

Intermodel-Multi-model comparison-assessment of the atmospheric and radiative composition-effects of supersonic transport aircraft changes due to emissions from a future supersonic aircraft fleet

Jurriaan A. van 't Hoff¹, Didier Hauglustaine², Johannes Pletzer³, Agnieszka Skowron⁴, Volker Grewe^{1,3},
5 Sigrun Matthes³, Maximilian M. Meuser^{3,5}, Robin N. Thor³, Irene C. Dedoussi^{1,5,6}

¹Aircraft Noise and Climate Effects, Delft University of Technology, Delft, 2629 HS, The Netherlands

²Laboratoire des Sciences du Climat et de l'Environnement (LSCE), CEA-CNRS-UVSQ, Gif-sur-Yvette, 91190, France

³Deutsches Zentrum für Luft- und Raumfahrt, Institut für Physik der Atmosphäre, Oberpfaffenhofen, 82234 Weßling, Germany

10 ⁴Faculty of Science and Engineering, Manchester Metropolitan University, Manchester, M1 5GD, United Kingdom

⁵[Deutsches Zentrum für Luft- und Raumfahrt, Institute of Air Transport, 21079 Hamburg, Germany](#)

⁶Department of Engineering, University of Cambridge, Cambridge, CB3 0DY, United Kingdom

Correspondence to: icd23@cam.ac.uk

Abstract. Commercial supersonic aircraft may return in the near future, offering ~~e~~considerably-reduced travel times while
15 flying higher in the atmosphere than ~~present-day~~subsonic aircraft, ~~and thus~~, and thus displacing ~~a part of the passenger traffic~~
~~and associated emissions to higher altitudes~~. ~~Their Supersonic aircraft~~For the first time since 2007, we present a
~~comprehensive multi-model assessment of the atmospheric and radiative effect of this displacement. We use four models~~ ~~Their~~
~~emissions can lead to long-lasting changes in the composition of our atmosphere, particularly in the spatial distribution of~~
~~ozone, aerosols, and other greenhouse gases. This poses a risk to the climate and public health. We present a comprehensive~~
20 ~~multi-model assessment of the impact of a supersonic fleet on a 2050 atmosphere using four state-of-the-art chemistry transport~~
~~models~~(EMAC, GEOS-Chem, LMDZ-INCA, MOZART-3) ~~to evaluate three scenarios where subsonic aviation is partially~~
~~replaced with supersonic aircraft. Replacing 4% of subsonic traffic with a Mach 2 aircraft with a NO_x emissions index of 13.8~~
~~g(NO₂)/kg leads to -model-ozone column loss of -0.3% (-0.9 DU, model range -0.4% to -0.1%), and it increases This radiative~~
25 ~~forcing by 19.1 mW/m² (model range 16.7 to 28.1). This forcing is driven by water vapour (18.2 mW/m²), ozone (11.4 mW/m²),~~
~~and aerosol emissions (-10.5 mW/m²). The use of a Mach 2 concept with low NO_x emissions (4.6 g(NO₂)/kg) reduces the~~
~~effect on forcing and ozone to 13.4 mW/m² (model range 2.4 to 23.4) and -0.1% (-0.3 DU, model range -0.2% to +0.0%),~~
~~respectively. If a Mach 1.6 aircraft with lower cruise altitudes and NO_x emissions of -index 4.6 g(NO₂)/kg is used instead, we~~
~~find a meannet-~~zero effect on the ozone column and an increase in radiative forcing of 3.7 mW/m² (model range 0.5 to 7.1).
~~were to be~~The supersonic concepts have ~~a larger (up to 185%)~~ greater radiative effect per passenger kilometre from non-CO₂
30 ~~emissions compared to subsonic aviation.~~

We show that the adoption of a fleet with 4.6 g(NO₂)/kg NO_x emissions index leads to a model-mean stratospheric H₂O burden
of +61.34 Tg for 46.2 Tg of annual H₂O emissions (model ranges from +20.14 to +116.53 Tg), and an ozone column loss of
0.11% (-0.18 to +0.03%). With an emissions index of 13.8 g(NO₂)/kg the average ozone column loss increases to -0.31% (-
0.57 to -0.09%). The adoption of a lower cruise altitude and speed reduces the mean H₂O burden to +9.34 Tg (+2.37 to +19.69
35 Tg) and instead leads to an ozone column increase of +0.02% (-0.01 to +0.04%). Compared to the most recent multi-model
assessment (2007), we find better agreement between the models, especially for the ozone response. Disagreement in H₂O
perturbation lifetimes remains, potentially driven by differences in vertical model resolutions. Our results reaffirm that
emissions from a supersonic fleet will lead to global changes in atmospheric composition, which can be reduced by adopting
lower cruise altitudes and lowering NO_x emissions.

40 1 Introduction

Over the past decades there has been growing global demand for fast intercontinental transportation. This demand has led to a search for faster alternatives to subsonic aircraft, such as supersonic or even hypersonic transport-vehicles (Kinnison et al. 2020; Pletzer et al. 2022; Matthes et al. 2022; Eastham et al. 2022). Supersonic vehicles transport aircraft (SSTs) have already attracted considerable commercial interest (Matthes et al. 2022, Eastham et al. 2024) and several parties are currently working towards the reintroduction of supersonic civil transport aircraft, supersonic transportation, relying on new technologies such as low-boom hull designs meant to minimize the environmental impact effect of the sonic boom (Berton et al. 2020). An example of this development is NASA's X-59 demonstrator aircraft, which has recently gone through engine testing and is planned to have its first flight this year in 2025.

Supersonic aircraft SSTs generally seek to use higher cruise altitudes to mitigate drag, with design cruise altitudes ranging from 14 to 21 km compared to subsonic altitudes aircraft which typically range cruise between 9 and 12 km. The increase in operational altitude changes the atmospheric response to the so-called non-CO₂ aircraft's emissions. Of particular concern is are the interaction emissions of nitrogen oxides (NO_x), water vapour (H₂O), and sulfur sulphur compounds, which affect emissions with the magnitude and the distribution and chemistry of ozone (O₃) layer and global radiative forcing (RF). The former two NO_x and H₂O emissions from SSTs lead to catalytic destruction of ozone through the NO_x and HO_x cycles (Matthes et al. 2022; Grewe et al. 2007; Solomon 1999; Crutzen 1972; Johnston 1971), while the latter leads to the formation of sulfate sulphate aerosols (SO₄) which that facilitate ozone destruction through heterogeneous chemistry (Pitari et al. 2014; Brasseur and Granier 1992). Through these emissions, the adoption of SSTs has been previously been linked to large-scale changes in the ozone distribution, with higher emission altitudes being linked to increased depletion of the global ozone column. Combined with increased ozone formation from smog chemistry and the self-healing effect, this leads to changes in the distribution of stratospheric ozone and net column ozone depletion for high emission altitudes (van 't Hoff et al., 2024a; Fritz et al. 2022; Zhang et al. 2021a; Speth et al. 2021; Fritz et al. 2022, van 't Hoff et al., 2024a). This is associated with poses a risk to public health, as the subsequent increased in surface UV-exposure has been linked to increased affects mortality (Eastham et al., 2018). Additionally, Furthermore, since ozone is also a greenhouse gas, the changes in its distribution also affect radiative forcing. In several studies this has been identified ozone the changes in the ozone distribution -as the primary warming driver of the radiative effect of non-CO₂ emissions from supersonic aircraft (van 't Hoff et al. 2024a; Zhang et al. 2023; Eastham et al. 2022), although others have also found this to have a net-cooling effect instead (Zhang et al. 2021b; Grewe et al. 2007).

Other non-CO₂ emissions that affect RF are water vapour and aerosols (black carbon, sulphates). Water vapour both directly impacts affects RFRF and it plays a pivotal role in the climate effect of subsonic aviation through the formation of contrails (Lee et al. 2021). At supersonic cruise altitudes contrail formation is expected to be much less common due to the drier conditions in the stratosphere (Stenke et al. 2008; Grewe et al 2007; IPCC 1999), however, the water vapour perturbation lifetime is higher compared to subsonic altitudes. Grewe and Stenke (2008) estimate that this lifetime is up to around 1.5 years at 20 km altitude, compared to lifetimes of 1 to 6 months at subsonic cruise altitudes. This facilitates more accumulation of stratospheric water vapour, which has a direct warming effect. The emission of water vapour has also been identified as a critical, if not the primary, driver of the radiative effect of SSTs and hypersonic vehicles (Pletzer and Grewe 2024; Pletzer et al. 2022; Zhang et al. 2021a; Grewe et al. 2010, 2007). The stratospheric accumulation of aerosols also affects RF, but they are commonly associated with a cooling effect instead (van 't Hoff 2024a; Zhang et al. 2023; Eastham et al. 2022; Speth et al. 2021). Combined, most studies find that these emissions result in net-warming RF in response to the adoption of supersonic aircraft (van 't Hoff 2024a; Zhang et al 2023, 2021a; Eastham et al. 2022; Speth et al. 2021; Grewe et al. 2007).

Besides an ozone impact, supersonic vehicles also have differing climate impacts compared to subsonic aviation. The climate impacts of supersonic vehicles are generally expected to be driven by H₂O emissions (Matthes et al. 2022, Pletzer et al. 2022, Zhang et al. 2021). Water vapour is a potent greenhouse gas which also plays an important role in the climate impact of subsonic aviation. At subsonic cruise altitudes (10 to 13 km) the perturbation lifetime of H₂O emissions is estimated to be between 1 and 6 months (Grewe and Stenke, 2008, Pletzer and Grewe, 2024). This limits its direct warming potential, but there is still considerable climate impact from the formation of contrails (Lee et al. 2021). At supersonic cruise altitudes (14–21 km) contrail formation is much less common as the stratosphere is drier (Stenke et al. 2008, Grewe et al. 2007, IPCC 1999). Instead, the perturbation lifetime of H₂O emissions is higher, up to around 1.5 years at 20 km (Grewe and Stenke, 2008). This leads to considerable accumulation of stratospheric H₂O, which is often found to be the main driver of the climate impact of emissions at these high altitudes (Grewe et al. 2010, Pletzer et al. 2022, Zhang et al. 2021a, Pletzer and Grewe 2024). Secondary to H₂O, the effect of changes in the global ozone distribution can have a warming effect, up to similar levels as those of H₂O emissions (Eastham et al. 2022).

Both the ozone and climate ~~impacts-effects~~ stem from changes in the chemical composition of the atmosphere, particularly the stratosphere. To adequately capture ~~the changes in the chemical composition~~ these changes we rely on chemistry transport models (CTMs) or climate chemistry models (CCMs), which model the chemistry, transport, removal, and conversion of species throughout the atmosphere. A variety of such models has already been used to evaluate the effects of high-altitude emissions on ozone and ~~the climate RFRF~~, and despite their similar scope and chemistry routines, ~~this often leads to~~ these models often yield different results ~~in the impact assessments for the future adoption of supersonic aircraft~~. These differences are ~~in part~~ partially driven by uncertainties about the future of supersonic civil aviation, resulting in the use of different emission scenarios and timelines across studies. ~~However, earlier~~ However, multi-model studies also highlight that there are considerable differences between ~~the CTMs and CCMs~~ different CTMs and CCMs even in the evaluation of identical scenarios, ~~which has been reported in studies of both supersonic (e.g. Pitari et al. 2008; Grewe et al., 2007; Kawa et al. 1999, Pitari et al. 2008) and subsonic aviation, thereby making previous results dependent on model choice (Olsen et al. 2013)~~. These differences are most prevalent in the evaluation ~~of changes in ozone, the impact on~~ of the ozone response, which is subject to complex feedback ~~mechanisms~~ mechanisms. ~~In earlier multi-model studies~~ Differences in the modelling thereof can result in a large spread in model predictions of the ozone response and its effect on RF, at times leading to contradictory results between models (e.g.g., Grewe et al. 2007; Kawa et al. 1999) ~~the ozone impact predictions sometimes conflict, with models predicting net column increases and decreases (Kawa et al. 1996) or if they agree on depletion there is still a large spread (Grewe et al. 2007)~~. ~~These differences are also observed through~~ The effect of these ~~se~~ differences ~~is also evident upon~~ when metrics such as sensitivities to specific emission species are compared between studies and models ~~comparison comparing of the ozone sensitivities to emissions between models (Eastham et al. 2022, van 't Hoff et al. 2024a; Eastham et al. 2022)~~.

~~They~~ The differences in model responses to SST emissions are often driven by different implementations of ~~key~~ chemical, transport, or radiative processes across the models, ~~especially or in~~ by differences in the interactions between these model components. ~~They are, while~~ also ~~being a~~ affected by ~~other~~ fundamental properties, such as the model resolutions.

Understanding the effect of model-driven differences ~~in the evaluation of high-altitude emission impacts~~ is vital to our capability to synthesize results across studies that use different models. Multi-model studies expose these differences, and can help us understand their drivers, potentially offering robust conclusions and policy advice. In the field of high-altitude SST emissions, the most recent multi-model study performed was by Grewe et al. (2007). They showed that ~~while all~~ the four atmospheric models they used agreed ~~on that~~ the introduction of supersonic SST emissions ~~leading led~~ to net depletion of ozone, accumulation of stratospheric water vapour ~~and increases in radiative forcing~~, and a net-warming radiative effect.

130 However, they also showed ~~, there~~ that there was a spread in the calculations of these effects, both in terms of the spatial distribution and in absolute numbers. For example, they report a model-mean ozone perturbation of -8 Tg with a range of -16 to -1 Tg and a standard deviation of 5.5 Tg ~~were still considerable differences between the models' estimates of changes in ozone distribution and the stratospheric H₂O accumulation.~~ They report a multi-model mean depletion of 8 Tg with a standard deviation of 5.49 Tg, and for H₂O a mean perturbation of 64 Tg with a standard deviation of 20.03 Tg. These differences are not to be underestimated, but also indicate a notable improvement over models used by Kawa et al. (1999) who, with 7 models, found a mean column ozone depletion of 0.16% with a standard deviation of 0.17% for a similar supersonic emission scenario. Before that, ~~Kawa et al. (1999) used seven different models to study the effect of SST emissions, reporting a similar spread in model calculations (e.g., they report a mean ozone column loss of -0.17% with a range of -0.6 to 0.23% and a standard deviation of 0.22%, HSR scenario 4).~~ In both cases the standard deviation of the model predictions is similar to the mean, highlighting the magnitude of model-driven differences.

140 ~~Since then,~~ Over the past decades there have been considerable advances in our understanding of the underlying chemistry and physics, and at the same time ~~rapid increases in~~ the increased availability of computational power ~~have has~~ expanded our capacity to model these processes. This has led to enhancements in the overall modelling capabilities of CTMs ~~and CCMs~~. To assess the effect of these developments Zhang et al. (2021a) have ~~recently~~ compared the ~~modern~~-WACCM6 model to models used by Kawa et al. (1999) in a reassessment of their scenarios, finding similar overall atmospheric ~~impacts-effects~~ despite the higher ~~detail-fidelity~~ in their model. While this does provide some insight with respect to older evaluations, it remains unclear ~~whether-how~~ the past two decades of model development ~~have led to better convergence in the assessment of supersonic emissions in currently widely used models.~~ affect model-driven differences in assessments of an identical scenario, Understanding these differences ~~which~~ can help us better synthesize results from studies that use different models ~~to assess different supersonic scenarios.~~

150 To close this gap, we present a comprehensive study of the effect of the partial replacement of subsonic traffic with SSTs ~~introduction~~ on atmospheric composition and RF, using four widely-used chemistry climate and chemistry transport models (EMAC, GEOS-Chem, LMDZ-INCA, MOZART-3). We evaluate three SST adoption scenarios based on the scenarios considered ~~by re-evaluate existing supersonic emission scenarios from the most recent multi-model study on the SCENIC project (Grewe et al., (2007), which reflect the partial replacement of subsonic traffic with different supersonic aircraft concepts or emission characteristics).~~ We do this with four state-of-the-science atmospheric chemistry climate and chemistry transport models (EMAC, GEOS-Chem, LMDZ-INCA, MOZART-3), ~~comparing the atmospheric changes induced by different supersonic emissions within these models with the earlier results~~ We and we also analyse differences in atmospheric responses between the models. In particular, we cover ~~emphasizing the effects of~~ the responses of water vapour-H₂O, NO_x, and O₃-ozone, odd oxygen loss rates, and RF, as well as how these differ between the models ~~perturbations as simulated by the different models. We present t~~ The output of these models is presented in a harmonized way, in order to provide a comprehensive, multi-~~model,~~ estimate overview of the atmospheric and radiative impacts-effects of supersonic aircraft of the adoption of supersonic aircraft. ~~emissions in the stratosphere.~~

2 Methodology

2.2.1 Emission scenarios

165 We study the impact of supersonic aircraft emission scenarios derived from the SCENIC project (Grewe et al., 2007) in a 2050 atmosphere based on the CMIP6 SSP3.7 scenario (Riahi et al. 2017). Our emission scenarios are based on emission

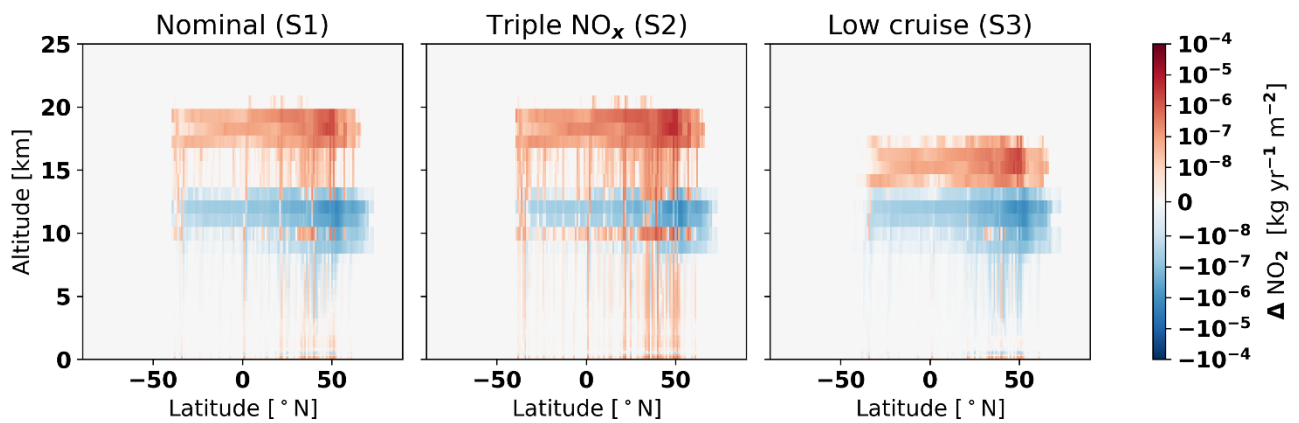
scenarios from the SCENIC project (Grewe and Stenke 2008; Grewe et al. 2007). The SCENIC emission inventories scenarios consider the adoption of a fleet of 501 supersonic transport aircraft SSTs in 2050, for the partial replacement-replacing part of the revenue passenger kilometres (RPK) of subsonic aviation. We consider a baseline scenario (S0) with only subsonic emissions (also S0 from Grewe et al. 2007). The nominal supersonic scenario (S1) considers the replacement of 4% of subsonic RPK with a fleet of 501 SSTs, operating at Mach 2.0 with cruise altitudes of 16.5 to 19.6 km (S5 of Grewe et al. 2007). This results in an increase of 6.3% in global aviation fuel usage. The triple NO_x scenario (S2) is a variant of the nominal scenario (S1) with tripled supersonic NO_x emissions, resulting in a fleet-average emission index of 13.80 kg NO₂/kg for the SSTs. This is closer to NO_x emission indices from recent SST concepts (Zhang et al. 2023, 2021a; Fritz et al. 2022; Eastham et al. 2022; Speth et al. 2021). In the low cruise scenario (S3) we consider the use of a SST with a lower cruise altitude of 13.1 to 16.7 km, and a cruise speed of Mach 1.6 (P6 from Grewe et al. 2007). Compared to the nominal emissions, this leads to a 5.5% reduction in supersonic RPK and a 31% reduction in SST fuel consumption. The characteristics of the emission scenarios are summarized in Table 1, and the resulting changes in the distribution of aviation emissions are shown in Figure 1.

(around 4% of revenue passenger km) of subsonic aviation. The supersonic aircraft operate at a cruise speed of Mach 2 at and cruise altitudes from 16.5 to 19.5 km (Grewe et al. 2007, Grewe and Stenke 2008). We use the same global distribution of supersonic flight routes, accounting for the partial substitution of subsonic traffic with the supersonic counterparts (Grewe and Stenke 2008). This leads to reduction in global fuel consumption of around 3.3% when compared to the emissions of the Grewe et al. (2007) study. The characteristics of the emission scenarios are summarized in Table 1.

Table 1: Summary of the sub- and supersonic aircraft emissions in the aircraft emission supersonic scenarios. The baseline emission scenario (A0S0) has no supersonic aviation, and there are three scenarios considering the partial replacement of subsonic aviation with supersonic vehicles aircraft. These are denoted as the The nominal supersonic emissions scenario (A1S1), thea considers the partial replacement of subsonic traffic with supersonic vehicles. Of this scenario two variants are included with triple supersonic NO_x emissions scenario (A2S2), and a the lower cruise supersonic altitude and speed low cruise scenario (A3S3). In all of the supersonic scenarios subsonic traffic is partially replaced by the supersonic aircraft, reducing the fuel consumption of subsonic aircraft compared to the baseline. -Within each category, the left (Sub.) columns summarizes the emission characteristics of all combined aircraft (subsonic and supersonic aircraft subsonic aircraft emissions), and the right (Sup.) columns summarizes the supersonic aircraft emissions.

Scenario	RPK		Fuel consumption		Avg. EI NO _x		NO _x emissions		Cruise altitude	
	(10 ¹¹ px. km)		(Tg yr ⁻¹)		(g (NO ₂) kg ⁻¹)		(Tg(NO ₂) yr ⁻¹)		(km)	
	Sub.	Sup.	Sub.	Sup.	Sub.	Sup.	Sub.	Sup.	Sub.	Sup.
Baseline (S0)	178.2	=	656.4	=	10.91	=	7.16	=	9-13	=
Nominal (S1)	171.1	7.3	639.9	57.9	10.91	4.60	6.98	0.27	9-13	16.5-19.5
Triple NO_x (S2)	171.1	7.3	639.9	57.9	10.91	13.80	6.98	0.80	9-13	16.5-19.5
Low cruise (S3)	171.5	6.9	639.0	40.0	10.84	5.62	6.93	0.22	9-13	13.1-16.7

We consider a baseline scenario (A0) with only subsonic aviation emissions (S0 from Grewe et al. 2007). The nominal supersonic scenario (A1) considers the partial replacement (4.1 % of passenger km) of subsonic aviation with a supersonic transport fleet (S5 of Grewe et al. 2007). This substitution results in an increase of 6.3% in global aviation fuel usage. The triple NO_x scenario (A2) is a variant of the nominal scenario with tripled supersonic NO_x emissions, resulting in a fleet average supersonic emission index of 13.80 kg NO₂/kg which is closer to supersonic NO_x emission estimates from more recent studies (Speth et al. 2021; Zhang et al. 2021a; Fritz et al. 2022). Finally, in the low cruise scenario we consider the use of a different aircraft concept with a lower cruise altitude of 13.1 to 16.7 km and a cruise speed of Mach 1.6 (P6 from Grewe et al. 2007). Compared to the nominal emissions this leads to a 5.5% reduction in supersonic passenger kilometres and a 31% reduction in supersonic fuel consumption. The resulting changes in the distribution of aviation emissions is shown in Fig. 1.



205 **Figure 1:** Zonal mean changes in the ~~vertical~~ distribution of annual NO_x emissions (expressed in kg NO₂ m⁻² yr⁻¹) due to the ~~introduction of supersonic aviation~~ partial replacement of subsonic traffic with SSTs. Differences are calculated with respect to the annual ~~A0-baseline (S0)~~ emissions.

2.2.3 Atmospheric mModelling

210 We evaluate the effect of the changes in aviation emissions on atmospheric composition and radiative forcing using four widely used chemistry transport models; EMAC, GEOS-Chem, LMDZ-INCA, and MOZART-3. Key characteristics of these models, including the horizontal and vertical resolution, chemistry processes, and dynamics, are summarized in Table 2. A direct comparison of the vertical grid of the models is also shown in Figure A1. We evaluate the effect of the SST adoption on a future atmosphere based on projections of the atmospheric composition and anthropogenic emissions in 2050, although there are some differences in how this is incorporated in the different models given model input availability and other technical

215 restrictions. The next subsections discuss the technical details and setup of each model individually. Numerical simulations are performed using four widely used global chemistry transport models: EMAC, GEOS-Chem, LMDZ-INCA, MOZART-3. A summary of the characteristics of the models, including resolution, chemistry processes covered, and dynamics is provided in Table 2 and the individual models are detailed in the following subsections.

220

Table 2: Summary of the atmospheric models characteristics, including resolution, chemistry, and dynamics.

Model	Resolution (lat × lon)	Vertical domain & resolution	Chemistry	Dynamics	Reference
EMAC	T42 (~2.8°×2.8°)	Surface to 0.01 hPa, 90 hybrid levels 22 layers between 400 and 50 hPa	1202 species 1839 gas phase rcts. 401 aqueous phase rcts. 401 photolytic rcts. 27 aqueous phase photolytic rcts. 21 heterogeneous rcts.	ECHAM5 nudged to ERA5, coupled online meteorology	Jöckel et al. 2016 Roeckner et al. 2003 Sander et al. 2011
GEOS-Chem	C48 (~2°×2.5°)	Surface to 0.01 hPa, 72 hybrid levels. 14 layers between 400 and 50 hPa	132 species 344 kinetic rcts. 154 photolytic rcts. 78 heterogeneous rcts.	MERRA -2, no onlineoffline meteorology	Eastham et al. 2018 Eastham et al. 2014 Bey et al. 2001
LMDZ-INCA	1.3°×2.5°	Surface to 0.04 hPa, 39 hybrid levels 11 layers between 400 and 50 hPa	154 species 234 homogeneous rcts. 43 photolytic rcts. 30 heterogeneous rcts.	LMDZ nudged to ERA5, offline meteorology	Hauglustaine et al. 2014. Terrenoire et al. 2022.
MOZART-3	T42 (~2.8°×2.8°)	Surface to 0.1 hPa, 60 hybrid layers 15 layers between 50 and 400 Hpa	108 species 218 gas phase rcts. 71 photolytic rcts. 18 heterogeneous rcts.	ERA-Interim, no onlineoffline meteorology	Kinnison et al., 2007 Skowron et al., 2021

2.23.1 EMAC

EMAC is an atmospheric chemistry general circulation model, consisting of the dynamical core ECHAM5 (European Centre
225 HAMBURG general circulation model, version 5, Roeckner et al. 2006) and MESSy (Modular Earth Submodel System, Jöckel
et al. 2016). ~~We use version 2.55.2 (The MESSY Consortium, 2021) of the EMAC model with a T42 global grid (approximately 2.8° × 2.8° latitude, longitude) and 90 hybrid vertical levels from the surface up to 80 km.~~ The chemical
mechanism incorporates 1839 gas phase and 21 heterogeneous phase reactions between 1202 species, which includes type 1ab
and type 2 polar stratospheric cloud ([PSC](#)) processes ([PSC](#), Kirner et al. ~~2010~~2011; Jöckel et al. 2010). The reaction rates are
230 from the most recent Jet Propulsion Laboratory evaluation, number 19 (Burkholder et al. 2020). Aerosol background
concentrations [of sulphates](#) are provided for heterogeneous chemistry [using inventories prepared for the Chemistry Climate
Model Initiative \(Jöckel et al. 2016; Gottschaldt et al. 2013\)](#). [Water vapour is accounted for as specific humidity-q, which is
influenced by gas-, solid- and liquid-phase processes at all altitudes. It is produced through 55 reactions and destroyed through
six reactions, and it is affected by physical processes such as rain-out and sedimentation. The radiation scheme incorporates
235 81 bands and recreates the solar cycle with high fidelity. This applies to the region from the top of the model domain \(0.01
hPa\) to 70 hPa \(Kunze et al. 2014; Dietmüller et al. 2016\).](#) RF is assessed at the tropopause with the radiative code of ECHAM5
(Roeckner et al. 2006), as well as a new radiative code based on the work by Pincus and Stevens (2013), as implemented by
Nützel et al. (2024).

240 [In this work we use EMAC version 2.55.2 \(The MESSY Consortium, 2021\) with a T42 global grid \(approximately 2.8° × 2.8°
latitude, longitude\) and 90 hybrid vertical levels from the surface up to 80 km. Twenty-two of these layers are located between
400 and 50 hPa, with an average thickness of 0.6 km.](#)

The model [has online meteorology which](#) is nudged towards ERA5 reanalysis data (2000-2010) between the surface and 10 hPa. Nudging is applied in the same way as earlier studies ([Pletzer et al. 2022](#); [Jöckel et al. 2016](#); [Pletzer et al. 2022](#)), affecting horizontal and vertical winds, temperature (wave 0 omitted), and the logarithm of surface pressure. ~~Water vapour is accounted for as specific humidity q , which is influenced by gas, solid and liquid phase processes at all altitudes. It is produced through 55 reactions and destroyed through six reactions, and it is affected by physical processes such as rain out and sedimentation. The radiation scheme incorporates 81 bands and recreates the solar cycle with high fidelity. This applies to the region from the top of the model domain (0.01 hPa) to 70 hPa ([Kunze et al. 2014](#); [Dietmüller et al. 2016](#)).~~ **The background atmosphere, surface boundary conditions,** and non-aviation anthropogenic emissions are based on the CMIP6 SSP3-7.0 scenario for the year 2050 ([Meinshausen et al. 2020](#)). **Volcanic emissions are included based on the AEROCOM emission inventory ([Dentener et al. 2006](#); [Ganzeveld et al. 2006](#)) for the year 2000, which is cycled throughout the model run. We also apply**

~~For EMAC model simulations a spin up method was applied, which allows~~ to reduce spin up times while maintaining annual quasi-equilibrium. ~~During This is done by applying the first year of simulations the annual aircraft emissions are increased by an altitude-dependent scaling factor to the emissions during the first year of the model run, and standard values are applied after. Through this approach so that the~~ annual quasi-equilibrium is achieved faster. For more detail on this method, we refer to the work by [Pletzer and Grewe \(2024\)](#) and its supplement. ~~The model is integrated for a total of 16 years to allow for a longer averaging period, which is done to improve the statistical significance of the EMAC results. The model is ran for a total~~ of 16 years to allow for a longer analysis period and better statistical significance of the results.

2.23.2 GEOS-Chem

GEOS-Chem is a community-developed tropospheric-stratospheric CTM with over 280 chemical species based on the Goddard Earth Observing System (GEOS) ([Bey et al. 2001](#)). ~~The model uses It incorporates stratospheric chemistry through the Unified Tropospheric-Stratospheric Chemistry Extension (UCX) by [Eastham et al. \(2014\)](#) using KPP for kinetic chemistry ([Damian et al. 2002](#)) and Fast-JX for photolytic reactions ([Bian and Prather, 2002](#)), incorporating stratospheric chemistry through the Unified Tropospheric-Stratospheric Chemistry Extension (UCX) by [Eastham et al. \(2014\)](#).~~ Within the troposphere, ~~H₂O water vapour~~ mixing ratios are prescribed by ~~the offline~~ meteorology, and in the stratosphere the ~~H₂O water vapour~~ tracer evolves freely subject to ~~photochemical-gas-phase~~ chemistry, [photochemistry](#), and ~~tropospheric-stratospheric~~ transport. GEOS-Chem's capability to model stratospheric chemistry ~~extension~~ has been demonstrated against satellite observations ~~aeross-in~~ several studies ([Fritz et al. 2022](#); [Speth et al. 2021](#); [Eastham et al. 2014](#)); ~~Speth et al. 2021; Fritz et al. 2022; van 't Hoff et al. 2024a~~), and it is incorporated into NASA GMAO's GEOS chemical composition forecast (GEOS-CF) ([Keller et al. 2021](#)). ~~The model simulates the distribution of various aerosols from anthropogenic and natural sources, and it models heterogeneous reactions in both the tropo- and stratospheric domain, including the formation, sedimentation and evaporation of PSCs ([Eastham et al. 2014](#)). RF is evaluated at the tropopause in the same manner as described in [van 't Hoff et al. \(2024a\)](#),~~ incorporating stratospheric adjustment following the implementation by [Eastham et al. \(2022\)](#).

We use version 14.1.1 ~~-of~~ the GEOS-Chem High Performance ~~(GCHP) variant model~~ (The International GEOS-Chem User Community, 2023) with a C48 ~~cubicoid~~-spherical global grid (approximately $2^\circ \times 2.5^\circ$ latitude, longitude) and 72 non-uniform vertical levels. ~~The vertical grid has 14 layers between 400 and 50 hPa, with an average thickness of 0.9 km.~~ We use historical meteorological data for the years 2000 to 2010 from the MERRA-2 reanalysis product by NASA/GMAO ([Gelaro et al. 2017](#)). Volcanic emissions are incorporated through historical emissions for the same time period following work by [Carn et al. \(2015\)](#). ~~Surface emissions and mixing ratios of long-lived species are prescribed following the 2050 boundary conditions of the SSP3-7.0 scenario. Simulatons~~ Simulations are ~~performed~~ ran for a total of 10 years using the ~~same~~ spin up method as EMAC, detailed in [Pletzer and Grewe \(2024\)](#).

The LMDZ-INCA global chemistry-aerosol-climate model couples ~~online~~ the LMDZ (Laboratoire de Météorologie Dynamique, version 6) General Circulation Model (GCM, Hourdin et al., 2020) and the INCA (INteraction with Chemistry and Aerosols, version 6) model (Hauglustaine et al., 2004; 2014; 2004). ~~In the present configuration, w~~ LMDZ-INCA is part of the IPSL Coupled Model, and we use the “Standard Physics” parameterization of the GCM (Boucher et al., 2020). ~~The model includes 39 hybrid vertical levels extending up to 70 km. The horizontal resolution is $1.3^\circ \times 2.5^\circ$ in latitude and longitude, respectively. The primitive equations in the GCM are solved with a 3 min time step, large-scale transport of tracers is carried out every 15 min, and physical and chemical processes are calculated at a 30 min time interval.~~ The large-scale advection of tracers is calculated based on a monotonic finite-volume second-order scheme (Van Leer, 1977; Hourdin and Armengaud 1999). Deep convection is parameterized according to the scheme of Emanuel (1991). The turbulent mixing in the planetary boundary layer is based on a local second-order closure formalism.

~~INCA includes a state-of-the-art $\text{CH}_4\text{-NO}_x\text{-CO-NMHC-O}_3$ tropospheric photochemistry (Folberth et al., 2006); Hauglustaine et al., 2004); Folberth et al., 2006) as well as. This version of the model also includes an interactive chemistry in the stratosphere and mesosphere (Terrenoire et al., 2022). For aerosols, the~~ The INCA model simulates the distribution of aerosols with anthropogenic sources such as ~~sulfates~~ sulphates, nitrates, black carbon (BC), and organic carbon ~~(OC)~~, as well as natural aerosols such as sea-salt and dust. ~~The heterogeneous reactions on b~~ Both natural and anthropogenic tropospheric aerosols are included in the model facilitate heterogeneous reactions (Hauglustaine et al., 2004; 2014; 2004). Heterogeneous processes on PSCs and stratospheric aerosols are parameterized following the scheme implemented in Lefèvre et al. (1994). ~~This version of the model also includes an interactive chemistry in the stratosphere and mesosphere (Terrenoire et al., 2022). Heterogeneous processes on PSCs and stratospheric aerosols are parameterized following the scheme implemented in Lefèvre et al. (1994).~~ Water vapour is affected by physical processes in the LMDZ GCM and an additional H₂O tracer is introduced in INCA incorporates a water vapour tracer which is linked to the LMDZ GCM. Similar to GEOS-Chem, in order to account for photochemical production and destruction. Below the model tropopause, the two water vapour tracers (i.e., physical water vapour tracer and full water vapour tracer) are this tracer is prescribed by imposed identical LMDZ at each time step below the tropopause, and only the full H₂O tracer is affected by and it evolves freely in the stratosphere subject to -chemistry (gas-phase and photochemical), (and aircraft emissions transport, condensation, sedimentation, and stratospheric emissions) in the stratosphere. In addition to gas phase chemistry, in the stratosphere, condensation and further sedimentation of water vapour can occur over stratospheric aerosols and PSCs at high (>60°) latitudes. RF is evaluated using an improved version of the ECMWF scheme developed by Fouquart and Bonnel (1980) in the solar part of the spectrum and by Morcrette (1991) in the thermal infrared. Aerosol forcing is assessed at the top of the atmosphere, similar to Hauglustaine et al. (2014), and forcing from ozone and water vapour is calculated at the tropopause with an offline version of the LMDZ GCM with stratospheric adjustment, similar to Terrenoire et al. (2022).

We use a configuration with a horizontal resolution of $1.3^\circ \times 2.5^\circ$ in latitude and longitude, with 39 hybrid vertical levels extending up to 70 km. Eleven of these layers are located between 300 and 50 hPa, with an average thickness of 1.1 km. The model simulations have a is ran for 15 years, -duration- with initial conditions representative of the year 2050 (Pletzer et al., 2022). -and with s Surface emissions and boundary conditions for 2050 are provided-prescribed by the CMIP6 SSP3-7.0 scenario (Meinshausen et al. 2020). Stratospheric volcanic aerosols are based historical data (2000-2014) from Input4MIP for the calculation of heterogeneous chemistry. In this study, the LMDZ GCM zonal and meridional wind components are nudged towards the meteorological data from the European Centre for Medium-Range Weather Forecasts (ECMWF) ERA-Interim reanalysis, with a relaxation time of 3.6 h (Hauglustaine et al., 2004). The ECMWF fields are provided every 6 h and interpolated onto the GCM grid for the years 2004-2018.

2.2.3.4 MOZART-3

The Model for OZone And Related chemical Tracers, version 3 (MOZART-3) is an offline ~~chemical transport mode~~ CTM (Kinnison et al., 2007) ~~which that~~ has been used for an extensive range of applications, ~~(e.g., Liu et al., 2009; Flemming et al., 2011)~~ including various aspects of the ~~impact-effect~~ of aircraft NO_x emissions on atmospheric composition (e.g. Skowron et al., 2021, 2015, 2013; Freeman et al., 2018; Sovde et al., 2014; ~~Skowron et al., 2013, 2015, 2021, Freeman et al., 2018~~ Flemming et al., 2011; Liu et al., 2009). MOZART-3 accounts for advection based on a flux-form semi-Lagrangian scheme, a shallow and mid-level convective and deep convective routines, boundary layer exchanges, and wet and dry deposition. MOZART-3 reproduces detailed chemical and physical processes from the troposphere through the stratosphere, including gas-phase, photolytic, and heterogeneous reactions. The latter includes four aerosol types: liquid binary sulphate, supercooled ternary solution, nitric acid tri-hydrate, and water-ice. Heterogeneous processes occurring on liquid sulphate aerosols and PSCs are also included, following the approach of Considine et al. (2000). The kinetic and photochemical data are based on the NASA/JPL evaluation (Sander et al., 2006). ~~The H₂O Water vapour emissions tracers~~ have been implemented into the model for the purpose of this work, allowing H₂O water vapour to evolve freely in the stratosphere subject to transport and chemistry. ~~and fixing it in the troposphere. However, it is still under exploration due to probable limitations with tropospheric-stratospheric transport.~~ We assess RF at the tropopause using the SOCRATES model of the UK Met Office (Manners et al. 2015).

~~In this work we~~ We use a model configuration with a T42 (~ 2.8° × 2.8°) horizontal resolution and 60 hybrid layers from the surface to 0.1 hPa. The vertical grid has 15 layers between 400 and 50 hPa, with an average thickness of 0.8 km. The transport of chemical compounds is driven by ~~the 6 hour reanalysis ERA-Interim data for the year 2006 meteorological fields~~ from the European Centre for Medium Range Weather Forecast (ECMWF), ~~6 h reanalysis ERA Interim data for the year 2006.~~ The 2050 gridded surface emissions (anthropogenic and biomass burning) ~~were determined~~ are prescribed by Integrated Assessment Models (IAMs) for the business-as-usual scenario of the Representative Concentration Pathways, RCP 4.5. The surface boundary conditions for long-lived species are set to fixed volume mixing ratio units with their concentrations determined using the methodology of Meinshausen et al. (2011). This future scenario does not include natural emissions, such as isoprene, NO_x from lightning and soil, or oceanic emissions of CO. The model ~~was run~~ is integrated for 8 years until ~~reaching~~ a steady-state is reached, and the last year of these simulations is considered for the analysis. ~~For t~~ The assessment of the H₂O water vapour perturbation ~~separate model runs were used~~ is performed using separate model runs, with outputs in limited ~~the output of which has a limited~~ vertical resolution ~~of with~~ 30 layers from 200 to 0.1 hPa.

2.2.5 Atmospheric conditions

~~We evaluate the impact of the supersonic aircraft emission scenarios in a 2050 atmosphere, which is an appropriate timeframe for large-scale civil application of these aircraft and matches the adoption timeframe considered by Grewe et al. (2007). Due to differences in the availability of datasets across all models, we make some compromises in the model setup to ensure better compatibility across the simulation setups. Notably we use historical data (2000-2020) for the inputs of background meteorology and volcanic emissions rather than future forecasts. In the EMAC, GEOS-Chem, and LMDZ-INCA models we base the atmosphere and surface emissions on the SSP 3.7 socioeconomic pathway from CMIP 6 (Riahi et al. 2017). This is different for the MOZART 3 model, where this is based on RCP 4.5 instead and the model is driven by more constrained meteorology (yearly data for 2006). Compared to the other models this means we expect less availability of methane (CH₄) and nitrogen compounds in MOZART 3's atmosphere (Meinshausen et al. 2020). Compared to the other models this means we expect less availability of methane (CH₄) and nitrogen compounds in MOZART 3's atmosphere (Meinshausen et al. 2020).~~

3.5 Approach for evaluating atmospheric and radiative effects

370 ~~These~~We identify quantify the effect of the supersonic emissions by comparing the perturbed atmospheric compositiones and forcing of the supersonic scenarios with that of the baseline atmosphere simulation, thereby also taking into account the effects of the reduction in subsonic emissions. To account for inter-annual variability, we calculate the effect of the emissions impacts are calculated over the last three years of the model integrations for GEOS-Chem and LMDZ-INCA. For the For EMAC results we use average over 6 years to improve the statistical significance of the results, considering the added variability from its online meteorology. For and the MOZART-3 results we show an annual average due to considering its cycling meteorology. We calculate the stratospheric perturbation lifetime (e-folding lifetime) of emission species by dividing the stabilized stratospheric perturbation by the increase in annual stratospheric emissions. Since not all models calculate forcing from aerosol perturbations, we first calculate model-mean RF from ozone, water vapour, and aerosols separately, which are then combined to produce a first-order estimate of the net radiative effect.

380 3.4 Results & Discussion

With this work we We present a comprehensive review of the effects of supersonic aviation of the partial replacement of subsonic traffic with SSTs on the atmospheric composition and RF using four atmospheric chemistry transport models as observed by several state-of-the-art models for the first time since the work by Grewe et al. (2007). Firstly, we will give a summary In section 4.1 we summarize of the model-mean (mean over all models) impact effect of the adoption of the supersonic SST emissions fleets on the stratospheric atmospheric composition and RF, and we compare the models' baseline atmospheres in section 3.1. Sections 4.2 to 4.6 discuss in more detail These impacts are calculated over the last three years of the model integrations for GEOS-Chem and LMDZ-INCA. For the EMAC results we use 6 years to improve the statistical significance, and the MOZART-3 results show an annual average due to its cycling meteorology. The individual how the supersonic scenarios affect impacts on stratospheric water vapour, NO_x and NO_y, nitrogen oxides, ozone ozone, and odd oxygen (O_x) loss rates, and RF, respectively are then discussed in sections 3.2 to 3.5. In these sections we also explore the differences between the individual models we use.

390 4.3.1 Global atmospheric and radiative impacteffect

Table 3 provides a summary of the key variables representing the changes in atmospheric composition and RF in response to the supersonic emissions scenarios across all models. Comprehensiveprehensive tables of the effects on water vapour, NO_x, and ozone, are included in the appendix (Tables A1 to A3). Similar to Grewe et al. (2007), we include the hemispheric fractionratio, which is the ratio of the perturbation mass in the northern hemisphere over the perturbation mass in the southern hemisphere, as a means to quantify interhemispheric transport the mixing of emissions between hemispheres. For reference, the hemispheric ratio for the SST fuel consumption is 10.14 for the nominal and triple NO_x scenarios, and 10.34 for the low cruise scenario, indicating the that the vast majority of SST emissions take place in the northern hemisphere.

400 ForIn response to the nominal supersonic supersonic scenario (A1)scenario (S1), we find a model-mean stratospheric H₂O water vapour perturbations perturbation of 46.9 Tg (model range 20.1 to 63.3 Tg) with ranging between 20.55 Tg (+0.55%) for the LMDZ-INCA model to +116.53 (+1.55%) for MOZART-3, with a multi-model mean perturbation of 61.34 Tg and a mean perturbation lifetime of 16.7 months. The mean perturbation lifetime (e-folding lifetime) is calculated by dividing the stratospheric perturbation by the increase in annual stratospheric emissions a lifetime of 12.0 months (model range 5.2 to 16.2). This perturbation is largely retained in the northern hemisphere, as indicated by the mean hemispheric fraction of 4.68. There is good agreement in the stratospheric The change in aviation emissionsintroduction leads to increases in stratospheric NO_x, with a model-mean perturbation across the models, ranging from +38.71 Tg for EMAC to +43.52 for GEOS-Chem with a

410 ~~model mean of +40.96 T of 38.9 Gg(NO₂) (model range 32.1 to 43.5)g, and global ozone column changes of -0.1% (-0.3 DU, model range -0.2% (-0.7 DU) to (0.0% (0.0 DU)). RF is also affected, with the~~ The emissions cause in a mean change of global column ozone by -0.11 %, with a range of -0.22 % for GEOS-Chem to +0.03% for EMAC, largest forcing due to being from water vapour (20.8 mW/m², model range 6.2 to 32.3), followed by ozone (3.2 mW/m², model range 1.3 to 6.8). Increases in stratospheric aerosols have a cooling effect, with forcing of -0.4 mW/m² from black carbon and -9.7 mW/m² from inorganic aerosols (sulphates & nitrates). We therefore estimate a model-mean net RF of 13.9 mW/m² when aerosols are included (model range 2.9 to 24.4).

420 ~~These results are similar to the results of Grewe et al. (2007), who report a model mean H₂O perturbation of 64 Tg with a range of 45 to 98 Tg between models. Compared to their work we do note an increase in the overall hemispheric fraction. Grewe et al. report a model mean value of 2.96 which is smaller than our mean, indicating reduced hemispheric exchange in our models. The source of this will be discussed further in section 3.2. Grewe et al. (2007) also report a mean change in the overall ozone column of -8 Tg, with a spread of -1 to -16 Tg between their models. Here we note a considerable improvement in the agreement of the ozone response in the models, as we find a smaller spread in the ozone perturbation mass and hemispheric fraction (Fig. A1).~~

425 ~~In the triple NO_x emission scenario (A2) the tripling of the NO_x emissions index increases the stratospheric NO_x accumulation by a factor of 3.4. There is little change in terms of the H₂O perturbation model, but the ozone depletion increases model The ozone RF+netRF to a mean ozone column change of -0.31 %, ranging between -0.57% for MOZART-3 to -0.09% for LMDZ-INCA. We note that the NO_x response is non-linear across all models. The tripling of supersonic NO_x emissions increases stratospheric O₃ loss by factors of 2.39 and 2.56 for the GEOS-Chem and LMDZ-INCA models, whereas this factor is 3.89 for MOZART-3 and 7.24 for EMAC (Table A3). The higher sensitivity of MOZART-3 may be driven by its lower background nitrogen availability (Table A2), whereas that of EMAC is enhanced by the low stratospheric O₃ loss for the nominal scenario. Still, the high factor for EMAC in particular may also be indicative of strong non-linear interactions. These drivers are expanded on in subsequent sections.~~

435 ~~RF~~ The impacts on stratospheric composition are reduced for the low-cruise altitude scenario (A3) Scenario S3. Here we find a mean H₂O perturbation of +9.34 Tg with a mean lifetime of 5.3 months. In this case very little H₂O reaches the southern hemisphere, resulting in high hemispheric fractions, with values of 25.07, 10.19, and 36.26 respectively for EMAC, GEOS-Chem, and LMDZ-INCA. The negative value for EMAC is due to a net decrease in southern hemispheric H₂O. The reduction in-cruise altitude also reduces the NO_x perturbation to a mean +20.82 Tg, ranging from +17.41 to +23.72 Tg. In this low-cruise

440 scenario we find a mean increase of the overall ozone column across the models with the exception of GEOS-Chem, which calculates a -0.01% change. This results in a model-mean ozone increase of +0.02% with a range of -0.01% to +0.04%.

445 **Table 3: Summary of impacts-effects on stratospheric water vapour budget, stratospheric NO_x, the and-ozone column, and RF changes for the emission-SST scenarios. These impacts-values are calculated as differences between the scenarios-perturbed and the baseline atmospheres. For more extensive summaries of the effects on H₂O, NO_x, and O₃-impacts, including background mass budgets, see Tables A1 ~~to~~ A3 in the appendix. The inorg. aer. column contains the RF from changes in nitrates and sulphates.**

450 **Notes:** ^aThe H₂O perturbation lifetime of the MOZART-3 model may be excessive due to some limitations in the H₂O evaluation, see the discussion at the end of section 3.2. ^bFor EMAC two numbers are shown for the RF assessment: F; the upper is calculated using the ECHAM5 radiative scheme, the bottom with the scheme by Pincus and Stevens (2013). Both are considered in the mean. ^cThese LMDZ-INCA aerosol forcings are calculated at the top of the atmosphere. ^dTotal forcing with aerosols is calculated with the model-mean aerosol forcings. model-mean

Nominal Scenario	Stratospheric H ₂ O			Stratospheric NO _x		Total O ₃	Radiative Forcing					
	H ₂ O Perturbation [Tg] (relative)	Perturbation lifetime [months]	Hemispheric ratio (increase only) [NH/SH]	NO _x Perturbation [Tg-NO ₂] (relative [%])	NO _x Perturbation n lifetime [months]	Ozone Perturbation column change [DU] (%)	O ₃	H ₂ O	Total (O ₃ +H ₂ O)	BC	Inorg. Aer.	Total ^c
	[Tg] (%)	[months]	[NH/SH]	[Tg NO ₂] (%)	[months]	[DU] (%)	[mW/m ²]					
EMAC	+69.63 (+1.625 %)	16.24	4.04	37.4 (1.6 %)	4.04	0.0 (0.0)	2.8 ^a 3.0 ^a	29.7 ^a 22.2 ^a	32.5 ^a 25.2 ^a	-	-	22.4 15.2
GEOS-Chem	+49.34 (+0.677 %)	12.73	4.04	43.5 (1.9 %)	4.74	-0.7 (-0.2 %)	1.3	13.4	14.7	-1.3	-9.3	4.6
LMDZ-INCA	+20.14 (+0.586 %)	5.25	5.45	42.6 (1.7 %)	4.64	-0.2 (-0.0 %)	6.8	6.2	13.0	0.5 ^b	-10.0 ^b	2.9
MOZART-3	+54.71 3 ^a (+1.556 %)	14.04	4.63	32.1 (1.6 %) (+3.16 %)	3.54	-0.6 (-0.2 %) 0.43	2.2	32.3	34.5	-	-	24.4
Model-mean	+61.34 (+1.14 %)	12.04	4.51	38.9 (1.7 %)	4.24	-0.3 (-0.1 %)	3.2	20.8	24.0	-0.4	-9.7	13.9
Triple NO _x												
EMAC	+61.86 (+1.54 %)	15.87	4.11	140.5 (6.0 %)	3.33	-0.6 (-0.2 %)	7.5 ^a 6.9 ^a	31.1 ^a 21.3 ^a	38.6 28.2	-	-	28.4 18.0
GEOS-Chem	+49.79 (+0.687 %)	12.83	3.91	173.6 (7.5 %)	4.14	-1.4 (-0.4 %)	13.3	14.0	27.3	-1.3	-9.2	17.1
LMDZ-INCA	+20.55 (+0.556 %)	5.35	5.25	119.5 (4.9 %)	2.82	-0.3 (-0.1 %)	20.9	6.3	27.2	0.5 ^b	-10.3 ^b	17.0
MOZART-3	-	-	-	112.8 (5.5 %)	2.62	-1.4 (-0.4 %)	8.6	-	-	-	-	-
Model-mean	+45.45 (+0.92 %)	11.35	4.47	136.6 (6.0 %)	3.23	-0.9 (-0.3 %)	11.4	18.2	29.6	-0.4	-9.8	19.4
Lower cruise												
EMAC	+19.69 (+0.446 %)	9.12	3.11	18.2 (0.8 %)	4.65	0.1 (0.0)	2.4 ^a 2.4 ^a	8.2 ^a 6.3 ^a	10.6 8.7	-	-	7.2 5.3
GEOS-Chem	+5.96 (+0.108 %)	3.41	10.43	23.7 (1.0 %)	6.06	-0.0 (-0.0 %)	2.1	1.9	4.0	-0.4	-3.1	0.6
LMDZ-INCA	+2.37 (+0.061 %)	1.33	38.14	17.4 (0.7 %)	4.44	0.1 (0.0)	4.6	0.7	5.3	0.2 ^b	-3.5 ^b	1.9
Model-mean	+9.34 (+0.20 %)	4.68	17.25	19.8 (0.8 %)	5.05	0.1 (0.0)	2.9	4.3	7.2	-0.1	-3.3	3.8

455 In case of the triple NO_x scenario (S2), the stratospheric NO_x accumulation increases by a factor of 3.5 to a model-mean of 136.6 Gg(NO₂) (model range 112.8 to 173.6). In this case the model-mean water vapour perturbation is 44.1 Tg (model range 20.6 to 61.8), and the model-mean ozone column depletion increases to -0.3% (-0.9 DU, model range -0.4% (-1.4 DU) to -0.1% (-0.3 DU)). RF from ozone is also enhanced, increasing to 11.4 mW/m² (model range 6.9 to 20.9), but RF from water vapour is still dominant with a mean value of 18.2 mW/m² (model range 6.3 to 31.1). We find RF of -0.4 mW/m² for black

carbon and -9.8 mW/m^2 for inorganic aerosols. Including these, the estimated model-mean net RF is 19.4 mW/m^2 (model range 17.0 to 28.4).

When the supersonic cruise altitude and speed are reduced (scenario S3), the effects of the SST adoption on the atmospheric composition and RF are reduced as well. Scenario S3 has 30% less SST fuel burn compared to the nominal scenario (S1), but the reduction in atmospheric and radiative effects exceeds that. In this case we find a model-mean water vapour perturbation of 8.1 Tg (model range 2.4 to 16.0) with a lifetime of 4.6 months (model range 1.3 to 9.1). The stratospheric NO_x perturbation is reduced to a model-mean of $19.8 \text{ Gg}(\text{NO}_2)$ (model range 17.4 to 23.7) and the ozone column changes by a global mean of 0.0% (0.1DU, model range 0.0% (0.0 DU) to 0.0% (0.1 DU)). The accumulation of stratospheric water vapour still has the largest contribution to radiative forcing (4.3 mW/m^2 , model range 0.7 to 8.2), followed by cooling from aerosols (-0.1 mW/m^2 for black carbon and -3.3 mW/m^2 for inorganic aerosols) and ozone (2.9 mW/m^2 , 0.7 to 4.6). The estimated total forcing is 3.8 mW/m^2 (range 0.6 to 7.2).

Despite some differences in the model configurations and inventories, we find that the models have similar budgets of water vapour, NO_x , ozone, and halogens in their baseline atmospheres (Tables A1 to A4). The GEOS-Chem model stands out as having more stratospheric water vapour than the other models. Furthermore, MOZART-3's baseline atmosphere has around 15% less stratospheric NO_x compared to the other models. This may be related to the use of RCP 4.5 boundary conditions rather than SSP3-7.0 (Meinshausen et al. 2020), and also to the use of ECMWF reanalysis meteorology, as this has been reported to lead to underestimations of stratospheric NO_x mixing ratios before with the MOZART-3 model (Kinnison et al., 2007). The effects of the differences in baselines on the response to the SST emissions are discussed further in the relevant sections.

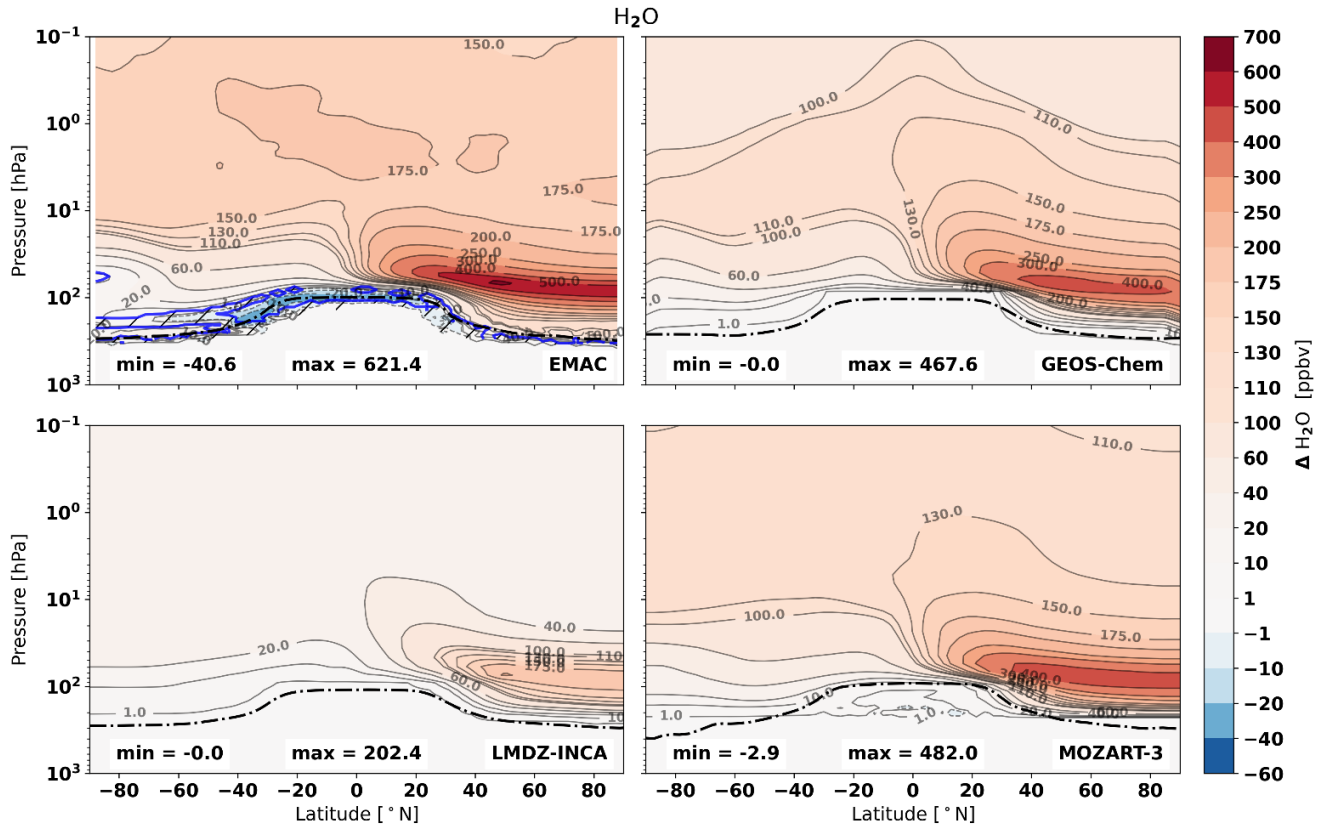
3.4.2 Water vapour

Figure 2 shows the zonal average H_2O -water vapour perturbations from the nominal supersonic scenario (SA1) as evaluated across-by the four models. ~~and, t~~ The vertical averages for all three scenarios are shown in Figure 3-A2. We find Overall, ~~t~~ the perturbation patterns of stratospheric water vapour ~~the zonal mean distributions~~ agree across the models. The strongest ~~changes~~ increases, ~~in terms of stratospheric H_2O concentrations-mixing ratios,~~ occur around the cruise altitude in the northern hemisphere, coinciding with the majority of ~~supersonic SST activity~~ emissions. From the cruise ~~areas~~ regions we see extensions transporting H_2O -water vapour to the northern polar latitudes, and upwards transport to the upper stratosphere in tropical latitudes. ~~Similar accumulation patterns have been observed across other studies (Zhang et al. 2023;2021a;2021b, Kinnison et al. 2020). Our results are similar to results from Grewe et al. (2007) up to pressure altitudes of 60 hPa. Above this altitude our model results show stronger perturbations, which may be related to the extended vertical domain.~~

Between the models we find a spread in the calculated water vapour perturbation lifetimes and hemispheric ratios, which is indicative of differences in transport processes or chemical sinks between the models. Earlier works have identified that the model resolution is important to the representation of transport, mixing, and diffusion processes (Revell et al. 2015; Roeckner et al. 2006; Strahan and Polansky, 2006), and we also find a trend between the model grids and water vapour perturbation lifetimes and hemispheric ratios (Figure 3). We find that the water vapour perturbation lifetime is linked to the model layer count between 400 and 50 hPa, with higher layer counts being associated with longer perturbation lifetimes. Transport of stratospheric water vapour emissions to the tropopause is a critical sink of the water vapour emissions, especially for the models using prescribed tropospheric water vapour mixing ratios (GEOS-Chem, LMDZ-INCA, MOZART-3), where the stratospheric water vapour tracer is effectively destroyed when it is transported into the model troposphere. We hypothesize

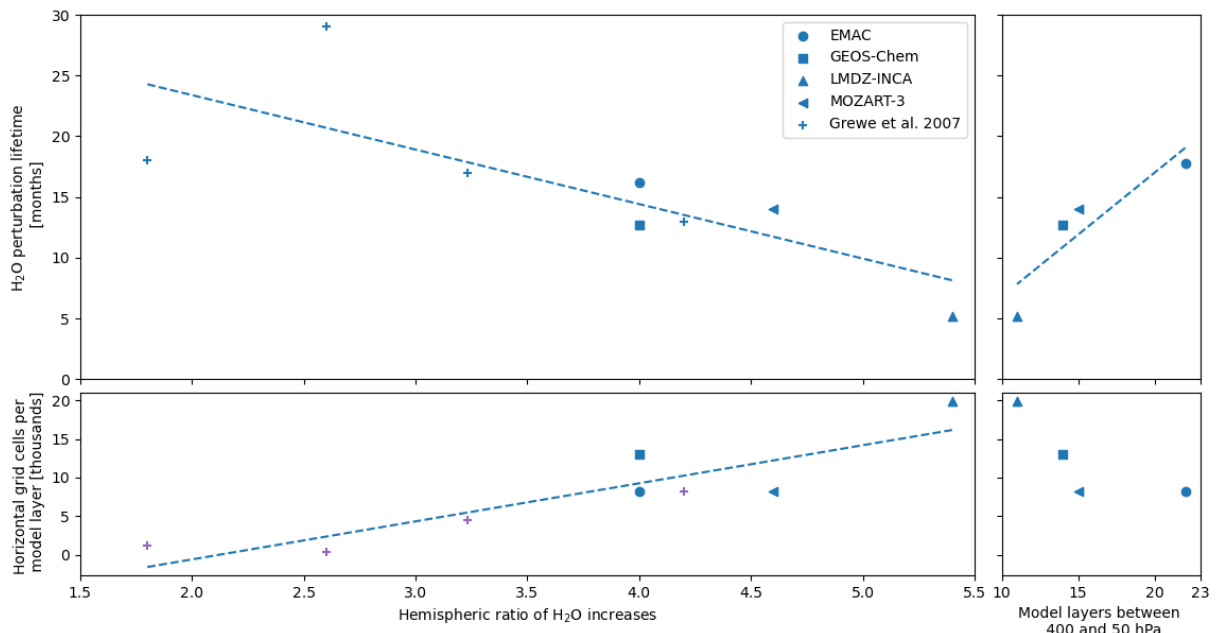
505

that the vertical model grid affects the modelling of the stratospheric to tropospheric transport, and furthermore that it introduces a secondary sink which affects stratospheric water vapour. During the model integration the tropopause altitude evolves over time, which causes parts of the model grid to switch from the stratosphere (evolving tracers) to troposphere (prescribed ratios), stripping stratospheric tracers in the process. This has been noted to reduce water vapour perturbation lifetimes of emissions near the tropopause in GEOS-Chem before (van 't Hoff et al. 2024a), and it also explains why we find larger reductions (relative to the nominal scenario) in water vapour perturbation lifetimes in the low cruise scenario (S3) for the models with coarser vertical grids



510

Figure 2: Zonal mean changes in H₂O-water vapour mixing ratios (ppbv) in response to the nominal supersonic emissions scenario (A0S1). Hatched areas enclosed by blue lines indicate regions which are not statistically significant for the EMAC results. The dash-dotted line indicates the mean tropopause pressure of each model. Similar figures for the triple NO_x and low cruise scenarios are provided in the appendix (Figures A32, and A34). ~~underlying processes in this work w/ the relationship number of layers altitude for altitude~~



515 **Figure 3: Mean changes in H₂O mixing ratio over altitude for the nominal supersonic (A1, left), triple NO_x (A2, middle) and low**
520 cruise (A3, right) emission scenarios. Entries with dashed lines are from data from Grewe et al. 2007. Comparison of the H₂O
perturbation lifetime in months and the hemispheric ratio of the H₂O increases of the nominal supersonic scenario (S1) with vertical
and horizontal model grid characteristics. The top left figure shows the relationship between the perturbation lifetime and the
hemispheric ratio, the top right the perturbation lifetime and the number of grid layers between 400 and 50 hPa, and the bottom
left shows the hemispheric ratio and the horizontal grid fidelity. The bottom right figure shows the vertical layer count against the
horizontal grid fidelity. Markers denote the different models. Results from Grewe et al. (2007) are included for their equivalent
scenario (S5, Grewe et al. (2007)). The other emission scenarios are included in Figure A5.

525 Figure 3 also shows that we find a trend between the hemispheric ratio and the horizontal grid fidelity. Strahan and Polansky
(2006) found that the use of coarse horizontal grids led to overestimations of interhemispheric mixing in modelled atmospheres,
and likewise we find smaller hemispheric ratios, suggesting that less water vapour emissions are transported to the southern
hemisphere in the models with coarser horizontal grids. However, given the inverse relationship between the vertical and
horizontal grid fidelities, we expect that this is primarily affected by the perturbation lifetime. The vast majority of water
530 vapour emissions is in the northern hemisphere, therefore shorter perturbation lifetimes affect transport of the water vapour
perturbation to the southern hemisphere, increasing the hemispheric ratio. We also see these trends in the responses to the other
emissions scenarios (Figure A5), indicating that differences in model grids may be a significant contributor to differences in
the lifetime and transport of high-altitude water vapour emissions.

535 As previously mentioned, we find larger hemispheric fractions in our results compared to those of Grewe et al. (2007),
indicating a reduced interhemispheric exchange in our models. Their hemispheric fractions range from 1.8 to 4.2 with a mean
of 2.96, whereas ours range between 3.96 to 5.37 with a model mean of 4.68. We expect that this difference is driven by an
improved representation of the tropical pipe acting as a transport barrier through a finer horizontal resolution in our models.
Previous work has shown that the horizontal resolution is important in the representation of horizontal mixing and diffusion,
and that coarse resolutions can lead to over-estimations of horizontal mixing (Strahan and Polansky, 2006). Consequently, we
note a trend between the horizontal model resolution and the hemispheric fraction, leading to reduced interhemispheric
540 exchange with finer horizontal resolutions (Fig. A4).

545 Between the models we find notable discrepancies in the stratospheric H₂O perturbation lifetime. Here we will first discuss
the difference between the EMAC, GEOS-Chem, and LMDZ-INCA models which model H₂O over the full tropo and
stratosphere. This is not the case for MOZART-3, which is discussed separately afterwards. Between the EMAC, GEOS-
Chem, and LMDZ-INCA models we hypothesize that the discrepancy in H₂O perturbation lifetimes may be driven by
differences in the model treatment of tropospheric H₂O and the models' vertical resolutions. In the GEOS-Chem and LMDZ-

INCA models tropospheric H₂O is fixed to the model meteorology. In this case the model troposphere acts as a sink for stratospheric H₂O tracers as the perturbation is removed when transported into the upper troposphere. As the tropopause height in high latitudes is adjusted seasonally, parts of the model grid switch from stratospheric to tropospheric, stripping the stratospheric H₂O near the boundary. This may lead to excessive removal of lower stratospheric H₂O, particularly at high latitudes, which is also enhanced by lower vertical resolution around the UTLS interface. This stripping effect has been observed to reduce H₂O perturbation lifetimes in the GEOS Chem model (van 't Hoff et al., 2024a) and we expect it may play a role here as well. In addition, similar to the effect of horizontal resolutions on horizontal transport modelling, the vertical resolution is also critical to the modelling of vertical transport and diffusion processes (Revell et al. 2015, Roeckner et al. 2006). Revell et al. (2015) have shown that the 90 layer EMAC model has reduced tropical upwards mass flux compared to the 47 layer model, and Brinkop et al. (in preparation, personal correspondence) also report that 90 layer EMAC simulations more accurately recreate stratosphere troposphere exchange patterns than the 47 layer counterpart.

This is reflected by the identification of a clear trend between the vertical model resolution and the H₂O perturbation lifetime between the EMAC, GEOS Chem, and LMDZ INCA results. The LMDZ INCA model, which has the coarsest vertical resolution at 39 levels, also has the lowest H₂O perturbation lifetimes. EMAC with 90 layers has the highest perturbation lifetimes, and GEOS Chem's resolution and lifetime fit well to a linear trend in between (Fig. A5). We also note that the shorter perturbation lifetime in LMDZ INCA may be enhanced by overestimations of cross tropopause transport at high latitudes (Cohen et al. 2023). The effect of the H₂O sink and vertical resolution is greatly enhanced for emissions in close proximity to the tropopause, and it reduces for high altitude emissions. This explains why we find larger discrepancies for the low cruise (A3) emissions scenario, respectively for these offline models. In this case we find a mean lifetime of 5.3 months, ranging from 1.3 months for LMDZ INCA to 11.2 months for EMAC. Compared to the nominal supersonic scenario (A1) the perturbation lifetime is reduced by 37% for EMAC, for the GEOS-Chem and LMDZ INCA models the respective lifetimes and decreases are 3.4 (73%) and 1.3 (75%) months. We also link this relationship to results from Pletzer et al. (2022) who used similar setups in the EMAC and LMDZ INCA models in tandem to study the impact of even higher altitude (26 to 35 km) emissions. In their results they also find LMDZ INCA has lower H₂O perturbation lifetimes compared to EMAC, with a relative difference of 8.6% at for 35 km emissions to 20.3% at 26 km cruise altitudes (Pletzer et al. 2022). Between these models we find a relative difference of 70.8% and 88.4% at mean cruise altitudes 18 and 14.9 km respectively, fitting the expected increase in stratospheric H₂O perturbation loss with lower emission altitudes.

In this consideration we have not included the MOZART 3 model, which has considerably higher perturbation lifetimes, as it is subject to some fundamental differences from the other models. Contrary to the other models which have H₂O as internal tracers, MOZART 3's perturbation is calculated through a separate model run with a different vertical grid. Like the GEOS-Chem and LMDZ INCA models this also uses fixed tropospheric H₂O mixing ratios, but the vertical grid does not extend past 200 hPa. Because of this limit it does not capture interactions of stratospheric H₂O with the tropopause outside of lower latitudes where there is predominantly upwards vertical transport, and as a result it may be missing crucial sinks of stratospheric H₂O at high latitudes. Furthermore, the separation of H₂O tracers from the CTM may mean that H₂O sinks from chemistry are not fully incorporated, or they could be weaker than in integrated models. Combined this results in the high H₂O perturbation lifetime in MOZART 3, which does not fit the other models.

34.3 Odd and reactive nitrogen Nitrogen oxides and reactive nitrogen

Figure 4 shows the perturbation of reactive nitrogen nitrogen oxides (NO_x) and odd reactive nitrogen (NO_y = NO + NO₂ + NO₃ + HNO₂ + HNO₃ + HNO₄ + ClNO₃ + 2 N₂O₅ + PAN + ClNO₂ + BrNO₃) from the nominal supersonic emissions scenario (SA1) over the four models. Similar figures for the triple NO_x and low cruise scenarios are provided in the appendix (Figures A6 and A7). We define NO_y as NO_y = NO + NO₂ + NO₃ + HNO₂ + HNO₃ + HNO₄ + ClNO₃ + 2 N₂O₅ + PAN + ClNO₂ +

590 ~~BrNO₃. In these perturbations we~~ We observe ~~find~~ similarities ~~perturbations~~ across all ~~offline models~~ models. The NO_x responses are primarily concentrated around the equator, with the strongest accumulation in the middle-stratosphere and a secondary zone near the northern equatorial tropopause. In contrast to the NO_x perturbation, the accumulation of NO_y is concentrated around the ~~region of cruise emissions~~ ~~area~~ ~~region in all models~~. The ~~NO_y is~~ perturbation, which includes that of NO_x, is mostly driven by ~~increased~~ ~~strong~~ formation of nitric acid (HNO₃) in these areas. NO_y is then transported to the north pole or southwards to the tropical pipes (a region of upwelling over the tropics), where it makes its way to the middle stratosphere. This results in similar accumulation patterns for NO_y as ~~is observed~~ ~~we find~~ for the H₂O water vapour emissions. ~~Similar NO_y perturbations from supersonic aviation have been observed by Zhang et al. (2023,2021a) and by Kinnison et al. (2020) with the WACCM model.~~

600 Contrary to the offline models, EMAC predicts that the SST adoption leads to loss of NO_x and NO_y in the upper stratosphere and southern hemisphere for all supersonic scenarios (Figures 4, A6, A7). We expect that these differences are predominantly driven by EMAC's use of online meteorology, which causes deviation of meteorological parameters between the baseline and the perturbed model run due to a combined result of the butterfly effect (noise) and meteorological feedbacks from the changes in stratospheric composition (Deckert et al. 2011). ~~Figure 5 shows the differences in the EMAC temperature fields.~~ It shows ~~that EMAC's~~ ~~a stratospheric~~ ~~ice cooling~~ ~~ing~~ in response to the three ~~supersonic~~ scenarios. The stratospheric cooling has several effects on EMAC's chemistry, some of which are reflected in the NO_x response. Near the south pole we see indications that the cooling facilitates increased formation of PSCs. We find regional depletion of gas phase NO_y reservoirs associated with PSC chemistry (ClONO₂, HNO₃, HNO₄) and increases in liquid phase HNO₃ particles and solid phase particles like nitric acid trihydrate (NAT). These changes suggest that PSC chemistry is enhanced, increasing the sedimentation of stratospheric
605 nitrogen compounds and leading to denitrification of the southern stratosphere. This likely drives the loss of NO_x and NO_y over the south pole. Near the North pole similar responses may occur, but this is hard to discern due to the proximity of the emission sources. Above pressure altitudes of 10 hPa, where nudging is no longer applied, there is stratospheric cooling of over -0.3 K in response to the nominal SST emissions. The cooling may contribute to the loss of NO_x and NO_y, as it slows down the N to NO_x reformation reactions (Rosenfield and Douglass, 1998), but it likely also has more complex effects on the
615 nitrogen chemistry cycles. Besides the change in temperature, there are also changes in EMAC's horizontal and vertical wind fields, but since these are nudged they are predominantly statistically insignificant (Figures A8 to A10). Some changes in wind fields can be seen above 10 hPa, which may alter mixing in this region. Altogether, the use of online meteorology leads to a very different response of stratospheric NO_x and NO_y compared to the offline models. Given the sensitivity of ozone to NO_x, this is also linked to differences in the ozone response which we discuss next.

620

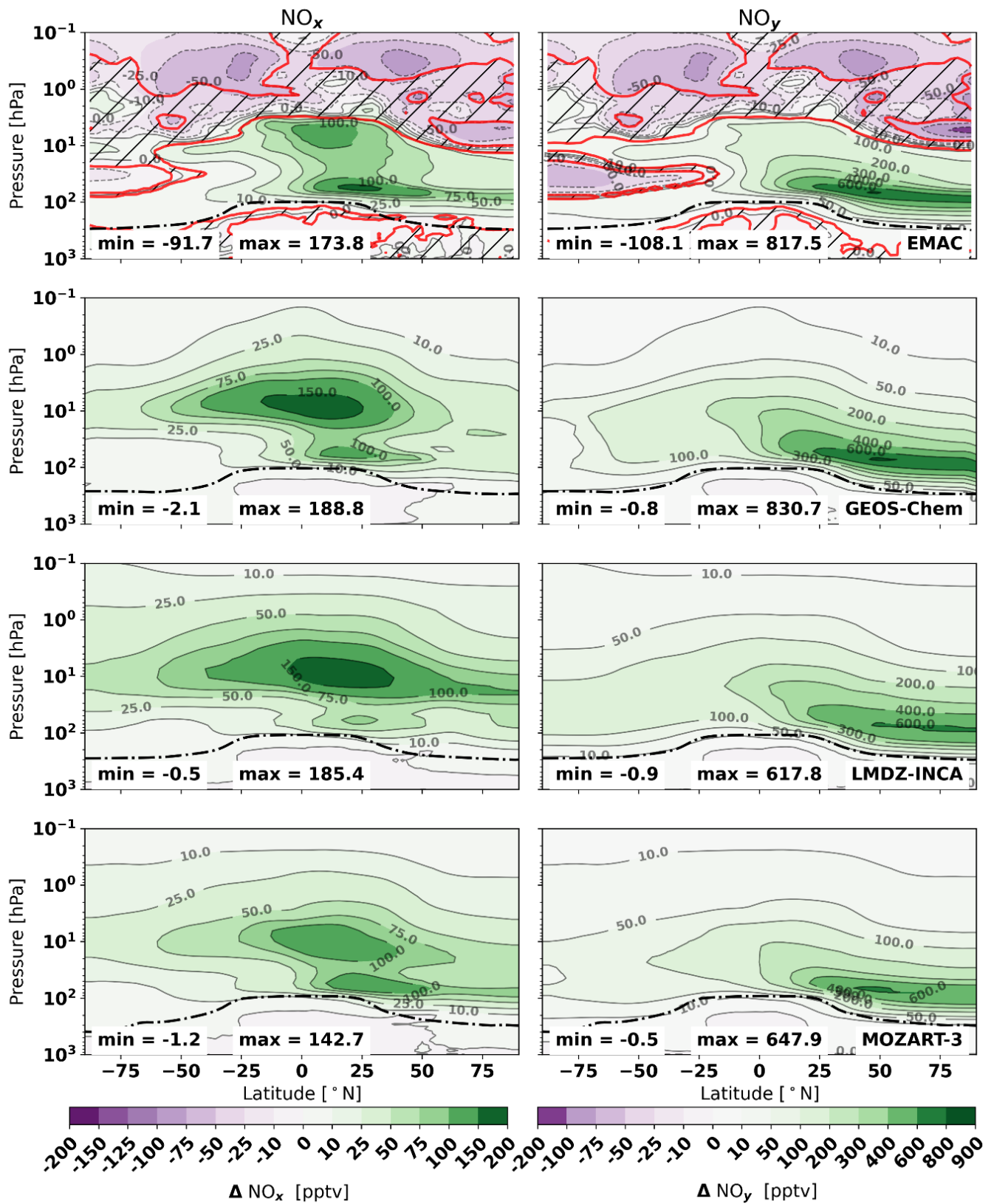
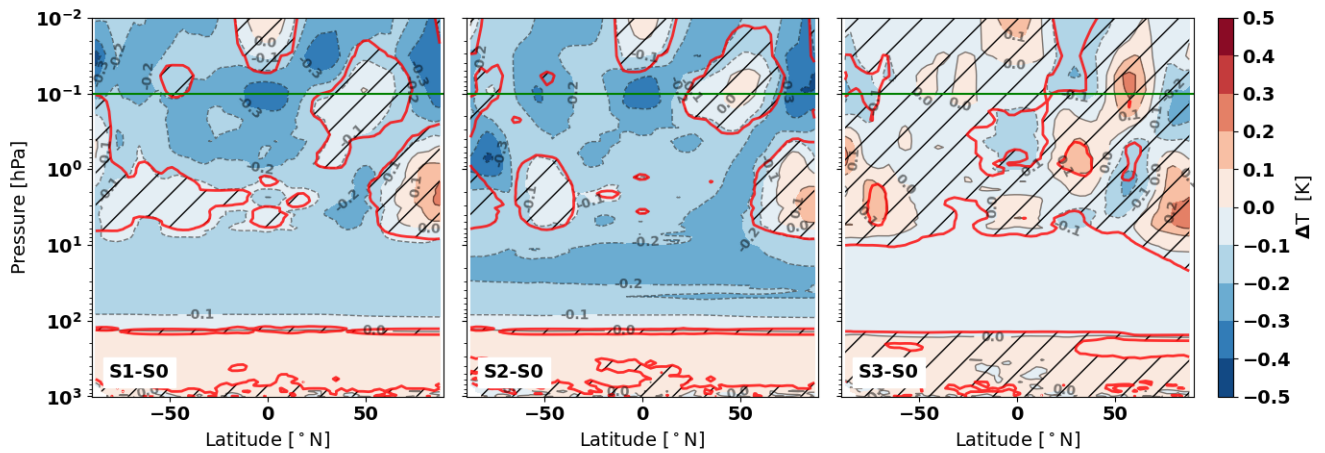


Figure 4: Zonal mean changes in NO_x (left) and NO_y (right) mixing ratios (pptv) in response to the nominal supersonic emissions (S1). Top to bottom: EMAC, GEOS-Chem, LMDZ-INCA, MOZART-3. Hatched areas enclosed by red lines indicate regions that are not statistically significant for the EMAC results. The dash-dotted line indicates the mean tropopause pressure for each of the models. Figures for triple NO_x (S2) and low cruise (S3) in the appendix (Figures A6, A7).

The NO_x and NO_y perturbations are similar across all models except for EMAC, where we find substantial differences in the upper stratosphere and southern hemisphere. Contrary to the other models EMAC predicts a loss of NO_x and NO_y in these areas, and the same can be observed for the triple NO_x and low cruise scenarios (Fig A6, A7). The differences are particularly striking above a pressure altitude of 10 hPa, where EMAC's meteorology is not nudged. This leads to a deviation of

635 meteorological parameters between the base run and the perturbed run, due to a combined result of the butterfly effect (noise) and meteorological feedbacks from the changes in stratospheric composition (Deckert et al. 2011). Because of this, parts of EMAC's upper atmospheric response are not statistically significant with the current model integration time. Still, we do find areas NO_x and NO_y depletion which are significant in the upper stratosphere, suggesting that we do also see the effect of feedback mechanisms,

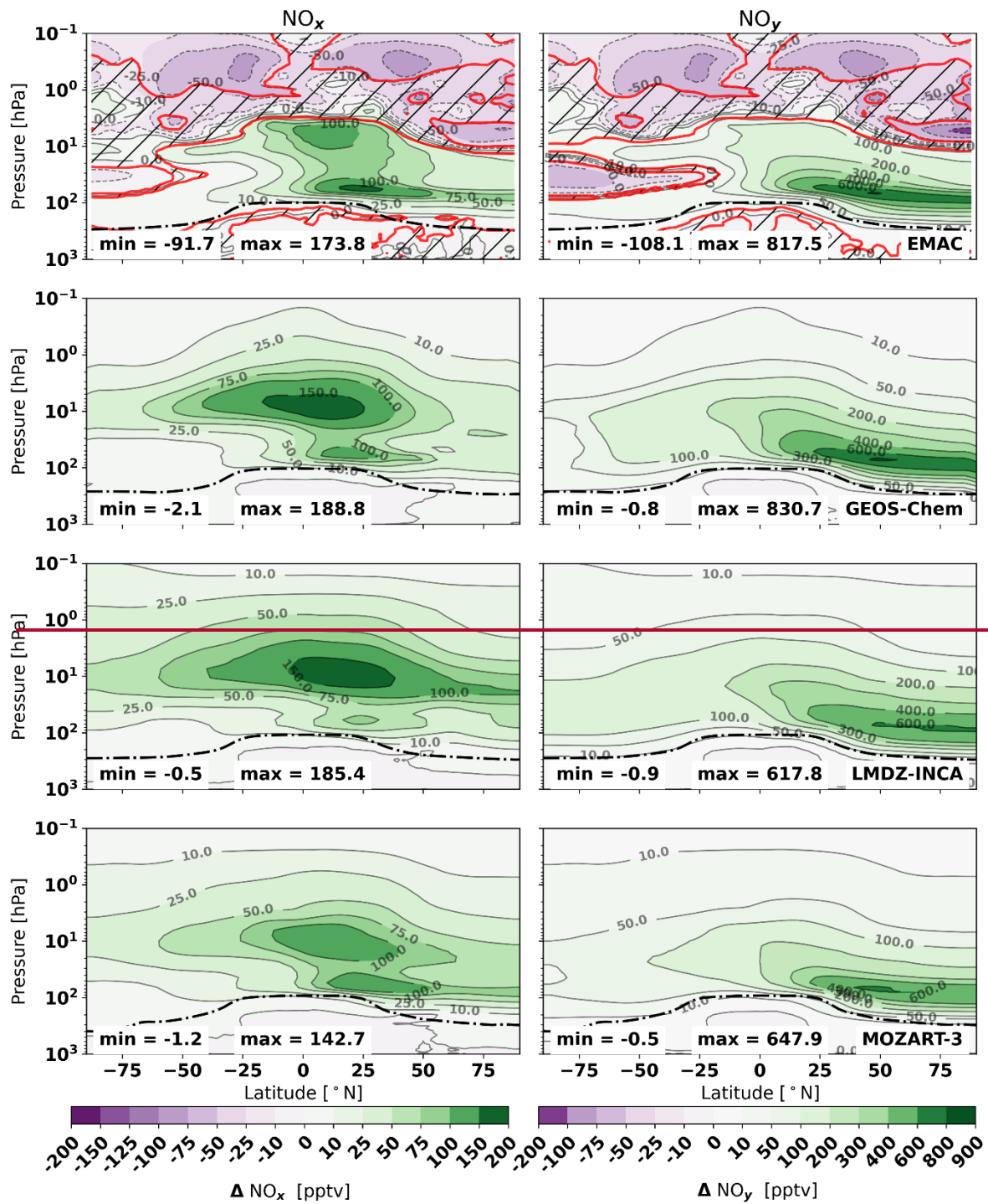
Comparing the model temperatures we find that the introduction of the supersonic emissions leads to overall cooling of EMAC's stratosphere (Fig A8).



640 **Figure 5: Zonal mean changes in temperature (in Kelvin) in the EMAC model, in response to the nominal (left), triple NO_x (middle), and low cruise (S3) scenarios. Hatched areas enclosed by red lines indicate regions that are not statistically significant. The green horizontal line at 0.1 hPa indicates the upper pressure shown in other figures.**

645 Near the south pole between 100 and 10 hPa this cooling is approximately 0.15 K, facilitating increased formation of polar stratospheric clouds (PSCs). This is observed in our result through regional depletion of gas phase NO_y reservoirs associated with PSC chemistry (ClONO₂, HNO₃, HNO₄) and increases in liquid phase HNO₃ particles and solid phase particles like nitric acid trihydrate (NAT). These changes suggest that PSC chemistry is enhanced, increasing the sedimentation of stratospheric nitrogen compounds and resulting in denitrification of the southern stratosphere. This likely leads to the NO_x and NO_y loss over the south pole. Near the North pole similar responses may occur, but this is hard to discern due to the proximity of the emission sources. Above pressure altitudes of 10 hPa we find areas of stratospheric cooling of up to 0.3 K. This may be contribute to the loss of NO_x and NO_y as it slows down the N to NO_x reformation reactions slow down (Rosenfield and Douglass, 1998). This is unlikely to be the sole driver however, as these NO_x and NO_y responses may be the result of complex interactions between the nitrogen chemistry cycles with the changes in stratospheric temperatures and

650



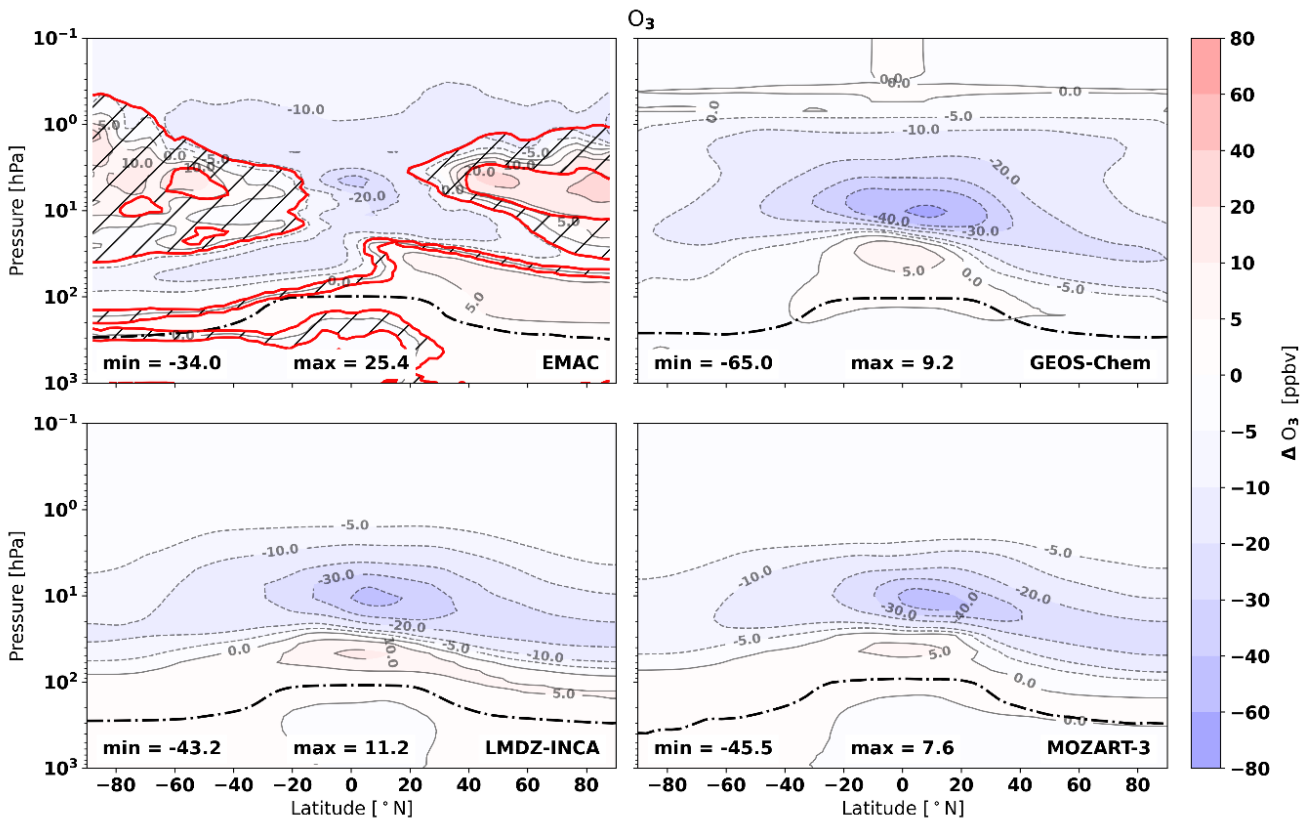
655 **Fig 4: Mean changes in NO_x (left) and NO_y (right) mixing ratios (pptv) in response to the nominal supersonic emissions (A1). Top to bottom: EMAC, GEOS Chem, LMDZ-INCA, MOZART-3. Hatched areas enclosed by red lines indicate regions which are not statistically significant for the EMAC results. Figures for triple NO_x (A2) and low-cruise (A3) in the appendix.**

660 This is unlikely to be the sole driver however, as these NO_x and NO_y responses may be the result of complex interactions between the nitrogen chemistry cycles with the changes in stratospheric temperatures and vertical mixing. Both this upper stratospheric behaviour and the denitrification of the southern hemisphere are not captured by the other models with offline meteorology. Given the importance of NO_x to the O_3 perturbation, the capture of these responses may also affect the O_3 response to emissions. This will be discussed in the next section.

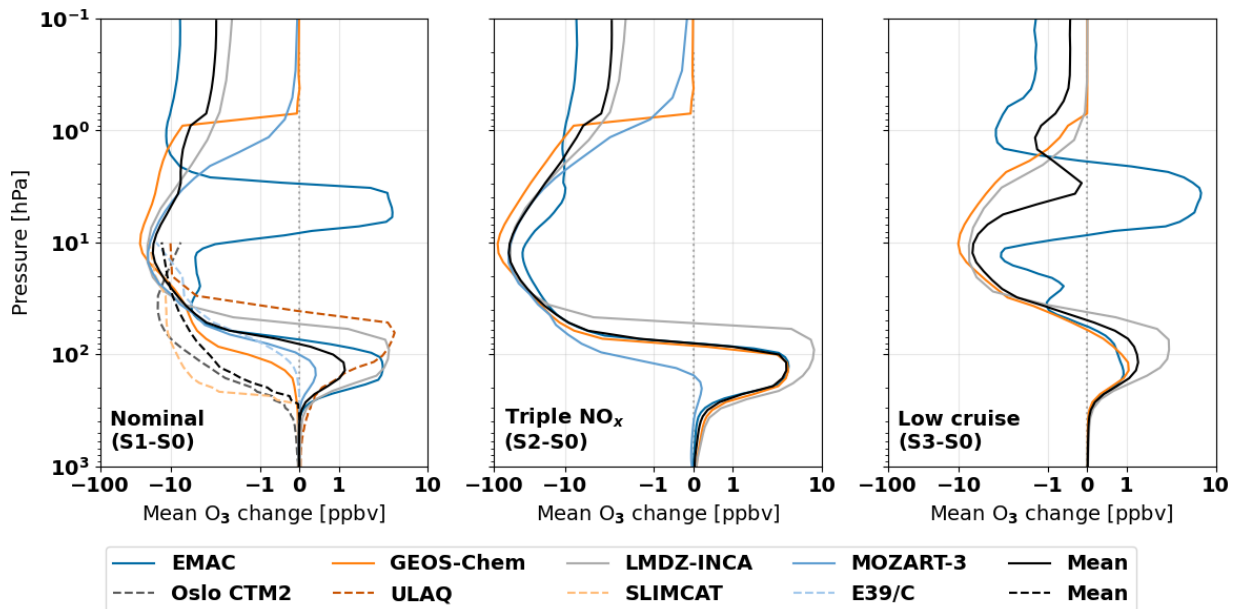
34.4 Ozone

We find similar changes in the stratospheric ozone composition between the models, with ozone loss in the upper stratosphere and areas of increases in the lower-stratosphere (Fig. 5). The changes in stratospheric H_2O and NO_x affect the ozone

665 concentrations through the HO_x-O_x and NO_x-O_x cycles. The emission of SO₂ forms sulfuric acid which facilitates heterogeneous chemistry, increasing the availability of chlorine and bromine radicals resulting in further ozone depletion. Across all models and scenarios we find increases in lower-stratospheric ozone mixing ratios paired with ozone depletion in the upper-stratosphere (Figure 6). Similar patterns are found for the other supersonic scenarios (Figures 7, A11, A12). Combined these effects This pattern has been reported in several other studies, where the ozone lead to depletion of ozone in the upper stratosphere paired with increases in the lower-stratosphere from are attributed to NO_x-driven ozone formation through smog processes or and the ozone layer's self-healing effect (Zhang et al. 2023₃; Eastham et al. 2022₂; Fritz et al. 2023₇; Zhang et al. 2021b). This increase is strongest in the LMDZ-INCA model where the ozone increase spans both hemispheres. In GEOS-Chem and MOZART-3 this increase is limited to the equatorial lower-stratosphere underneath the main lobe of ozone depletion, and in EMAC it only occurs in the northern hemisphere. This increase is strongest in the LMDZ-INCA model, where the ozone increase spans both hemispheres. In GEOS-Chem and MOZART-3 this increase is limited to the equatorial lower-stratosphere underneath the main lobe of ozone depletion, and this may be driven by the self-healing effect.



680 **Figure 6:** Mean changes in O₃-ozone volume mixing ratios [ppbv] in response to the nominal supersonic (SA1) emissions. Hatched areas enclosed by red lines indicate regions which that are not statistically significant for the EMAC results. The dash-dotted line indicates the mean tropopause pressure for each of the models. Similar figures for the triple NO_x and low cruise scenarios are provided in the appendix (Figures, A911 and, A102).



685 **Figure 67:** Mean changes in O_3 ozone volume mixing ratio [ppbv] over altitude for the nominal supersonic (SA1, left), triple NO_x (SA2, middle) and low cruise (AS3, right) emission scenarios. Dashed lines show results from models used by Grewe et al. (2007).

690 The similarity in ozone responses, particularly between the models with offline meteorology, also extends to the low-altitude and triple NO_x perturbation scenarios (Fig 6.). Across all models and scenarios we find increases in lower-stratospheric ozone mixing ratios. Such increases were previously only captured by one of the models used by Grewe et al. (2007), but now they have been observed across multiple recent studies using the GEOS-Chem and WACCM-CTMs (Eastham et al. 2022, Zhang et al. 2023; 2021a; 2021b, Kinnison et al. 2020). We expect that this shift in lower-stratospheric responses may be related to overall improvements in the representation of Non-Methane Hydrocarbon (NMHC) chemistry (Houweling et al. 1998). We also observe a shift in the NO_y species towards more formation of HNO_3 around the emission areas, reducing the availability of HO_x and NO_x . This may further suppress lower stratospheric ozone depletion. When the supersonic NO_x emissions are 695 tripled, the changes in O_3 are enhanced, the effect on ozone is enhanced, particularly over the tropics around in the middle-stratosphere a pressure altitude of 100 hPa (Figure A9A11). In the low cruise emissions scenario both the magnitude of ozone increases and losses are reduced considerably (Fig. A10).

700 Similar to the NO_x and NO_y responses, the O_3 perturbation is different in EMAC than in the other models (Figs. 5, 6). This is likely driven by the inclusion of composition-meteorology feedbacks and online meteorology. The most notable difference is the presence of two lobes of ozone increases at high latitudes above 10 hPa, both of which are partially statistically significant. We hypothesize that their formation is driven by stratospheric cooling and enhancements of PSC chemistry. In the southern hemisphere the latter causes shifts in the abundance of nitrogen and chlorine ($ClONO_2$) reservoir species, which correlate with areas of ozone decreases and increases. In the northern lower stratosphere ozone increase correlates with HNO_3 705 increase. The patterns that should be associated with PSC chemistry tend to vanish for the triple NO_x emission scenario (Fig A9), which points toward the limited magnitude of PSC processes. The regions of ozone increases around 10 hPa can also be observed in other studies using the EMAC model with online meteorology (Pletzer et al. 2022, Kirner et al. 2014). Kirner et al. (2014) explain the dynamical changes in ozone as a combination of changes in vertical stratospheric transportation and slowdowns of the Chapman mechanism in response to stratospheric cooling. It is likely that these mechanisms also drive part 710 of the dynamical response in the EMAC model, as the increased reduction in the Chapman mechanism can also be observed in the Odd O_x loss rates, which will be evaluated in the next section. Furthermore Kinnison et al. (2020) also demonstrated

~~that the inclusion of interactive dynamics leads to increases in upper stratospheric ozone formation from supersonic emissions, although their results do not share the characteristics unique to the EMAC model.~~

715 We ~~note~~ find that there is a nonlinear relationship between the ~~supersonic-SST~~ NO_x emissions and the global O₃-ozone losses across all models. In GEOS-Chem and LMDZ-INCA the tripling of NO_x emissions increases ~~ozone column~~ stratospheric ozone budget losses (Table A3) by factors of 2.394 and 2.656 respectively, whereas these factors are 3.89 and 7.244 for MOZART-3 and EMAC, respectively. ~~The high sensitivity of the EMAC model compared to the others is related to the aforementioned differences. Under the triple NO_x emissions EMAC's middle stratospheric ozone response becomes more similar to that of the~~
720 ~~other models, leading to more uniform O₃ losses and a large increase in O₃ column losses relative to the nominal scenario.~~ Between the ~~fixed-offline meteorology~~ models MOZART-3 is most sensitive to NO_x emissions, which could be related to its lower background NO_x levels. ~~–In the low cruise emissions scenario both the magnitude of ozone increases and losses are reduced considerably (Figure A10A12). This may be related to the lower availability of background NO_x in its stratosphere (Table A2), which has been observed when it is used with the ECMWF reanalysis meteorology (Kinnison et al. 2007).~~

725 Similar to the NO_x and NO_y responses, EMAC's ozone response differs from the offline models (Figs. 65, 67), which is likely coupled to feedbacks with its online meteorology. The most notable difference is the presence of ozone increases at high northern and southern latitudes above 10 hPa, both being partially statistically significant. We hypothesize that their formation is driven by the previously discussed stratospheric cooling and enhancements of PSC chemistry. In the southern hemisphere,
730 the meteorological feedbacks cause shifts in the abundance of nitrogen and chlorine (ClONO₂) reservoir species, which correlate with areas of ozone changes. In the northern lower stratosphere, the ozone increase correlates with an increase in HNO₃ formation. The patterns that should be associated with PSC chemistry tend to vanish for the triple NO_x emission scenario (Figure A121), which may point towards their limited magnitude. –The regions of ozone increases could also be related to slowdowns of the Chapman mechanism due to cooling and perturbations in local transport (Kirner et al., 2014). The former is
735 also seen in the odd O_x loss rates, which are evaluated in the next section.

~~Even though the zonal and vertical averages of the ozone changes are similar across the models, we note that the effects on net column ozone differ between the models over latitude.~~ Differences between the model responses become more evident when the changes in ozone columns are compared. Figure 78 shows the mean ozone column change over latitude for the emission scenarios alongside the multi-model mean profile. Across all emission scenarios
740 It shows that the spread –the disagreement between the models is biggest in the northern hemisphere for all emission scenarios, with the spread between models increasing particularly near towards the north pole. Expanding this into seasonal ozone column changes (Figure 89), we find shows that the mean ozone column impacts over the year differs between all models. These differences are particularly notable in polar areas all models show different seasonal behaviour as well. – In EMAC we observe clear increases in northern hemispheric ozone which are strongest in the local winter season, with slight enhancements of southern polar ozone loss from July to November. For example, GEOS-Chem shows enhancement of seasonal ozone column loss during both the arctic Arctic and Antarctic ozone hole formation. These both of which enhancements are also slightly present present in LMDZ-INCA, albeit at a smaller scale. In contrast, MOZART-3 does not show them, and is it instead calculates estimating the highest Arctic ozone depletion from June to November in the northern hemisphere. EMAC shows year-round increases in the ozone column
745 in the northern hemisphere. – We expect that such differences are These differences may be indicative results of differences in the modelling of processes important to ozone, such as the –PSC processes and feedbacks from emissions on heterogeneous chemistry. Only GEOS-Chem and LMDZ-INCA capture the effect of the emissions on PSC formation and the available surface area for heterogeneous chemistry, which may explain why only these models find enhancement of the seasonal ozone holes. but they
750 The differences may may also further be driven affected by differences in the availability of stratospheric

755 halogens (Table A4). For example, the enhancement of the ozone hole formation is most visible in GEOS-Chem is stronger in
 GEOS-Chem, which also has the highest background halogen availability higher stratospheric halogen availability. We note
 the seasonal O₃ column changes of our models also differ from evaluations of a similar emissions scenario using the WACCM6
 model by Zhang et al. (2023), who instead find increases in southern hemispheric ozone from September to March with
 enhanced southern polar losses in between.

760

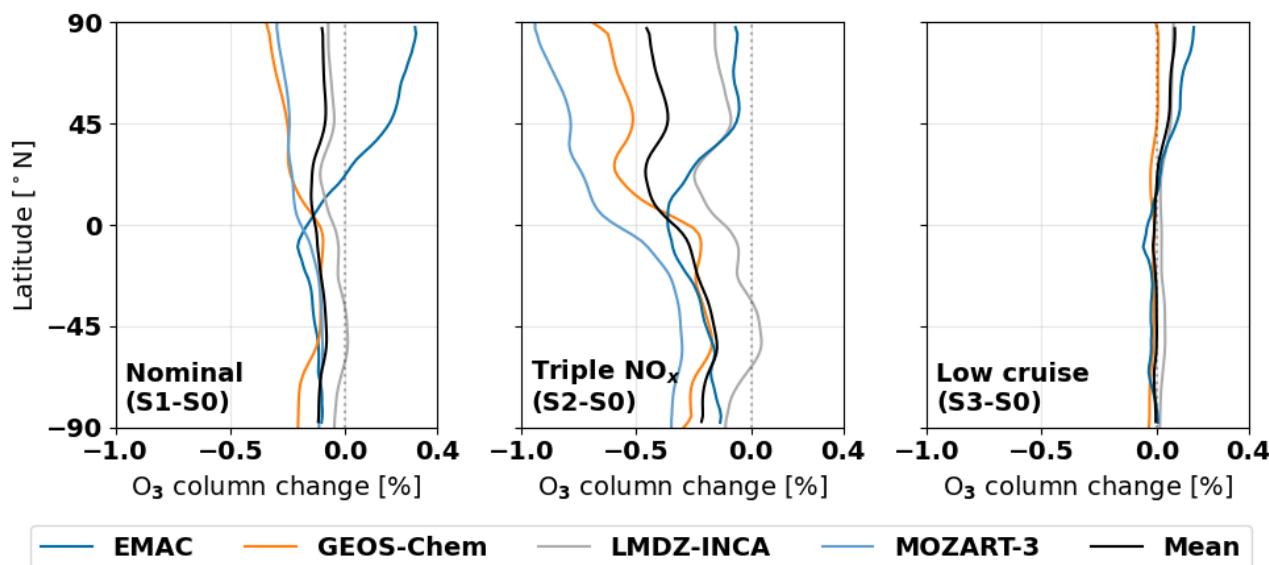
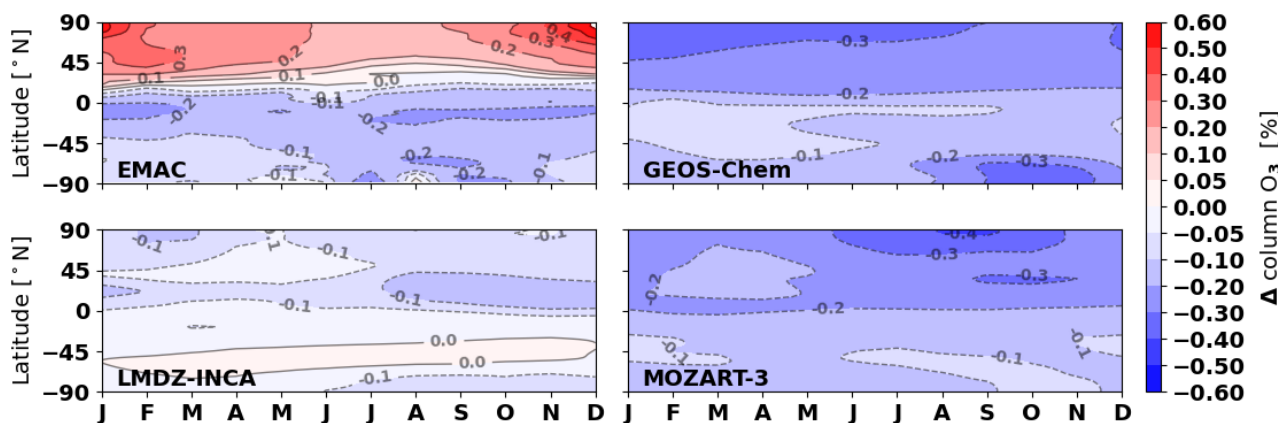


Figure 78: Zonal mean annually averaged changes in O₃ ozone columns (percentage) for nominal supersonic (S1-S0, left), triple NO_x (S2-S0, middle), and low cruise (S3-S0, right) emission scenarios.



765 Figure 89: Mean monthly changes in percentage of the ozone columns in response to the nominal supersonic emissions scenario (AS1 - AS0). Similar figures for the other emission scenarios are provided in the appendix (Figures A13 & A14)

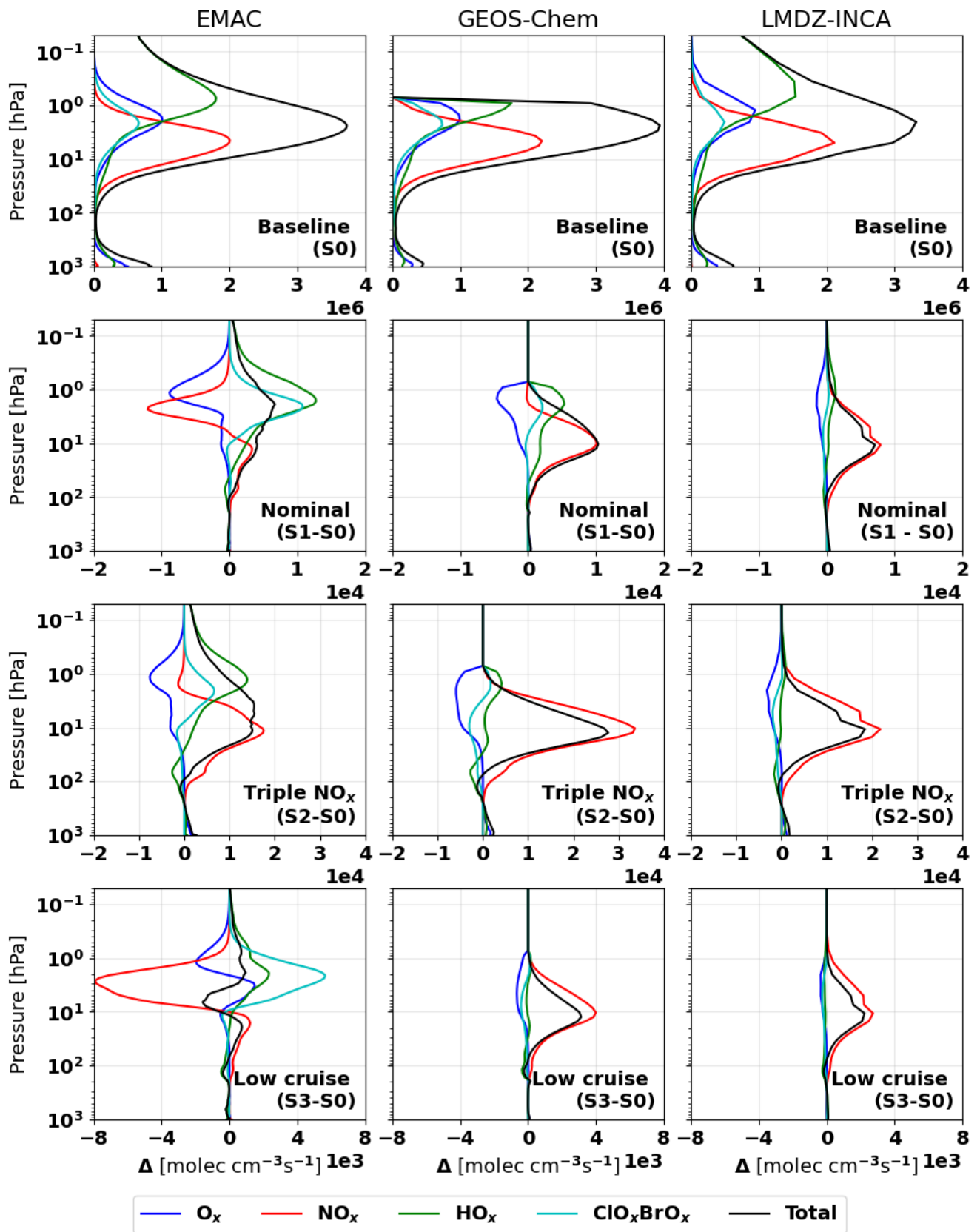
34.5 Odd oxygen loss

To better understand the source of the differences in the ozone responses we evaluate the changes in odd oxygen (O_x) reaction rates for EMAC, GEOS-Chem, and LMDZ-INCA. We use the same reaction grouping as Zhang et al. (2023; 2021a). Across
 770 all models the supersonic emissions These models all find that the supersonic scenarios lead to net-increases in O_x loss. When averaged over altitude, the responses are similar across the models (Fig. 9), we find similar baseline O_x loss rates across all models (Figure 10), and the responses of the GEOS-Chem and LMDZ-INCA models appear to share similar profiles whereas that of EMAC is very different. When the O_x loss responses are seen as zonal averages (Figure 11), further but the zonal average of the O_x reaction changes also reveals notable differences in the spatial distribution of these O_x loss responses processes
 775 between the model atmospheres (Fig. 10 become evident).

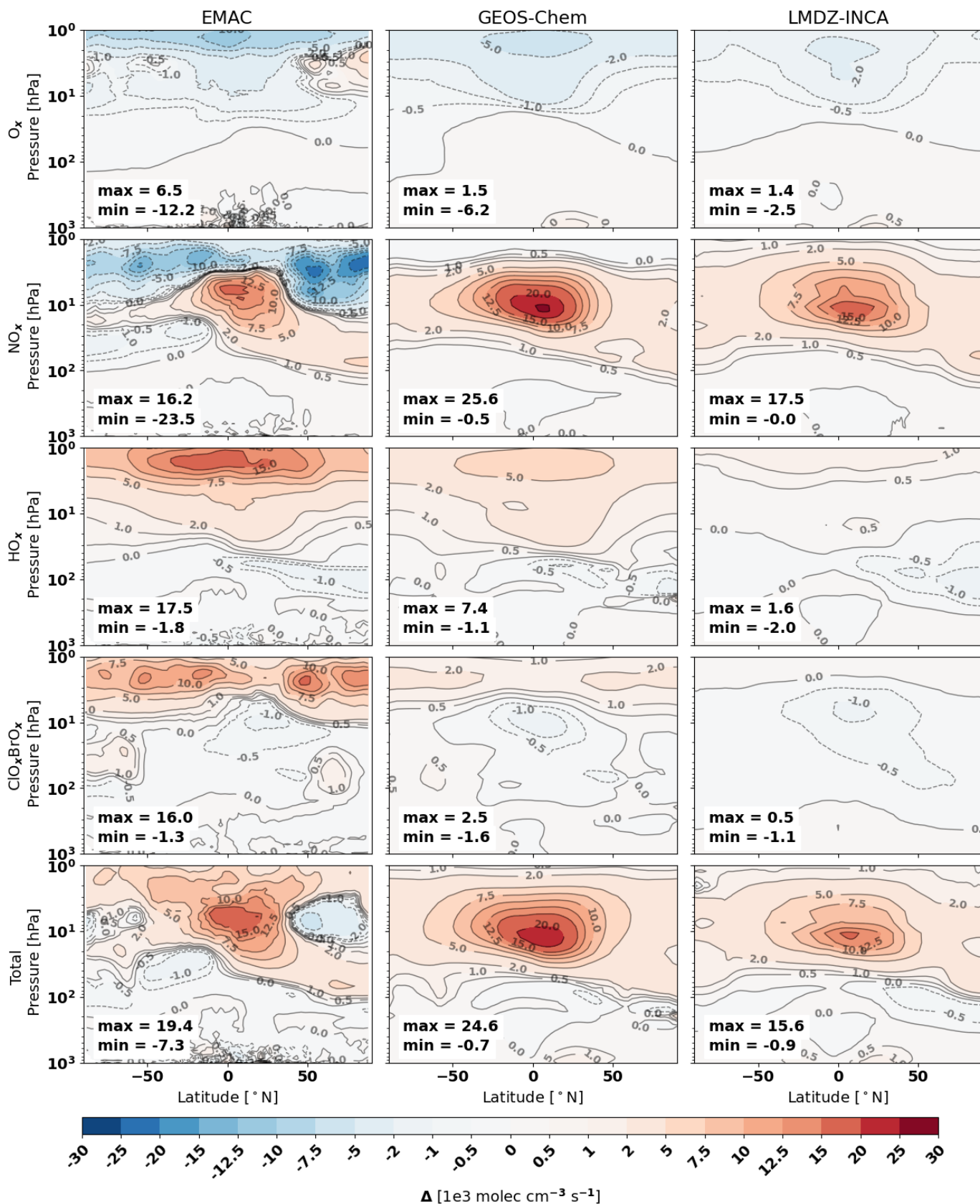
In the GEOS-Chem and LMDZ-INCA models the increases in O_x losses are primarily driven by increases in NO_x -driven losses at from 200 to 20 hPa and HO_x -driven losses from 20 hPa to 0.1 hPa (1 hPa for GEOS-Chem). These increases are paired with decreases in O_x - O_x losses, as the availability of O_x reduces from the other loss channels. Across all models we also find an increase in ClO_x / BrO_x -driven losses above 10 hPa. In the EMAC model the change in NO_x -driven losses is more complex. The zonal average (Fig. 10) shows that this response is more complex due to the presence of areas with reductions in NO_x -driven losses, coinciding with areas of NO_x decreases in the upper stratosphere and southern hemisphere (Fig. 4). In case of HO_x -driven losses we observe similar decreases around the emission areas in all models, with varying degrees of increases in the upper stratosphere coinciding, the magnitude of which coincides with the H_2O perturbation lifetimes across the models. For the triple NO_x scenario (A2) we find increased NO_x -driven O_x losses across all models. The enhancement of NO_x -driven O_x loss slightly reduces HO_x and ClO_x / BrO_x -driven O_x losses. For the lower cruise altitude scenario (A3) we find similar changes in O_x loss rates as the nominal supersonic scenario but at smaller magnitudes. In the case of the GEOS-Chem and LMDZ-INCA models the reduction in cruise altitude also sharply reduces upper-stratospheric HO_x -driven odd O_x losses, resulting from the previously discussed reduction in H_2O perturbation lifetimes.

The changes in ClO_x / BrO_x -driven losses differ across all of the models, with increases in loss rates being considerably smaller in the LMDZ-INCA model. This difference is likely driven by the differences in halogen availability. Table A4 (SI) shows mean background mixing ratios for key halogens at the surface and from 200 to 10 hPa for the models. Compared to LMDZ-INCA the GEOS-Chem atmosphere has higher availability of all halogens, which may explain its higher ClO_x / BrO_x response near the poles. Comparison of surface and stratospheric CFC11 levels suggest that this may be driven by enhanced CFC destruction in GEOS-Chem.

As previously discussed, we see unique characteristics in EMAC's zonal average O_x -loss perturbations due to the inclusion of meteorological feedback. Contrary to the previously shown changes in O_3 - and NO_x -mixing ratios, the changes in odd O_x -loss reactions are statistically significant. The enhancement of PSC chemistry leads to increased southern hemispheric ClO_x / BrO_x losses while subsequent denitrification reduces NO_x -driven losses in this area. The cooling of the stratosphere also slows the Chapman mechanism, leading to reductions in upper-stratospheric O_x - O_x losses with the exceptions of the areas where there is a net increase of ozone. Combined the inclusion of this feedback leads to differences in the NO_x , NO_y , and O_3 perturbations throughout the stratosphere compared to the models which do not account for it. The incorporation of this feedback may be crucial to adequately assess the impact of high altitude emissions on the stratospheric composition, especially if the composition of the ozone layer is to be considered. In the consideration of increasing future emissions at high altitudes, whether it be from aviation or spaceflight, the incorporation of meteorological feedbacks may be an important direction for the future development chemistry transport models.



810 **Figure 910:** Mean background O_x loss rates (top) and O_x loss rate perturbations from emission scenarios over pressure altitude for EMAC (left), GEOS-Chem (middle) and LMDZ-INCA (right). From top to bottom: background loss rates, loss rate perturbation from nominal supersonic emissions (A1), loss rate perturbation from triple NO_x emissions (A2), loss rate perturbation from low cruise emissions (A3).



815 **Figure 10**: Zonal average mean changes in O_x loss reactions in response to the nominal supersonic emissions for EMAC (left), GEOS-Chem (middle) and LMDZ-INCA (Right). Loss perturbations are split into O_x-driven loss (top), NO_x-driven loss (second row), HO_x-driven loss (third), ClO_x/BrO_x driven loss (fourth) and total changes in O_x loss (bottom). Values in molec cm⁻³ s⁻¹. Similar figures for the triple NO_x (SA2) and low cruise (SA3) scenarios are provided in the [SI Appendix \(Figures A15 & A16\)](#).

820 The O_x loss reaction responses of the GEOS-Chem and LMDZ-INCA models are similar. In these models, the largest response to the nominal scenario is an increase in NO_x -driven O_x losses from 200 to 20 hPa. HO_x -driven losses also increase, but mostly at higher altitudes from 20 hPa to 0.1 hPa. These increases are paired with decreases in O_x - O_x losses, as the availability of O_x reduces. The models also calculate increases in ClO_xBrO_x driven losses above 10 hPa. In response to the triple NO_x scenario, the NO_x -driven O_x losses increase by around threefold, reducing the effect on ClO_xBrO_x -driven losses. For the lower cruise altitude scenario (S3) we find similar changes in O_x loss rates as the nominal supersonic scenario but at smaller magnitudes. In the case of the GEOS-Chem and LMDZ-INCA models, the reduction in cruise altitude also sharply reduces HO_x -driven O_x losses. This is related to the shorter water vapour perturbation lifetimes at this cruise altitude.

830 Figures 10 and 11 show that the increased complexity of EMAC's response extends to odd O_x loss rates. Contrary to the previously shown changes in ozone and NO_x mixing ratios, the response in EMAC's O_x loss reactions is entirely statistically significant. Both figures show that there are areas where NO_x -driven O_x losses are reduced, coinciding with the previously discussed areas of denitrification in the upper-stratosphere and over the south pole (Figure 4). The reduction in NO_x -driven O_x losses is coupled with local increases of HO_x and ClO_xBrO_x driven losses, the latter of which is also affected by the enhancement of PSC chemistry. The cooling of the stratosphere also slows the Chapman mechanism, leading to reductions in upper-stratospheric O_x - O_x losses, with the exceptions of the areas where there is a net increase of ozone and therefore also O_x availability.

840 The perturbation of ClO_xBrO_x -driven O_x losses differs across the three models, with EMAC's ClO_xBrO_x response showing peak values up to five times larger than GEOS-Chem, whereas ClO_xBrO_x losses are mostly unaffected in LMDZ-INCA. The large response in EMAC is likely coupled to the local decreases in NO_x -driven losses in these areas, which are of similar magnitude (Figure 11). Between GEOS-Chem and LMDZ-INCA, we expect that these differences may be related to the availability and distribution of halogens. Table A4 (appendix) shows mean background mixing ratios for key halogens at the surface and from 200 to 10 hPa in the models' baseline atmospheres. While we find similar background halogen levels near the surface, GEOS-Chem has lower stratospheric CFC mixing ratios, and higher values of other halogens compared to LMDZ-INCA. This could suggest that CFC destruction is faster in GEOS-Chem, which may affect the role of ClO_xBrO_x -driven O_x losses. Another difference is the upper limit of the O_x chemistry domain, which is around 1 hPa in GEOS-Chem but extends further in the other models. Above this altitude GEOS-Chem has no O_x chemistry, yet other species related to ozone chemistry are allowed to evolve freely. This may lead to an accumulation of HO_x and halogens in the mesosphere, contributing to increased HO_x and ClO_xBrO_x driven O_x losses when they are transported downwards into the region of O_x chemistry.

850 ~~We use the same O_x loss reaction grouping as Zhang et al. (2021b) to facilitate comparison with their results. Overall, we find agreement in background loss rates across the models (Fig. 9), with LMDZ-INCA having slightly smaller overall O_x loss rates. Our background loss rates, in particular those of the GEOS-Chem model, also closely match loss rates from the WACCM4 model as reported by Zhang et al. (2021b). The most notable difference between the models occurs above 1 hPa, which marks the upper boundary of GEOS-Chem's stratospheric chemistry domain. Above this altitude GEOS-Chem has no O_x chemistry, yet other species related to ozone chemistry are allowed to evolve freely. This may lead to an accumulation of excessive HO_x , which then leads to excessive HO_x -driven O_x loss when it is transported downwards into the region of O_x chemistry. This may be what drives the stronger HO_x - O_x losses in the GEOS-Chem model, and it may contribute to the higher O_3 loss in GEOS-Chem from 5 to 1 hPa compared to the MOZART-3 and LMDZ-INCA models. Similar emission scenarios to our nominal supersonic and triple NO_x scenarios were also studied by Zhang et al. (2021b) using WACCM4. Our results agree well with their evaluations. We note a strong similarity in the changes in odd O_x losses between GEOS-Chem and WACCM4 for the nominal supersonic (A1) and triple NO_x (A2) and comparable scenarios (Case A & C, Zhang et al. 2021b). The overall~~

860

~~magnitude of changes in loss rates is lower in GEOS-Chem, but we find similar vertical profiles across all loss rate families up to 1 hPa.~~

4.6 Radiative Forcing

865 From non-CO₂ emissions we ~~we~~ estimate a net-warming effect of 13.9 mW/m² for the nominal supersonic ~~emissions~~ scenario (S1). This is predominantly driven by the accumulation of stratospheric water vapour (20.8 mW/m²) and warming from changes in the distribution of ozone (3.2 mW/m²). The calculated ozone forcing ranges from 1.3 mW/m² (GEOS-Chem) to 6.8 mW/m² (LMDZ-INCA), where EMAC and MOZART-3 find forcings of 3.0 and 2.2 mW/m² respectively. The largest spread is in the water vapour forcing, ranging from 6.2 mW/m² (LMDZ-INCA) to 32.4 mW/m² (MOZART-3). This is affected by the differences in water vapour perturbation lifetime within the models, but also by the radiative schemes used to assess RF. For example, the two radiative schemes applied to EMAC find water vapour forcings of 29.7 and 22.2 mW/m² in this scenario, a relative difference of 33%. The SOCRATES model used with MOZART-3 also finds a larger water vapour forcing relative to the water vapour perturbation and lifetime. This suggests that the differences between radiative schemes may be a more important contributor to uncertainties in radiative forcing assessments than differences in atmospheric perturbations calculated by CTMs or CCMs.

Only the GEOS-Chem and LMDZ-INCA models assess the effect of aerosols on RF, and the aerosol perturbations in these models are shown in Figures A17 and A18. These models do assess aerosol RF at different altitudes, which likely causes them to find differences forcing from BC aerosols (Eastham et al. 2022; Speth et al. 2021). ~~the values for LMDZ-INCA show~~ For the nominal scenario LMDZ-INCA calculates RF of 0.5 mW/m² from BC and -10.0 mW/m² from inorganic aerosols, and GEOS-Chem calculates -1.3 mW/m² and -9.3 mW/m² respectively. Between the models we calculate a mean aerosol forcing of -10.1 mW/m², resulting in a net forcing of 13.9 mW/m² from the nominal supersonic scenario. Considering the altitude dependency of the BC forcing, this value may change by up to ±0.5 mW/m² depending on the assessment altitude.

885 The tripling of NO_x emissions (S2) has affects the radiative effect of ~~from~~ ozone, which increases to a model-mean of 11.4 mW/m² (range 6.9 to 20.9). In this case we calculate model-mean RF from water vapour of 18.2 mW/m² (model range 6.3 to 31.1) and RF from aerosols of -0.4 mW/m² for BC and -9.7 mW/m² for inorganic aerosols. This results in a model-mean net RF of 19.4 mW/m² from non-CO₂ emissions (model range 16.7 to 28.1). The reduction of the cruise altitude and speed (S3) reduces the RF from ozone to 2.9 mW/m² (model range 2.1 to 4.6) and water vapour to -4.3 mW/m² (model range 0.7 to 8.2). RF from aerosols is also smaller, with -0.1 mW/m² from BC and -3.3 mW/m² from inorganic aerosols. This results in a model-mean net RF of 3.8 mW/m² from non-CO₂ emissions (range 0.5 to 7.1). ~~RF~~

3.6 Modelling considerations

895 ~~In the previous sections we have identified some notable differences between the models which we use in this study. Here we summarize the most important differences between the model and their effects, as they may provide fruitful directions for further development of these models and future work which aims to utilize them.~~

5 Discussion

900 ~~Across all models and assessments, we find that the partial replacement of subsonic aviation with supersonic aircraft leads to extensive changes to the atmospheric composition, particularly in the stratosphere, and global radiation budgets. RF. The extent of these effects appears to scale with fleetwide NO_x emissions and the cruise altitude, increases of which enhance ozone column~~

loss and associated radiative effects in all models. Therefore, we also find the largest effect on the ozone column and RF in response to the Mach 2 concept with higher NO_x emissions (Scenario S2). In terms of NO_x emissions, this scenario is closest to SST concepts studied in other recent works (Zhang et al. 2023, 2021a; Eastham et al. 2022; Speth et al. 2021), which is why we consider it as a basis for comparison with literature and as the most plausible outlook for future SST adoption.

The stratospheric changes we identify in response to this scenario matches patterns identified in several recent works (van 't Hoff 2024a; Zhang et al. 2023, 2021a; Eastham et al 2022; Kinnison et al. 2020). Here, we find a model-mean change in the global ozone column of -0.3% (-0.9 DU). Scaling by fuel consumption, this is similar to the -0.74% ozone column loss reported by Zhang et al (2023), who considered a larger SST fleet with around 2.1 times the fuel burn. It does not match with results from Eastham et al. (2022), who reported a larger ozone column loss (-0.77%) for a smaller SST fleet (14.9 Tg of annual SST fuel burn). This may be related to differences in background conditions and in the emission scenarios. ~~spatial~~The scenarios considered by Eastham et al. (2022) have higher SST NO_x emissions, and they consider a more prominent role of the Asian market in SST adoption than the inventories we use, displacing more SST traffic to lower latitudes (Speth et al. 2021). The ozone column is substantially more sensitive to SST emissions near the tropics (van 't Hoff 2024a; Fritz et al. 2022), which may explain why they find higher ozone loss relative to the fuel consumption. The nominal and triple NO_x scenarios we evaluate are also similar to scenarios evaluated by Zhang et al. (2021b, case A & C). In comparison to their results, we find also find similar ozone column losses (-0.1 % and -0.3%, compared to their -0.2% and -0.4%). We also find similar O_x loss rate perturbations, in particular between GEOS-Chem and the WACCM4 model they used. Several recent studies have identified that the perturbation of ozone can be the primary source of radiative forcing from SST emissions (van 't Hoff 2024a; Zhang et al. 2023; Eastham et al. 2022), but we instead find water vapour to be dominant in all scenarios, matching the results from Zhang et al. (2021b) and Grewe et al. (2007). This is not agreed upon in all models however, as in some cases LMDZ-INCA and GEOS-Chem find that the ozone perturbation is the primary forcer (Scenarios S1 to S3 for LMDZ-INCA, scenario S3 for GEOS-Chem). We expect that this difference is related to fleetwide NO_x emissions. Previous works have shown that RF from ozone perturbations scales with fleetwide NO_x emissions (van 't Hoff 2024a; Zhang et al. 2021b), and even in in the triple NO_x scenario our NO_x emissions index is lower than indices used by the works that find forcing from ozone to be dominant (van 't Hoff 2024a; Zhang et al. 2023; Eastham et al. 2022). Therefore, it is plausible that we'd also find the primary radiative effect to be from ozone if higher supersonic NO_x emissions are considered.

Since the nominal scenario that we consider is almost identical to scenario S5 from Grewe et al. (2007) we also compare to their results, although we note that there are considerable differences between our models and the ones they used. ~~We note that~~ For example, ~~and~~our models have higher resolutions (horizontal and vertical) and upper grid levels (0.1 to 0.01 hPa, compared to their 10 hPa). Compared to their results, we find lower stratospheric perturbations of water vapour (47 Tg compared to 64 Tg) and ozone (-3.1 Tg compared to -8 Tg). Considering the perturbation mass and the hemispheric ratios, we also find smaller spread in our models compared to theirs (Figure A19). In terms of radiative forcing we calculate this at the tropopause level, whereas they calculated it at the top of the atmosphere, hindering direct comparison. For the scattering inorganic aerosols, which should not be affected much by the assessment altitude, we find similar RF (-9.7 mW/m² compared to their -11.4 mW/m²). At the top of the atmosphere we find smaller RF for black carbon (0.5 mW/m² for LMDZ-INCA, 1.7 mW/m² for GEOS-Chem, compared to their 4.8 mW/m²), which could be related to differences in radiative modelling, aerosol size distributions, or the simulated transport of the black carbon.

Like earlier works, we find that the perturbation of stratospheric water vapour plays a key role in the radiative effect of SSTs. ~~Earlier works have identified that the accumulation of stratospheric H₂O plays a key role in the climate impact of~~

~~supersonic aviation~~ (Zhang et al. 2023; Eastham et al. 2022; Matthes et al. 2022; Grewe et al. 2007), but we note that RF
945 from water vapour is prone to several uncertainties. Foremost, we find that the RF depends on the radiative schemes, with
relative differences of up to 30% between the two radiative schemes which we apply to EMAC. The radiative effect from
water vapour is also directly related to the stratospheric water vapour burden, and therefore it depends on the water vapour
perturbation lifetime within the models. We find indications that this lifetime is affected by the vertical resolution and model
950 grid, linking increased grid layers between 400 and 50 hPa to higher perturbation lifetimes. Therefore, our results suggest that
both the model grid itself and the choice of radiative scheme may be important contributors to uncertainties surrounding
radiative effects of water vapour emissions. We expect that these factors may be influential in all assessments of high-altitude
water vapour emissions, and not exclusively to supersonic aircraft.

~~In our results we find indications that the accumulation of stratospheric H₂O and its distribution across hemispheres may be~~
~~related to the vertical and horizontal model resolutions, which affect the modelling of critical transport processes. The use of~~
955 ~~higher vertical resolutions may lead to higher stratospheric H₂O perturbation lifetimes and higher horizontal resolutions reduce~~
~~interhemispheric mixing. The link between vertical resolution and perturbation lifetime may be strengthened by the use of~~
~~fixed tropospheric H₂O mixing ratios in the LMDZ-INCA and GEOS-Chem models. In these cases, the troposphere acts as a~~
~~sink for stratospheric H₂O emissions, which may lead to underestimation of perturbation lifetimes for lower stratospheric~~
960 ~~emissions. Combined, this explains why we don't see the same level of improvement in model agreement for H₂O perturbations~~
~~as we see for O₃ compared to the results of Grewe et al. (2007). We expect that the adoption of a common vertical grid and~~
~~resolution may remove a factor contributing to model disagreement of stratospheric H₂O perturbation lifetimes, and this may~~
~~therefore be desirable in future multi-model studies. Improvements in model agreement does not necessarily indicate better~~
~~model performance however, for this validation with observations and measurements remains to be crucial.~~

965 We find considerable differences between the responses of the online and offline models. Between the offline models (GEOS-
Chem, LMDZ-INCA, MOZART-3) we find good agreement in all perturbations of the stratospheric composition. The most
notable difference is the lower vertical domain of GEOS-Chem's extensive stratospheric ozone chemistry. With regards to the
ozone impact, we find considerable improvement in model agreement compared to the previous multi-model assessment by
970 Grewe et al. (2007). Between the models with offline meteorology the biggest difference is identified in the GEOS-Chem
model, which has a lower upper altitude for its stratospheric ozone chemistry than all other models (Eastham et al. 2014).
Comparing perturbations in odd O_x loss rates, we expect that this lower domain, which may lead to Above this limit species
such as HO_x still evolve freely in the model's mesosphere, and we expect this may result in excessive increased influx of HO_x
975 at the upper-stratospheric boundary. Ultimately, but although our findings results do not indicate that this has an a large effect
on the observed changes in the total ozone columns for the supersonic emission scenarios. on our the calculated ozone column
responses. It may however become a more relevant restriction for the study of the effects of higher altitude emissions, such as
from hypersonic vehicles or spaceflight. Comparing the online EMAC model to the offline models, we see some substantial
differences from the inclusion of meteorological feedbacks (predominantly stratospheric cooling) on chemistry. However, w
980 Finally, we find that the use of online meteorology in the EMAC model has considerable effects on the impact of all supersonic
emission scenarios. The inclusion of this feedback allows EMAC to capture interactions that are not included in the offline
models. For example, we find that the stratospheric cooling enhances PSC chemistry in EMAC, leading to denitrification over
the south pole in response to the SST adoption. To our knowledge, this feedback from SST emissions has not previously been
identified in earlier works. We also identify denitrification of the upper-stratosphere in response to the SST emissions This is
particularly influential for the accumulation of stratospheric nitrogen compounds, likely due to slowdown of NO_x reformation
reactions and interactions with nitrogen chemistry cycles. and by extend it also affects the changes in global ozone distribution
985 du This contributes to increases in upper-stratospheric ozone at high latitudes, which has also been shown other works that use
EMAC in a similar configuration (Pletzer et al. 2022; Kirner et al. 2014). We find these differences even when the

990 meteorological feedbacks are still constrained. Within the model the horizontal and vertical winds are still nudged for the majority of the stratosphere, and furthermore some feedbacks like local temperature changes from black carbon perturbations are not included. The inclusion of these feedbacks would likely further alter the response to high-altitude emissions. We expect that the consideration meteorological feedbacks might be critical to the complete assessment of the effects of high altitude emissions, as some important feedbacks may be overlooked otherwise. ~~e to the emissions. Notably, the inclusion of chemistry-meteorological feedback allowed EMAC to observe some interactions overlooked by the other models such as the denitrification of the southern stratosphere due to enhancements of PSC chemistry from stratospheric cooling. A downside of the use of online meteorology is that it makes models more susceptible to noise, requiring longer model integration times to ensure results are statistically significant. This is less practical than working with offline meteorology, but our results indicate that some critical interactions may be overlooked otherwise. Therefore, we recommend that the effect of chemistry-meteorology feedback is considered and explored further in future studies regarding the impact of high altitude emissions.~~

1000 The adoption of a fleet of SSTs should be considered in context of other options for air travel, both in terms of their CO₂ and non-CO₂ effects. For the nominal and triple NO_x scenarios, we calculate a fuel burn to RPK ratio of 79.3 g/ RPK, and for the low cruise concept a ratio of 58.0 g/ RPK. In comparison, from Lee et al. (2021) we calculate a fuel burn to RPK ratio of around 38.0 g/ RPK for the 2018 subsonic fleet. This suggests that replacing a RPK with these SST concepts increases the associated fuel consumption, and by extension the emission of CO₂ and its radiative effects, by 109% and 53% for the respective nominal and low cruise concepts. A similar trend also holds for the radiative effects of non-CO₂ emissions. In the triple-NO_x scenario we find that replacing 7.3×10^{11} subsonic RPK with SSTs increases RF from non-CO₂ emissions by 19.4 mW/m². From this we calculate an increase in the RF:RPK ratio of 26.6×10^{-12} mW/m² / RPK. In case of the nominal and low cruise scenarios we find increases in this ratio of 19.0×10^{-12} and 5.2×10^{-12} mW /m² / RPK, respectively. These estimates incorporate the removal of the equivalent RPKs from the subsonic fleet, thereby representing the additional RF from non-CO₂ emissions per RPK when an RPK is flown by a SST rather than a subsonic aircraft. We note that our results do not reflect the RF benefits of practically eliminating contrail impacts from the subsonic RPK, but do reflect aerosol RF. In comparison, using non-CO₂ RF estimates from the 2018 subsonic aviation from Lee et al. (2021), we calculate a RF:RPK ratio of 14.4×10^{-12} mW/m² / RPK for subsonic radiative effects from non-CO₂ emissions. Our results therefore indicate that the replacement of subsonic RPKs with the triple NO_x scenario SST would increase the non-CO₂ RF:RPK ratio by 185% compared to the estimate of Lee et al. (2021), and that the nominal SST and low cruise (Mach 1.6) SST would increase the RPK cost by 132% and 36%, respectively. These discrepancies would differ if contrails were to be included in the RF assessment, but they provide an estimate of the additional climate impacts of SSTs over subsonic aircraft. The disparity that we identify has also been reported in earlier works (Eastham et al. 2022; Speth et al. 2021; Grewe et al. 2007), and while our results suggest that this disparity may be mitigated by reducing supersonic NO_x emissions, cruise speed, and altitude, we expect it will nonetheless persist due to the more sensitive emission altitudes, the higher fuel requirements, and the lower passenger numbers of supersonic aircraft.

1020 Our results provide some actionable information for consideration in sustainability discussions related to SSTs. We find the atmospheric and radiative effects are predominantly driven by NO_x and water vapour emissions, which indicates that the use of sustainable aviation fuels is not likely to lead to substantial differences in these effects. On the contrary, sustainable aviation fuels are likely to have lower sulphur and black carbon emissions, which will increase SST radiative effects by reducing the emissions responsible for the cooling RF, as also identified by Speth et al. (2021). We also remark that the effect on the ozone column could be considered in the context of the effects on human health. For example, in response to the triple-NO_x scenario, we find a model-mean global ozone column loss of -0.3 % (-0.9 DU), but some models calculate year-round depletion of up to -0.7% (-2.1 DU) over the northern hemisphere. Considering the distribution of population, the effect on human health is likely larger than what the global average would imply. Estimating the effect on human health lies outside of the scope of this

1030 work, but it may be an effective means to communicate the effect of changes in the ozone column. Such an approach may also
account for the changes in air quality from tropospheric ozone perturbations, which are otherwise not included in discussions
surrounding global column ozone perturbations.

64 Conclusions

1035 For the first ~~time in about eighteen years~~ time since 2007, we present a comprehensive multi-model assessment review of the
~~effects~~ effects of the partial replacement of subsonic aviation traffic with a fleet of supersonic transport aircraft ~~of~~ on
atmospheric composition and global radiative forcing. With four widely-used models (~~supersonic aviation on the stratospheric~~
~~composition of a future atmosphere as calculated by four widely-used state-of-the-art chemistry transport models. We use the~~
EMAC, LMDZ-INCA, GEOS-Chem, and MOZART-3) we evaluate three supersonic adoption scenarios based on models to
~~make an updated assessment of~~ the emission scenarios of the SCENIC project (Grewe et al. 2007). Two of these scenarios
1040 consider ~~to evaluate the effects of advancements in atmospheric chemistry and modelling since then. In this scenario we~~
~~consider~~ the adoption of a Mach 2 supersonic aircraft operating at cruise altitudes of 16.5 to 19.5 km ~~that~~ to replace around
4% of ~~partially replaces~~ subsonic aviation traffic, differing in fleetwide NO_x emissions (13.80 and 4.60 g(NO₂)/kg) ~~e.~~ . ~~We also~~
~~evaluate two variants of this scenario. One considers increased NO_x emissions that are more comparable to modern emission~~
~~estimates for supersonic vehicles.~~ The ~~other~~ third scenario considers a aircraft with a lower cruise speed (Mach 1.6) and altitude
1045 instead (13.1 to 16.7 km).

The partial replacement of subsonic aviation with ~~B~~ both Mach 2 concepts results in a reduction in the global ozone column.
For the Mach 2 concept with NO_x emissions of 13.80 g (NO₂)/kg we calculate model-mean global ozone column loss of -0.3%
(-0.9 DU), with higher losses across the northern hemisphere (model-mean up to -0.5%, -1.5DU). The replacement of subsonic
1050 aviation with this concept increases ~~and~~ radiative forcing by of 19.4 mW/m². The biggest forcing is from changes in
stratospheric water vapour (18.2 mW/m²), followed by ozone (11.4 mW/m²), and aerosols (-10.2 mW/m²). If the fleetwide
NO_x emissions are reduced by 67%, the net forcing also reduces ~~d~~ to 13.9 mW/m² because of the smaller ozone perturbation (-
0.1% (-0.3 DU)) and its associated forcing (3.2 mW/m²). If part of the subsonic aviation is instead replaced by the Mach 1.6
1055 concept, which has a lower cruise altitude and fleetwide NO_x emissions, the effects on stratospheric composition and radiative
forcing are reduced ~~as well. In this case we find an increase in radiative forcing by~~ ~~to~~ 3.8 mW/m². These values do not account
for potential changes in contrail formation and the increase in CO₂ emissions. Compared to estimates of subsonic aviation, we
find that the replacement of subsonic passenger revenue kilometres with supersonic aircraft ~~strongly~~ increases the associated
radiative forcing from non-CO₂ emissions by up to 185% compared to subsonic aircraft.

1060 Compared to the previous multi-model assessment of the atmospheric and radiative effects of supersonic aircraft (Grewe et al.
2007), we see a smaller spread in our model evaluations of the water vapour and ozone perturbations. We find good agreement
in the composition changes between the three models which use offline meteorology, but we also see large differences with
the model with online meteorology (EMAC). The inclusion of meteorological feedbacks in the model captures several
1065 responses to the emissions that are not captured in the offline models, leading to denitrification of the upper-stratosphere and
south pole. These feedbacks have substantial effects on the stratospheric ozone and nitrogen responses, and we expect that
they may be of critical importance to the assessment of the effects of high-altitude emissions.

~~In the nominal supersonic emission scenario, the partial replacement of subsonic traffic with supersonic vehicles leads to~~
~~substantial accumulation of stratospheric water vapor (H₂O) which is often associated with positive radiative forcing. This~~
1070 ~~accumulation is contained almost entirely within the lower altitudes of the northern stratosphere, yielding a model-mean~~

1075 perturbation of +61.34 Tg with a spread of +20.14 to +116.53 Tg. This value closely agrees with estimates from the earlier assessment of the SCENIC scenario, but we find a larger spread in perturbation masses. We expect that this originates from differences in H₂O perturbation lifetime, which are primarily driven by differences in vertical model resolutions and the treatment of tropospheric water vapour. The H₂O perturbation lifetime may be a function of the vertical model resolution, and low resolutions may lead to excessive removal of stratospheric H₂O emissions. This is most influential in the low cruise altitude emissions, where we find reduced model mean H₂O increases of +9.34 Tg with a range of +2.37 to +19.69 Tg. This is paired with large reductions in H₂O perturbation lifetimes which depend on vertical model resolution. We also find that the use of higher horizontal resolutions reduced interhemispheric transport of the H₂O perturbation in current models compared to the previous assessment of these scenarios.

1080 In most cases the supersonic emissions lead to loss of the global ozone column, driven by depletion of middle and upper-stratospheric ozone paired with lower stratospheric increases, of smaller magnitude. For the nominal emissions scenario we find a model average decrease in the global ozone column of -0.11%, with a range of -0.22% to +0.03%. Compared to the earlier multi-model assessment of the SCENIC project we find considerable improvements in the agreement of the ozone perturbation across the models, which may be indicative of substantial improvements in the modelling of ozone chemistry. The ozone response is primarily driven by the emission of NO_x, followed by sulfur emissions and then H₂O, leading to lower-stratospheric ozone increases and upper stratospheric losses. Consequently, we find that in the scenario with triple the supersonic NO_x emissions the global column ozone loss increases to -0.31%, ranging between -0.57% to -0.09%. The increase in global ozone losses is not linearly tied to the supersonic NO_x emissions, and we find that the degree of nonlinearity varies across models. When a low cruise altitude is used, the ozone impact is strongly reduced, yielding a net increase in the global ozone column of +0.02% instead (range -0.01% to +0.04%).

1090 The adoption of a lower cruise speed and altitude sharply reduces the impacts of supersonic emissions on atmospheric composition. It leads to reductions in the perturbations of stratospheric O₃, NO_y, H₂O, and aerosol loadings, which will implicitly also reduce the effect on radiative forcing. Limitations on cruise altitude and speed may prove to be the most effective means to minimize the environmental impact of a future supersonic fleet. The impact on the distribution of atmospheric ozone in particular may be further reduced by the reduction of fleetwide NO_x emissions.

1100 Finally, we find that the use of online meteorology in the EMAC model leads to differences in the assessment of high altitude emissions compared to the other models. In EMAC, the introduction of supersonic emissions lead to a cooling of the stratosphere. This enhances PSC formation in the southern hemisphere, increasing the availability of halogens for heterogeneous chemistry and contributing to denitrification of the southern hemisphere through sedimentation of PSC particles. These effects lead to a loss of ozone in the southern mid-stratosphere which is not captured by the models with offline meteorology. At the upper model domain above 10 hPa the slowing of the Chapman mechanism and changes in vertical mixing lead to a complex upper stratospheric ozone response, including areas of ozone increases. These interactions are not captured by other models with offline meteorology, but they have considerable consequences for the impact of high altitude emissions. From this we identify that the inclusion of such feedback may be of necessary to adequately capture the effects of high altitude emissions on the stratosphere. This is particularly true for changes in ozone chemistry, and it may prove a fruitful direction for future developments in chemistry transport models.

1110 **75 Acknowledgements**

This work was funded by the European Union's Horizon 2020 research and innovation programme. Authors (J.A.H, R.T., J.P., V.G., D.H., I.C.D., M.M.M.) were funded by the MORE & LESS project (MDO and REgulations for Low-boom Environmentally Sustainable Supersonic aviation, grant No. 101006856). Others (A.S. & S.M.) were funded by the SENECA project ((LTO) Noise and Emissions of Supersonic Aircraft, grant No.101006742). The GEOS-Chem simulations were supported by the Dutch national e-infrastructure and supercomputer with the support of the SURF Cooperative (Grant no. EINF-5945). The EMAC model simulations were computed at the German Climate Computing Center (DKRZ). The resources for the simulations were provided by the German Bundesministerium für Bildung und Forschung (BMBF). [Ruben Rodriguez de Leon is thanked for maintaining and running the SOCRATES RTM.](#)

86 Data availability

1120 The data supporting the results of this work is publicly available at DOI: **10.4121/dd38833d-6c5d-47d8-bb10-7535ce1eecf1** (van 't Hoff et al. 2024b). Reserved DOI, dataset to be minted on acceptance. Reviewers can preview the dataset through https://data.4tu.nl/private_datasets/_qffTJdRitRConukkBmBTegk9CJTJZD36xRUN6lif5M.

9 Author contribution

Conceptualization: ICD, VG, DH, JAH, RNT; Formal analysis: DH, JAH, JP, AS; Investigation: ICD, VG, DH, JAH, SM, JP, AS; Data Curation: DH, JAH, MMM, JP, AS, RNT; Writing - Original Draft: JAH; Writing - Review & Editing: all; Visualization: JAH, JP; Supervision: ICD; Funding acquisition: ICD, VG, DH, SM, AS.

10 Competing interests

The authors declare that they have no conflict of interest.

1130 **References**

- Matthes, S., Lee, D. S., De Leon, R. R., Lim, L., Owen, B., Skowron, A., Thor, R. N., and Terrenoire, E.: Review: The Effects of Supersonic Aviation on Ozone and Climate, *Aerospace*, 9, 41, <https://doi.org/10.3390/aerospace9010041>, 2022.
- Berton, J. J., Huff, D. L., Geiselhart, K., and Seidel, J.: Supersonic Technology Concept Aeroplanes for Environmental Studies, in: AIAA Scitech 2020 Forum, American Institute of Aeronautics and Astronautics, <https://doi.org/10.2514/6.2020-0263>, 2020.
- 1135 Solomon, S.: Stratospheric ozone depletion: A review of concepts and history, 1999.
- Johnston, H.: Reduction of stratospheric ozone by nitrogen oxide catalysts from supersonic transport exhaust, *Science*, 173, 517–522, 1971.
- Pitari, G., Aquila, V., Kravitz, B., Robock, A., Watanabe, S., Cionni, I., De Luca, N., Di Genova, G., Mancini, E., and Tilmes, S.: Stratospheric ozone response to sulfate geoengineering: Results from the Geoengineering Model Intercomparison Project (GeoMIP), *Journal of Geophysical Research*, 119, 2629–2653, <https://doi.org/10.1002/2013jd020566>, 2014.
- 1140 Granier, C. and Brasseur, G.: Impact of heterogeneous chemistry on model predictions of ozone changes, *Journal of Geophysical Research: Atmospheres*, 97, 18015–18033, <https://doi.org/10.1029/92JD02021>, 1992.
- Zhang, J., Wuebbles, D., Kinnison, D., and Baughcum, S. L.: Stratospheric Ozone and Climate Forcing Sensitivity to Cruise Altitudes for Fleets of Potential Supersonic Transport Aircraft, *Journal of Geophysical Research: Atmospheres*, 126, <https://doi.org/10.1029/2021jd034971>, 2021a.

- 1145 Zhang, J., Wuebbles, D., Kinnison, D., and Baughcum, S. L.: Potential Impacts of Supersonic Aircraft Emissions on Ozone and Resulting Forcing on Climate: An Update on Historical Analysis, *Journal of Geophysical Research: Atmospheres*, 126, <https://doi.org/10.1029/2020JD034130>, 2021b.
- Speth, R. L., Eastham, S. D., Fritz, T. M., Sanz-Morère, I., Agarwal, A., Prashanth, P., Allroggen, F., and Barrett, S. R. H.: Global Environmental Impact of Supersonic Cruise Aircraft in the Stratosphere, 2021.
- 1150 Crutzen, P. J.: SST's: A Threat to the Earth's Ozone Shield, *Ambio*, 1, 41–51, 1972.
- [van 't Hoff, J.A., Grewe, V., Dedoussi, I.C. :Sensitivities of Ozone and Radiative Forcing to Supersonic Aircraft Emissions Across Two Flight Corridors. *Journal of Geophysical Research: Atmospheres* 129, e2023JD040476. <https://doi.org/10.1029/2023JD040476>, 2024a.](https://doi.org/10.1029/2023JD040476)
- [van 't Hoff, J.A., Hauglustaine D., Pletzer, J., Skowron S., Grewe V., Matthes, S., Meuser, M., Thor, R.N., Dedoussi, I.C. : Supporting dataset for “Multi-model assessment of the atmospheric and radiative effects of supersonic transport aircraft.” *Journal of Geophysical Research: Atmospheres*, 2024b](https://doi.org/10.4121/dd38833d-6c5d-47d8-bb10-7535ce1eefcf)
- 1155 ~~[Van 't Hoff, J.A., Grewe V., and Dedoussi I.C.: Sensitivities of atmospheric ozone and radiative forcing to supersonic aircraft emissions across two flight corridors. *Journal of Geophysical Research: Atmospheres*, 2024a \(under review\).](https://doi.org/10.4121/dd38833d-6c5d-47d8-bb10-7535ce1eefcf)~~
- Eastham, S. D., Weisenstein, D. K., Keith, D. W., and Barrett, S. R. H.: Quantifying the impact of sulfate geoengineering on mortality from air quality and UV-B exposure, *Atmospheric Environment*, 187, 424–434, <https://doi.org/10.1016/j.atmosenv.2018.05.047>, 2018.
- 1160 Pletzer, J., Hauglustaine, D., Cohen, Y., Jöckel, P., and Grewe, V.: The climate impact of hydrogen-powered hypersonic transport, *Atmospheric Chemistry and Physics*, 22, 14323–14354, <https://doi.org/10.5194/acp-22-14323-2022>, 2022.
- Lee, D. S., Fahey, D. W., Skowron, A., Allen, M. R., Burkhardt, U., Chen, Q., Doherty, S. J., Freeman, S., Forster, P. M., Fuglestedt, J., Gettelman, A., De León, R. R., Lim, L. L., Lund, M. T., Millar, R. J., Owen, B., Penner, J. E., Pitari, G., Prather, M. J., Sausen, R., and Wilcox, L. J.: The contribution of global aviation to anthropogenic climate forcing for 2000 to 2018, *Atmospheric Environment*, 244, <https://doi.org/10.1016/j.atmosenv.2020.117834>, 2021.
- 1165 Stenke, A., Grewe, V., and Pechtl, S.: Do supersonic aircraft avoid contrails?, 2008.
- Grewe, V., Stenke, A., Ponater, M., Sausen, R., Pitari, G., Iachetti, D., Rogers, H., Dessens, O., Pyle, J., Isaksen, I. S. A., Gulstad, L., Søvde, O. A., Marizy, C., and Pascuillo, E.: Climate impact of supersonic air traffic: an approach to optimize a potential future supersonic fleet – results from the EU-project SCENIC, *Atmospheric Chemistry and Physics*, 7, 5129–5145, <https://doi.org/10.5194/acp-7-5129-2007>, 2007.
- 1170 IPCC: Special report on aviation and the global atmosphere, edited by: Penner, J. E., Lister, D. H., Griggs, D. J., Dokken, D. J., and McFarland, M., Intergovernmental Panel on Climate Change, 1999.
- Grewe, V., Plohr, M., Cerino, G., Di Muzio, M., Deremaux, Y., Galerneau, M., de Saint Martin, P., Chaika, T., Hasselrot, A., Tengzelius, U., and Korovkin, V. D.: Estimates of the climate impact of future small-scale supersonic transport aircraft-results from the HISAC EU-project, 2010.
- 1175 Pletzer, J. and Grewe, V.: Sensitivities of atmospheric composition and climate to altitude and latitude of hypersonic aircraft emissions, *Atmospheric Chemistry and Physics*, 24, 1743–1775, <https://doi.org/10.5194/acp-24-1743-2024>, 2024.
- Eastham, S. D., Fritz, T., Sanz-Morère, I., Prashanth, P., Allroggen, F., Prinn, R. G., Speth, R. L., and Barrett, S. R. H.: Impacts of a near-future supersonic aircraft fleet on atmospheric composition and climate, *Environmental Science: Atmospheres*, <https://doi.org/10.1039/d1ea00081k>, 2022.
- 1180 Kawa, S. R., Anderson, J. G., Baughcum, S. L., Brock, C. A., Brune, W. H., Cohen, R. C., Kinnison, D. E., Newman, P. A., Rodriguez, J. M., and Stolarski, R. S.: Assessment of the effects of high-speed aircraft in the stratosphere: 1998, 1999.
- Pitari, G., Iachetti, D., Mancini, E., Montanaro, V., De Luca, N., Marizy, C., Dessens, O., Rogers, H., Pyle, J., Grewe, V., Stenke, A., and Søvde, O. A.: Radiative forcing from particle emissions by future supersonic aircraft, *Atmospheric Chemistry and Physics*, 8, 4069–4084, <https://doi.org/10.5194/acp-8-4069-2008>, 2008.
- 1185 Riahi, K., van Vuuren, D. P., Kriegler, E., Edmonds, J., O'Neill, B. C., Fujimori, S., Bauer, N., Calvin, K., Dellink, R., Fricko, O., Lutz, W., Popp, A., Cuaresma, J. C., Kc, S., Leimbach, M., Jiang, L., Kram, T., Rao, S., Emmerling, J., Ebi, K., Hasegawa, T., Havlik, P., Humpenöder, F., Da Silva, L. A., Smith, S., Stehfest, E., Bosetti, V., Eom, J., Gernaat, D., Masui, T., Rogelj, J., Strefler, J., Drouet, L., Krey, V., Luderer, G., Harmsen, M., Takahashi, K., Baumstark, L., Doelman, J. C., Kainuma, M., Klimont, Z., Marangoni, G., Lotze-Campen, H., Obersteiner, M., Tabeau, A., and Tavoni, M.: The Shared Socioeconomic Pathways and their energy, land use, and greenhouse gas emissions implications: An overview, *Global Environmental Change*, 42, 153–168, <https://doi.org/10.1016/j.gloenvcha.2016.05.009>, 2017.
- 1190 Grewe, V. and Stenke, A.: AirClim: An efficient tool for climate evaluation of aircraft technology, *Atmospheric Chemistry and Physics*, 8, 4621–4639, <https://doi.org/10.5194/acp-8-4621-2008>, 2008.

- Jöckel, P., Tost, H., Pozzer, A., Kunze, M., Kirner, O., Brenninkmeijer, C. A. M., Brinkop, S., Cai, D. S., Dyroff, C., Eckstein, J., Frank, F., Garny, H., Gottschaldt, K.-D., Graf, P., Grewe, V., Kerkweg, A., Kern, B., Matthes, S., Mertens, M., Meul, S., Neumaier, M., Nützel, M., Oberländer-Hayn, S., Ruhnke, R., Runde, T., Sander, R., Scharffé, D., and Zahn, A.: Earth System Chemistry integrated Modelling (ESCiMo) with the Modular Earth Submodel System (MESSy) version 2.51, *Geoscientific Model Development*, 9, 1153–1200, <https://doi.org/10.5194/gmd-9-1153-2016>, 2016.
- The MESSy Consortium. (2021). The Modular Earth Submodel System (2.55.2). Zenodo. <https://doi.org/10.5281/zenodo.8360276>
- Roeckner, E., Bäuml, G., Bonaventura, L., Brokopf, R., Esch, M., Giorgetta, M., Hagemann, S., Kirchner, I., Kornblüeh, L., Manzini, E., Rhodin, A., Schlese, U., Schulzweida, U., and Tompkins, A.: The atmospheric general circulation model ECHAM 5. PART I: Model description, <https://doi.org/10.17617/2.995269>, 2003.
- Sander, R., Baumgaertner, A., Gromov, S., Harder, H., Jöckel, P., Kerkweg, A., Kubistin, D., Regelin, E., Riede, H., Sandu, A., Taraborrelli, D., Tost, H., and Xie, Z.-Q.: The atmospheric chemistry box model CAABA/MECCA-3.0, *Geoscientific Model Development*, 4, 373–380, <https://doi.org/10.5194/gmd-4-373-2011>, 2011.
- Eastham, S., Long, M., Keller, C., Lundgren, E., Yantosca, R., Zhuang, J., Li, C., Lee, C., Yannetti, M., Auer, B., Clune, T., Kouatchou, J., Putman, W., Thompson, M., Trayanov, A., Molod, A., Martin, R., and Jacob, D.: GEOS-Chem High Performance (GCHP v11-02c): a next-generation implementation of the GEOS-Chem chemical transport model for massively parallel applications, *Geoscientific Model Development*, 11, 2941–2953, <https://doi.org/10.5194/gmd-11-2941-2018>, 2018.
- Eastham, S. D., Weisenstein, D. K., and Barrett, S. R. H.: Development and evaluation of the unified tropospheric–stratospheric chemistry extension (UCX) for the global chemistry-transport model GEOS-Chem, *Atmospheric Environment*, 89, 52–63, <https://doi.org/10.1016/j.atmosenv.2014.02.001>, 2014.
- The International GEOS-Chem User Community: geoschem/GCHP: GCHP 14.1.1, , <https://doi.org/10.5281/zenodo.7696683>, 2023.
- Hauglustaine, D. A., Hourdin, F., Jourdain, L., Filiberti, M.-A., Walters, S., Lamarque, J.-F., and Holland, E. A.: Interactive chemistry in the Laboratoire de Météorologie Dynamique general circulation model: Description and background tropospheric chemistry evaluation, *Journal of Geophysical Research: Atmospheres*, 109, 2004.
- Hauglustaine, D. A., Balkanski, Y., and Schulz, M.: A global model simulation of present and future nitrate aerosols and their direct radiative forcing of climate, *Atmospheric Chemistry and Physics*, 14, 11031–11063, 2014.
- Terrenoire, E., Hauglustaine, D. A., Cohen, Y., Cozic, A., Valorso, R., Lefèvre, F., and Matthes, S.: Impact of present and future aircraft NO_x and aerosol emissions on atmospheric composition and associated direct radiative forcing of climate, *Atmospheric Chemistry and Physics*, 22, 11987–12023, <https://doi.org/10.5194/acp-22-11987-2022>, 2022.
- Kinnison, D. E., Brasseur, G. P., Walters, S., Garcia, R. R., Marsh, D. R., Sassi, F., Harvey, V. L., Randall, C. E., Emmons, L., Lamarque, J. F., Hess, P., Orlando, J. J., Tie, X. X., Randel, W., Pan, L. L., Gettelman, A., Granier, C., Diehl, T., Niemeier, U., and Simmons, A. J.: Sensitivity of chemical tracers to meteorological parameters in the MOZART-3 chemical transport model, *Journal of Geophysical Research: Atmospheres*, 112, <https://doi.org/10.1029/2006JD007879>, 2007.
- Skowron, A., Lee, D. S., De León, R. R., Lim, L. L., and Owen, B.: Greater fuel efficiency is potentially preferable to reducing NO_x emissions for aviation’s climate impacts, *Nat Commun*, 12, 564, <https://doi.org/10.1038/s41467-020-20771-3>, 2021.
- Kirner, O., Ruhnke, R., Buchholz-Dietsch, J., Jöckel, P., Brühl, C., and Steil, B.: Simulation of polar stratospheric clouds in the chemistry-climate-model EMAC via the submodel PSC, *Geoscientific Model Development*, 4, 169–182, <https://doi.org/10.5194/gmd-4-169-2011>, 2011.
- Jöckel, P., Kerkweg, A., Pozzer, A., Sander, R., Tost, H., Riede, H., Baumgaertner, A., Gromov, S., and Kern, B.: Development cycle 2 of the modular earth submodel system (MESSy2), *Geoscientific Model Development*, 3, 717–752, 2010.
- Burkholder, J. B., Sander, S. P., Abbatt, J. P. D., Barker, J. R., Cappa, C., Crouse, J. D., Dibble, T. S., Huie, R. E., Kolb, C. E., Kurylo, M. J., Orkin, V. L., Percival, C. J., Wilmouth, D. M., and Wine, P. H.: Chemical kinetics and photochemical data for use in atmospheric studies; evaluation number 19, 2020.
- Kunze, M., Godolt, M., Langematz, U., Grenfell, J. L., Hamann-Reinus, A., and Rauer, H.: Investigating the early Earth faint young Sun problem with a general circulation model, *Planetary and Space Science*, 98, 77–92, <https://doi.org/10.1016/j.pss.2013.09.011>, 2014.
- Dietmüller, S., Jöckel, P., Tost, H., Kunze, M., Gellhorn, C., Brinkop, S., Frömming, C., Ponater, M., Steil, B., Lauer, A., and Hendricks, J.: A new radiation infrastructure for the Modular Earth Submodel System (MESSy, based on version 2.51), *Geoscientific Model Development*, 9, 2209–2222, <https://doi.org/10.5194/gmd-9-2209-2016>, 2016.

- 1240 Bey, I., Jacob, D. J., Yantosca, R. M., Logan, J. A., Field, B. D., Fiore, A. M., Li, Q., Liu, H. Y., Mickley, L. J., and Schultz, M. G.: Global modeling of tropospheric chemistry with assimilated meteorology: Model description and evaluation, *Journal of Geophysical Research: Atmospheres*, 106, 23073–23095, 2001.
- Damian, V., Sandu, A., Damian, M., Potra, F., and Carmichael, G. R.: The kinetic preprocessor KPP—a software environment for solving chemical kinetics, *Computers & Chemical Engineering*, 26, 1567–1579, 2002.
- 1245 Bian, H. and Prather, M. J.: Fast-J2: Accurate simulation of stratospheric photolysis in global chemical models, *Journal of Atmospheric Chemistry*, 41, 281–296, 2002.
- Fritz, T. M., Dedoussi, I. C., Eastham, S. D., Speth, R. L., Henze, D. K., and Barrett, S. R. H.: Identifying the ozone-neutral aircraft cruise altitude, *Atmospheric Environment*, 276, 119057, <https://doi.org/10.1016/j.atmosenv.2022.119057>, 2022.
- Keller, C. A., Knowland, K. E., Duncan, B. N., Liu, J., Anderson, D. C., Das, S., Lucchesi, R. A., Lundgren, E. W., Nicely, J. M., Nielsen, E., Ott, L. E., Saunders, E., Strode, S. A., Wales, P. A., Jacob, D. J., and Pawson, S.: Description of the NASA GEOS Composition Forecast Modeling System GEOS-CF v1.0, *J Adv Model Earth Syst*, 13, e2020MS002413, <https://doi.org/10.1029/2020MS002413>, 2021.
- 1250 Gelaro, R., McCarty, W., Suárez, M. J., Todling, R., Molod, A., Takacs, L., Randles, C. A., Darmenov, A., Bosilovich, M. G., Reichle, R., Wargan, K., Coy, L., Cullather, R., Draper, C., Akella, S., Buchard, V., Conaty, A., da Silva, A. M., Gu, W., Kim, G.-K., Koster, R., Lucchesi, R., Merkova, D., Nielsen, J. E., Partyka, G., Pawson, S., Putman, W., Rienecker, M., Schubert, S. D., Sienkiewicz, M., and Zhao, B.: The Modern-Era Retrospective Analysis for Research and Applications, Version 2 (MERRA-2), *Journal of Climate*, 30, 5419–5454, <https://doi.org/10.1175/JCLI-D-16-0758.1>, 2017.
- Carn, S. A., Yang, K., Prata, A. J., and Krotkov, N. A.: Extending the long-term record of volcanic SO₂ emissions with the Ozone Mapping and Profiler Suite nadir mapper, *Geophysical Research Letters*, 42, 925–932, <https://doi.org/10.1002/2014GL062437>, 2015.
- Hourdin, F., Rio, C., Grandpeix, J.-Y., Madeleine, J.-B., Cheruy, F., Rochetin, N., Jam, A., Musat, I., Idelkadi, A., and Fairhead, L.: LMDZ6A: The atmospheric component of the IPSL climate model with improved and better tuned physics, *Journal of Advances in Modeling Earth Systems*, 12, e2019MS001892, 2020.
- 1260 Boucher, O., Servonnat, J., Albright, A. L., Aumont, O., Balkanski, Y., Bastrikov, V., Bekki, S., Bonnet, R., Bony, S., and Bopp, L.: Presentation and evaluation of the IPSL-CM6A-LR climate model, *Journal of Advances in Modeling Earth Systems*, 12, e2019MS002010, 2020.
- 1265 Van Leer, B.: Towards the ultimate conservative difference scheme. IV. A new approach to numerical convection, *Journal of Computational Physics*, 23, 276–299, 1977.
- Hourdin, F. and Armengaud, A.: The use of finite-volume methods for atmospheric advection of trace species. Part I: Test of various formulations in a general circulation model, *Monthly Weather Review*, 127, 822–837, 1999.
- Emanuel, K. A.: A scheme for representing cumulus convection in large-scale models, *Journal of the atmospheric sciences*, 48, 2313–2329, 1991.
- 1270 Folberth, G. A., Hauglustaine, D. A., Lathière, J., and Brocheton, F.: Interactive chemistry in the Laboratoire de Météorologie Dynamique general circulation model: model description and impact analysis of biogenic hydrocarbons on tropospheric chemistry, *Atmospheric Chemistry and Physics*, 6, 2273–2319, 2006.
- Lefevre, F., Brasseur, G. P., Folkins, I., Smith, A. K., and Simon, P.: Chemistry of the 1991–1992 stratospheric winter: Three-dimensional model simulations, *Journal of Geophysical Research: Atmospheres*, 99, 8183–8195, 1994.
- 1275 Liu, Y., Liu, C. X., Wang, H. P., Tie, X. X., Gao, S. T., Kinnison, D., and Brasseur, G.: Atmospheric tracers during the 2003–2004 stratospheric warming event and impact of ozone intrusions in the troposphere, *Atmospheric Chemistry and Physics*, 9, 2157–2170, <https://doi.org/10.5194/acp-9-2157-2009>, 2009.
- Flemming, J., Inness, A., Jones, L., Eskes, H. J., Huijnen, V., Schultz, M. G., Stein, O., Cariolle, D., Kinnison, D., and Brasseur, G.: Forecasts and assimilation experiments of the Antarctic ozone hole 2008, *Atmospheric Chemistry and Physics*, 11, 1961–1977, <https://doi.org/10.5194/acp-11-1961-2011>, 2011.
- 1280 Søvde, O. A., Matthes, S., Skowron, A., Iachetti, D., Lim, L., Owen, B., Hodnebrog, Ø., Di Genova, G., Pitari, G., Lee, D. S., Myhre, G., and Isaksen, I. S. A.: Aircraft emission mitigation by changing route altitude: A multi-model estimate of aircraft NO_x emission impact on O₃ photochemistry, *Atmospheric Environment*, 95, 468–479, <https://doi.org/10.1016/J.ATMOSENV.2014.06.049>, 2014.
- 1285 Skowron, A., Lee, D. S., and De León, R. R.: The assessment of the impact of aviation NO_x on ozone and other radiative forcing responses – The importance of representing cruise altitudes accurately, *Atmospheric Environment*, 74, 159–168, <https://doi.org/10.1016/J.ATMOSENV.2013.03.034>, 2013.

- Skowron, A., Lee, D. S., and De León, R. R.: Variation of radiative forcings and global warming potentials from regional aviation NO_x emissions, *Atmospheric Environment*, 104, 69–78, <https://doi.org/10.1016/j.atmosenv.2014.12.043>, 2015.
- 1290 Freeman, S., Lee, D. S., Lim, L. L., Skowron, A., and De León, R. R.: Trading off Aircraft Fuel Burn and NO_x Emissions for Optimal Climate Policy, *Environ. Sci. Technol.*, 52, 2498–2505, <https://doi.org/10.1021/acs.est.7b05719>, 2018.
- Sander, S. P., Finlayson-Pitts, B., Friedl, R. R., Golden, D. M., Huie, R., Keller-Rudek, H., Kolb, C. E., Kurylo, M., Molina, M., Moortgat, G., Orkin, V., Ravishankara, A. R., and Wine, P.: Chemical Kinetics and Photochemical Data for Use in Atmospheric Studies, *Evaluation No. 15*, 2006.
- 1295 Meinshausen, M., Nicholls, Z. R. J., Lewis, J., Gidden, M. J., Vogel, E., Freund, M., Beyerle, U., Gessner, C., Nauels, A., Bauer, N., Canadell, J. G., Daniel, J. S., John, A., Krummel, P. B., Luderer, G., Meinshausen, N., Montzka, S. A., Rayner, P. J., Reimann, S., Smith, S. J., van den Berg, M., Velders, G. J. M., Vollmer, M. K., and Wang, R. H. J.: The shared socio-economic pathway (SSP) greenhouse gas concentrations and their extensions to 2500, *Geosci. Model Dev.*, 13, 3571–3605, <https://doi.org/10.5194/gmd-13-3571-2020>, 2020.
- Houweling, S., Dentener, F., and Lelieveld, J.: The impact of nonmethane hydrocarbon compounds on tropospheric photochemistry, *Journal of Geophysical Research: Atmospheres*, 103, 10673–10696, <https://doi.org/10.1029/97JD03582>, 1998.
- 1300 Zhang, J., Wuebbles, D., Pfaender, J. H., Kinnison, D., and Davis, N.: Potential Impacts on Ozone and Climate From a Proposed Fleet of Supersonic Aircraft, *Earth's Future*, 11, e2022EF003409, <https://doi.org/10.1029/2022EF003409>, 2023.
- Kinnison, D., Brasseur, G. P., Baughcum, S. L., Zhang, J., and Wuebbles, D.: The Impact on the Ozone Layer of a Potential Fleet of Civil Hypersonic Aircraft, *Earth's Future*, 8, <https://doi.org/10.1029/2020ef001626>, 2020.
- 1305 Strahan, S. E. and Polansky, B. C.: Meteorological implementation issues in chemistry and transport models, *Atmospheric Chemistry and Physics*, 6, 2895–2910, <https://doi.org/10.5194/acp-6-2895-2006>, 2006.
- Revell, L. E., Tummon, F., Stenke, A., Sukhodolov, T., Coulon, A., Rozanov, E., Garny, H., Grewe, V., and Peter, T.: Drivers of the tropospheric ozone budget throughout the 21st century under the medium-high climate scenario RCP 6.0, *Atmospheric Chemistry and Physics*, 15, 5887–5902, <https://doi.org/10.5194/acp-15-5887-2015>, 2015.
- 1310 Roeckner, E., Brokopf, R., Esch, M., Giorgetta, M., Hagemann, S., Kornbluch, L., Manzini, E., Schlese, U., and Schulzweida, U.: Sensitivity of Simulated Climate to Horizontal and Vertical Resolution in the ECHAM5 Atmosphere Model, *Journal of Climate*, 19, 3771–3791, <https://doi.org/10.1175/JCLI3824.1>, 2006.
- Cohen, Y., Hauglustaine, D., Sauvage, B., Rohs, S., Konjari, P., Bundke, U., Petzold, A., Thouret, V., Zahn, A., and Ziereis, H.: Evaluation of modelled climatologies of O₃, CO, water vapour and NO_x in the upper troposphere–lower stratosphere using regular in situ observations by passenger aircraft, *Atmospheric Chemistry and Physics*, 23, 14973, <https://doi.org/10.5194/acp-23-14973-2023>, 2023.
- 1315 Rosenfield, J. E. and Douglass, A. R.: Doubled CO₂ effects on NO_y in a coupled 2D model, *Geophysical Research Letters*, 25, 4381–4384, <https://doi.org/10.1029/1998GL900147>, 1998.
- Van 't Hoff, J.A., Hauglustaine, D., Pletzer, J., Skowron, A., Grewe, V., Matthes, S., Meuser, M.M., Thor, R. N., Dedoussi, I.C.: Supporting dataset for “Intermodel comparison of the atmospheric composition changes due to emissions from a potential future supersonic aircraft fleet”, Dataset, <https://doi.org/10.4121/dd38833d-6c5d-47d8-bb10-7535ce1eeecf1> (reserved DOI, to be minted on acceptance), 2024b
- 1320 Olsen, S.C., Brasseur, G.P., Wuebbles, D.J., Barrett, S.R.H., Dang, H., Eastham, S.D., Jacobson, M.Z., Khodayari, A., Selkirk, H., Sokolov, A., Unger, N., 2013. Comparison of model estimates of the effects of aviation emissions on atmospheric ozone and methane. *Geophysical Research Letters* 40, 6004–6009. <https://doi.org/10.1002/2013GL057660>
- [Manners, J., Edwards, J.M., Hill, P., Thelen, J.C., 2015. SOCRATES \(Suite of Community Radiative Transfer codes based on Edwards and Slingo\). Code available at https://code.metoffice.gov.uk/trac/socrates](https://code.metoffice.gov.uk/trac/socrates)
- 1325 [Paths to accuracy for radiation parameterizations in atmospheric models - Pincus - 2013 - Journal of Advances in Modeling Earth Systems - Wiley Online Library \[WWW Document\], n.d. URL https://agupubs.onlinelibrary.wiley.com/doi/10.1002/jame.20027 \(accessed 11.22.24\).](https://doi.org/10.1002/jame.20027)
- [Nützel, M., Stecher, L., Jöckel, P., Winterstein, F., Dameris, M., Ponater, M., Graf, P., Kunze, M., 2024. Updating the radiation infrastructure in MESSy \(based on MESSy version 2.55\). Geoscientific Model Development 17, 5821–5849. https://doi.org/10.5194/gmd-17-5821-2024](https://doi.org/10.5194/gmd-17-5821-2024)
- 1330 [Penner, J.E., Lister, D., Griggs, D.J., Dokken, D.J., McFarland, M., 1999. Aviation and the global atmosphere: a special report of the Intergovernmental Panel on Climate Change. Cambridge University Press.](https://doi.org/10.1007/s10584-011-0156-z)
- [Meinshausen, M., Smith, S. J., Calvin, K., Daniel, J. S., Kainuma, M. L. T., Lamarque, J-F., Matsumoto, K., Montzka, S. A., Raper, S. C. B., Riahi, K., Thomson, A., Velders, G. J. M., and van Vuuren, G. J. M.: The RCP greenhouse gas concentrations and their extensions from 1765 to 2300, *Clim. Change* 109, 213–241, <https://doi.org/10.1007/s10584-011-0156-z>, 2011.](https://doi.org/10.1007/s10584-011-0156-z)

- 1335 [Considine, D. B., A. R. Douglass, D. E. Kinnison, P. S. Connell, and D. A. Rotman.: A polar stratospheric cloud parameterization for the three dimensional model of the global modeling initiative and its response to stratospheric aircraft emissions. *J. Geophys. Res.*, 105, 3955–3975, <https://doi.org/10.1029/1999JD900932>, 2000.](#)
- [Fouquart, Y. and Bonel, B.: Computations of solar heating of the earth's atmosphere: a new parameterization, *Beitr. Phys. Atmos.*, 53, 35–62, 1980.](#)
- 1340 [Hauglustaine, D. A., Balkanski, Y., and Schulz, M.: A global model simulation of present and future nitrate aerosols and their direct radiative forcing of climate, *Atmos. Chem. Phys.*, 14, 11031–11063, <https://doi.org/10.5194/acp-14-11031-2014>, 2014.](#)
- [Morcrette, J.-J.: Radiation and cloud radiative properties in the European Centre for Medium Range Weather Forecasts forecasting system, *J. Geophys. Res.*, 96, 9121–9132, 1991.](#)
- [Ganzeveld, L.N., Aardenne, J.A. van, Butler, T.M., Lawrence, M.G., Metzger, S.M., Stier, P., Zimmermann, P., Lelieveld, J., 2006.](#)
- 1345 [Technical Note: Anthropogenic and natural offline emissions and the online Emissions and dry DEPosition submodel EMDEP of the Modular Earth Submodel system \(MESSy\). <https://doi.org/10.5194/acpd-6-5457-2006>](#)
- [Dentener, F., Kinne, S., Bond, T., Boucher, O., Cofala, J., Generoso, S., Ginoux, P., Gong, S., Hoelzemann, J.J., Ito, A., Marelli, L., Penner, J.E., Putaud, J.-P., Textor, C., Schulz, M., van der Werf, G.R., Wilson, J., 2006. Emissions of primary aerosol and precursor gases in the years 2000 and 1750 prescribed data-sets for AeroCom. *Atmospheric Chemistry and Physics* 6, 4321–4344. \[https://doi.org/10.5194/acp-6-\]\(https://doi.org/10.5194/acp-6-4321-2006\)](#)
- 1350 [4321-2006](#)
- [Kirner, O., Ruhnke, R., Sinnhuber, B.-M., 2014. Chemistry–Climate Interactions of Stratospheric and Mesospheric Ozone in EMAC Long-Term Simulations with Different Boundary Conditions for CO₂, CH₄, N₂O, and ODS. *Atmosphere-Ocean* 53, 140–152. <https://doi.org/10.1080/07055900.2014.980718>](#)
- [Gottschaldt, K., Voigt, C., Jöckel, P., Righi, M., Deckert, R., Dietmüller, S., 2013. Global sensitivity of aviation NO_x effects to the HNO₃-forming channel of the HO₂ + NO reaction. *Atmospheric Chemistry and Physics* 13, 3003–3025. <https://doi.org/10.5194/acp-13-3003-2013>](#)
- 1355

Appendices

Table A1: Summary of stratospheric H₂O perturbations in all scenarios. Values calculated as triannual averages

	<u>Strat.</u> <u>b</u> Background H ₂ O [Tg]	<u>Strat.</u> -H ₂ O perturbation [Tg]	Perturbation lifetime [month]	Hemispheric <u>fraction-ratio</u> [NH/SH]	<u>Absolute-H₂O</u> <u>Increase</u> Hemispheric <u>fraction-ratio</u> [NH/SH]
<u>Nominal (SA1)</u>	[Tg]	[Tg]	[months]	[NH/SH]	[NH/SH]
EMAC	4295.14 <u>1133.5</u>	+ 69.34 <u>63.3</u> (+ 1.62 <u>5</u> %)	176.82	4.82 <u>5.9</u>	4.03 <u>11</u>
GEOS-Chem	7344.8	+49.34 (+ 0.67 <u>7</u> %)	12.7	3.96 <u>4.0</u>	4.03 <u>98</u>
LMDZ-INCA	3743.8	+20.14 (+ 0.58 <u>6</u> %)	5.2	5.37 <u>4</u>	5.45 <u>37</u>
MOZART-3	7520.63 <u>519.8</u>	+ 116.55 <u>4.73</u> (+ 1.55 <u>6</u> %)	30.01 <u>14.0</u>	4.56	4.6 <u>48</u>
<u>Model-M</u> mean		+ 61.34 <u>46.9</u> (+ 1.11 %)	16.12 <u>0.4</u>	4.68 <u>5.0</u>	4.24 <u>5</u>
<u>Triple NO_x (SA2)</u>					
EMAC	4295.14 <u>1133.5</u>	+ 66.27 <u>61.8</u> (+ 1.54 <u>1.5</u> %)	17.01 <u>5.8</u>	7.05 <u>6.6</u>	3.17 <u>4.1</u>
GEOS-Chem	7344.8	+49.79 <u>8</u> (+ 0.68 <u>7</u> %)	12.8	3.88 <u>9</u>	3.83 <u>9</u>
LMDZ-INCA	3743.8	+20.55 <u>6</u> (+ 0.55 <u>6</u> %)	5.3	5.11 <u>2</u>	5.10 <u>5.2</u>
<u>Model-M</u> mean		+ 45.44 <u>54.1</u> (+ 0.92 %)	7.48 <u>11.3</u>	5.35 <u>2</u>	4.05 <u>4</u>
<u>Low cruise (SA3)</u>					
EMAC	4295.14 <u>1133.5</u>	+ 19.69 <u>16.0</u> (+ 0.46 <u>4</u> %)	11.29 <u>1</u>	25.07 <u>3.2</u>	2.39 <u>3.1</u>
GEOS-Chem	7344.8	+ 5.96 <u>6.0</u> (+ 0.08 <u>1</u> %)	3.4	10.19 <u>3</u>	10.39 <u>4</u>
LMDZ-INCA	3743.8	+2.37 <u>4</u> (+ 0.06 <u>1</u> %)	1.3	36.26 <u>6.4</u>	39.41 <u>38.1</u>
<u>Model-M</u> mean		+ 9.34 <u>8.1</u> (+ 0.20 %)	5.34 <u>6</u>	8.89 <u>16.6</u>	17.42 <u>0</u>

Table A2: Summary of stratospheric NO_x perturbations due to the emission scenarios. Values calculated as triannual averages.

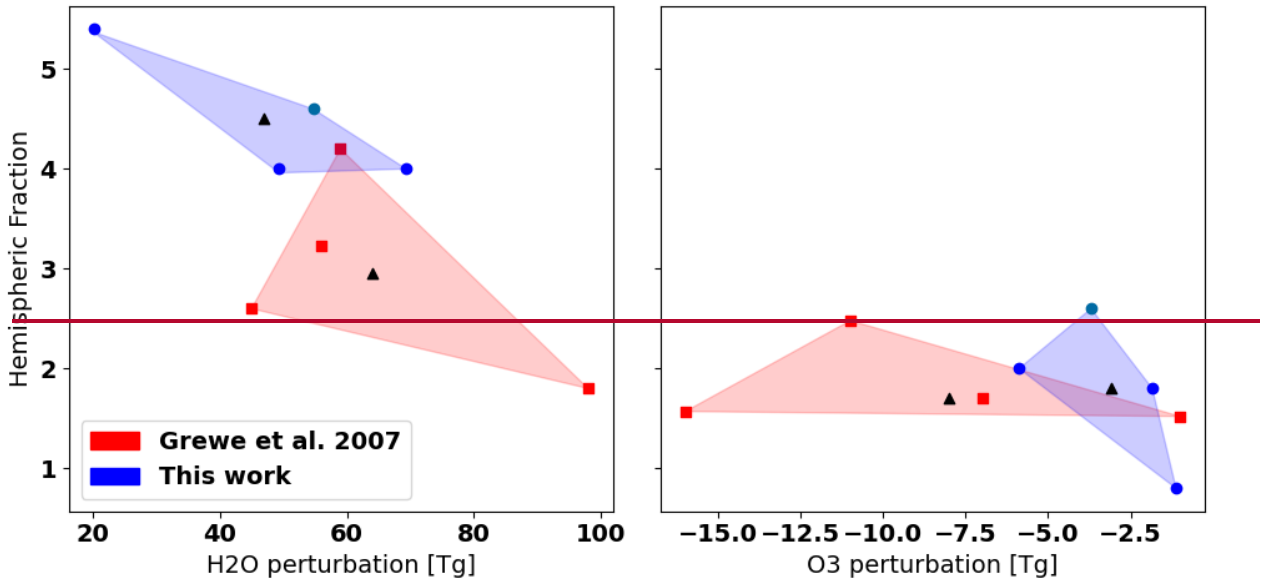
	<u>Strat</u> <u>b</u> Background NO _x [<u>Gg</u> NO ₂]	<u>Strat</u> -NO _x perturbation [<u>Gg</u> -NO ₂]	Perturbation lifetime [<u>months</u>]	<u>Absolute</u> -NO _x <u>increase</u> hemispheric <u>fraction-ratio</u> [<u>NH</u> / <u>SH</u>]
<u>Nominal (AS1)</u>	[<u>Gg</u> NO ₂]	[<u>Gg</u> NO ₂]	[<u>months</u>]	[<u>NH</u> / <u>SH</u>]
EMAC	2321.7 2329.6	+378.714 (+1.67%)	4.20	4.52 4.41
GEOS-Chem	2302.0	+43.52 (+1.89%)	4.7	2.637
LMDZ-INCA	2457.8	+42.56 (+1.73%)	4.6	2.237
MOZART-3	1233.1 2035.74	+39.0732.1 (+3.1.646%)	4.23 5	2.95 6.7
<u>Model-mean</u>		+40.9638.9 (+1.72.11%)	4.24	2.57 4.1
<u>Triple NO_x (SA2)</u>				
EMAC	2329.6 2321.7	+139.640.5 (+6.04%)	3.3	3.067
GEOS-Chem	2302.0	+173.6 (+7.54%)	4.1	2.485
LMDZ-INCA	2457.8	+119.54 (+4.869%)	2.8	2.34
MOZART-3	1233.14 2035.7	+120.74112.8 (+9.795.5%)	2.82 6	3.08 6.2
<u>Model-mean</u>		+1368.376 (+7.6.005%)	3.23	2.3 773
<u>Low cruise (AS3)</u>				
EMAC	2329.6 2321.7	+21.3218.2 (+0.928%)	5.44 6	1.96 3.7
GEOS-Chem	2302.0	+23.72 (+1.03%)	6.0	2.67
LMDZ-INCA	2457.8	+17.41 (+0.71%)	4.4	2.34
<u>Model-mean</u>		+1920.82 (+0.89%)	5.03	2.93

Table A3: Summary of O₃ perturbations due to the emission scenarios. Values calculated as triannual averages.

	Strat. background O ₃ [Tg]	Strat. O ₃ perturbation [Tg]	O ₃ increase hemispheric mass ratio	O ₃ loss hemispheric ratio	Background column [DU]	Column perturbation [DU]	Column O ₃ loss hemispheric ratio
Nominal (SA1)	[Tg]	[Tg]	[NH/SH]	[NH/SH]	[DU]	[DU]	[NH/SH]
EMAC	3152.837.3	-1.13 (-0.04 %)	4.4	0.8	342.9340.0	+0.09 (+0.03 %)	0.9
GEOS-Chem	3002.9	-5.889 (-0.20 %)	1.3	2.0	333.1321.92	-0.72 (-0.22 %)	2.4
LMDZ-INCA	3092.0	-1.84 (-0.061 %)	1.3	1.8	33328.57.6	-0.152 (-0.050 %)	2.6
MOZART-3	1907.42926.5	-2.393.7 (-0.13 %)	0.4	2.6	238331.2	-0.463 (-0.182 %)	19.4
Model-mean		-2.813.1 (-0.14 %)	1.9	1.8	312.9330.4	-0.30 (-0.14 %)	6.3
Triple NO_x (SA2)							
EMAC	313752.83	-8.19 (-0.263 %)	5.4	1.5	342.9340.0	-0.611.6 (-0.218 %)	1.3
GEOS-Chem	3002.9	-14.061 (-0.465 %)	1.1	1.9	333.12321.9	-1.364 (-0.41 %)	3.2
LMDZ-INCA	3092.0	-4.72 (-0.152 %)	1.3	1.8	337.6328.5	-0.30 (-0.091 %)	2.5
MOZART-3	1907.42926.5	-9.1714.1 (-0.485 %)	0.2	3.2	238331.2	-1.354 (-0.574 %)	20.3
Model-mean		-10.259.04 (-0.34 %)	2.0	2.1	312.9330.4	-0.991 (-0.34 %)	6.8
Low cruise (AS3)							
EMAC	3137.352.8	+0.211 (+0.04 %)	3.5	1.2	342.9340.0	+0.11 (+0.03 %)	1.6
GEOS-Chem	3002.9	-0.63 (-0.02 %)	2.2	1.5	333.12321.9	-0.04 (-0.04 %)	2.6
LMDZ-INCA	3092.0	+0.827 (+0.03 %)	1.6	1.4	337.6328.5	+0.14 (+0.04 %)	7.4
Model-mean		+0.5561 (+0.02 %)	2.4	0.9	3307.91	+0.107 (+0.02 %)	3.9

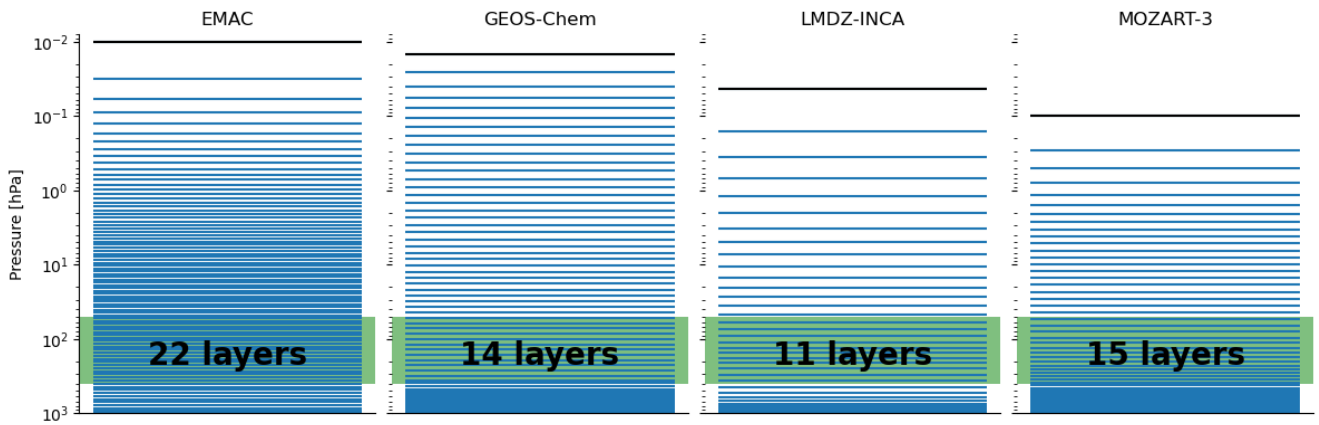
Table A4: Summary of mean background halogen mixing ratios in the last 3 years of ~~for~~ the baseline (AS0) scenario. Units in pptv. Values denoted by – indicate species which are not present in ~~that specific~~ that model.

	Surface				200 to 10 hPa			
	EMAC	GEOS-Chem	LMDZ-INCA	MOZART-3	EMAC	GEOS-Chem	LMDZ-INCA	MOZART3
Br	0.0002	0.0002	0.0001	3.0153e-5	0.1730	0.1252	0.1026	0.1709
BrCl	1.9678e-6	0.0015	5.652e-7	4.5890e-7	0.5050	1.3526	0.3435	0.4528
BrO	0.0060	0.0028	0.0020	0.0006	2.7007	1.8154	1.3145	2.6226
CFC11	-	138.19	138.1999	248.0824	-	59.7229	70.9768	120.1767
Cl	1.8753e-6	2.0481	2.5670	3.3410	0.0189	0.02414	0.0213	0.0262
Cl ₂	4.9708e-6	0.0028	1.9384	2.6432	7.5453	5.6160	4.3763	2.0720
Cl ₂ O ₂	1.7003e-11	1.243e-9	7.8370	2.1778	4.4737	18.0780	8.6143	13.3571
ClNO ₂	3.2010e-8	0.0706	0.0005	-	0.0303	0.0050	0.1487	-
ClONO ₂	0.02210	0.0106	0.2481	0.2723	201.1863	265.0219	197.7726	309.8003
HBr	0.1244	0.01407	0.1085	0.0131	0.4284	0.1884	0.1691	0.2867
HCl	1.4150	3.2963	2.5572	1.6588	669.4262	680.3545	561.8869	936.3695
HOBr	0.0806	0.0116	0.0113	0.0032	1.0023	0.8293	1.1495	1.1218
HOCl	0.1142	0.0973	0.0587	0.0626	9.3144	20.2350	10.6867	8.4008
OCIO	4.5830e-5	7.906e-5	0.2534	4.2968e-7	1.7333	1.9323	1.8834	2.1081



1375

Fig A1: Comparison of the H₂O (left) and O₃ (right) perturbations and hemispheric fractions for the models used in this work and Grewe et al. (2007). Black triangles represent the multi-model means.



1380

Figure A1: Comparison of the vertical grid of the EMAC, GEOS-Chem, LMDZ-INCA, and MOZART-3 models. The green region denotes the region between 400 and 50 hPa, which is important to the stratospheric-tropospheric exchange. The count of model layers within this region is shown in the figure.

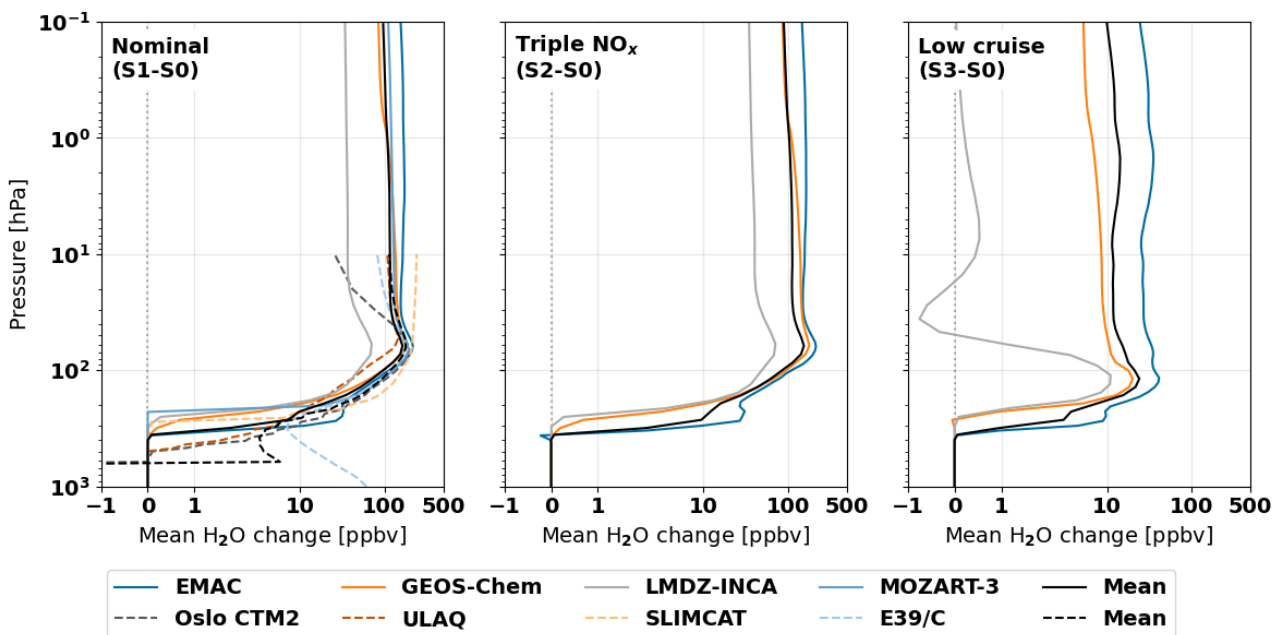


Figure A2: Mean changes in water vapour mixing ratio over altitude for the nominal supersonic (S1, left), triple NO_x (S2, middle) and low cruise (S3, right) emission scenarios. Entries with dashed lines are from data from Grewe et al. (2007).

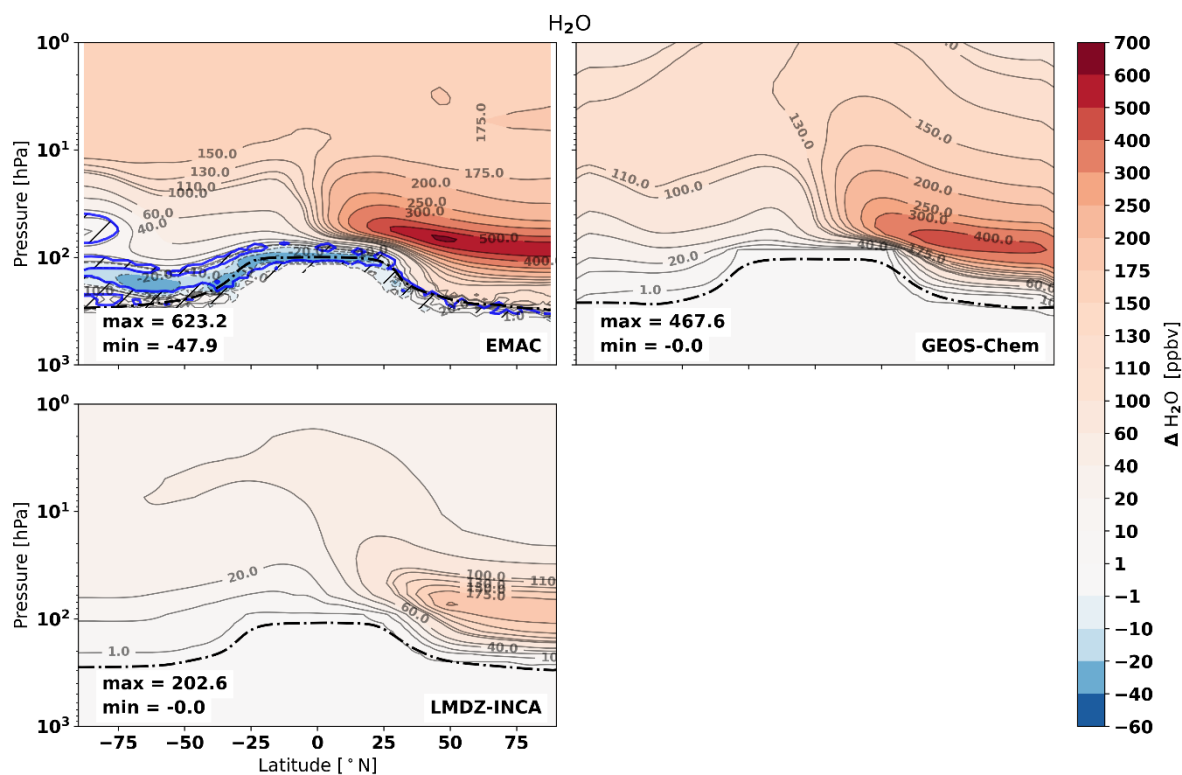


Figure A3: Changes in H₂O volume mixing ratios for the triple NO_x (SA2) emission scenario. Hatched areas enclosed by blue lines indicate regions which are not statistically significant for the EMAC results. Dash-dotted lines show the mean tropopause pressure, calculated per model.

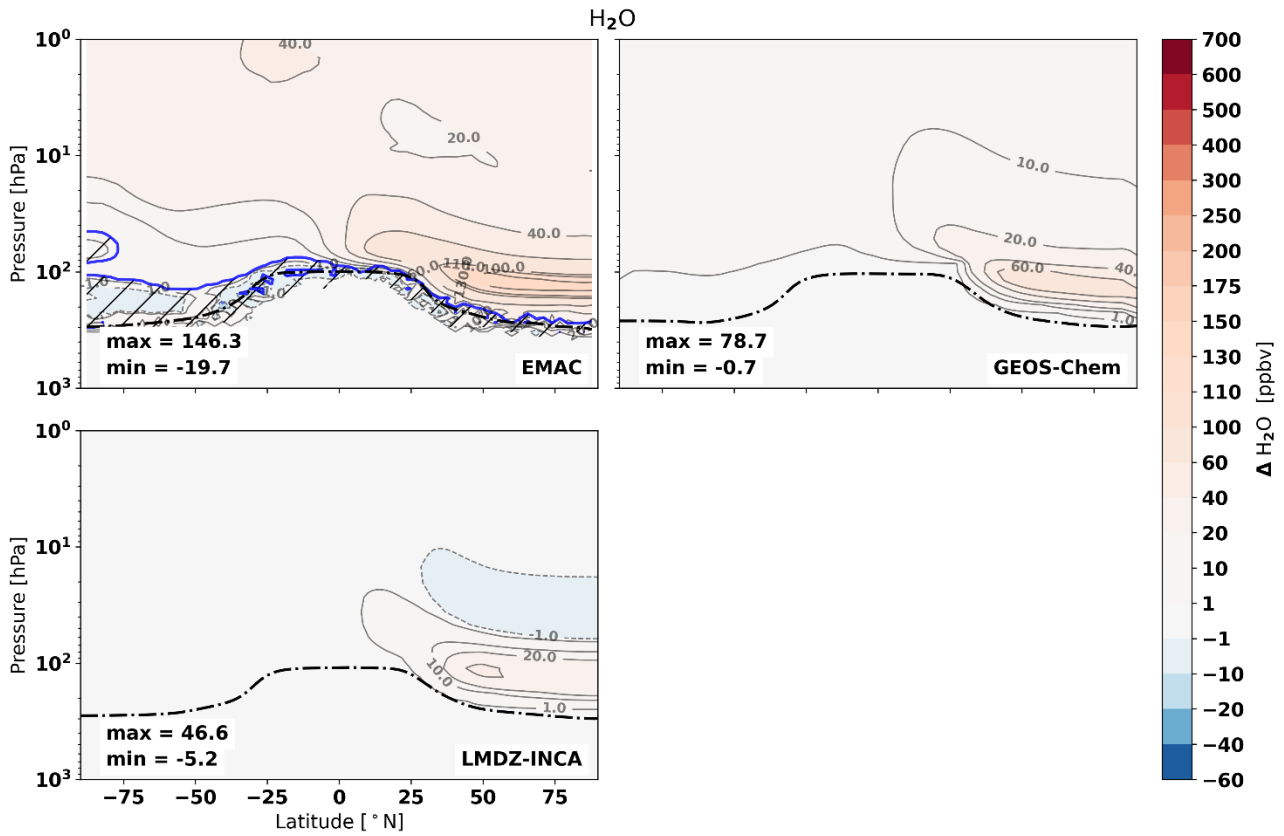


Figure A34: Changes in H₂O volume mixing ratios for the low cruise (SA3) emission scenario. Hatched areas enclosed by blue lines indicate regions which are not statistically significant for the EMAC results. Dash-dotted lines show the mean tropopause pressure, calculated per model.

1395

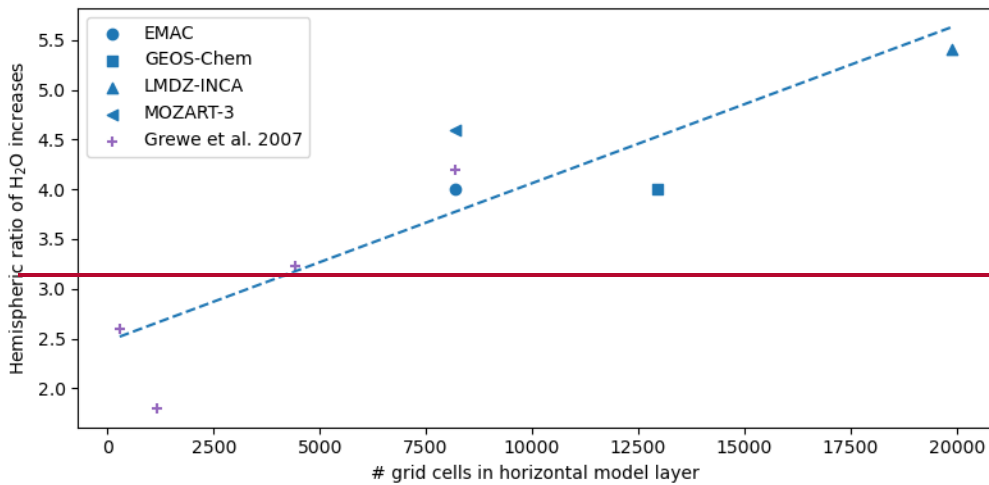
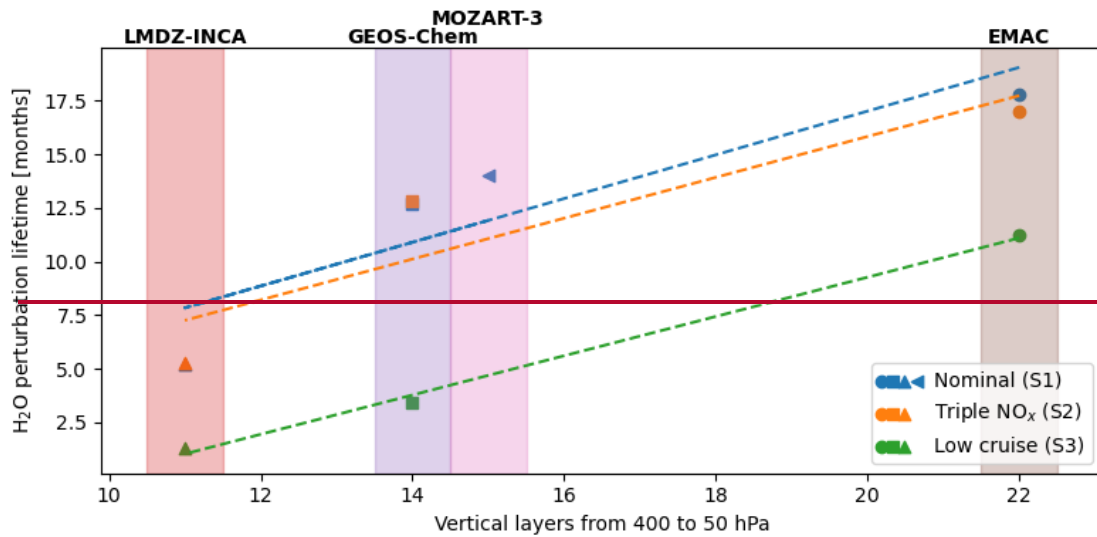
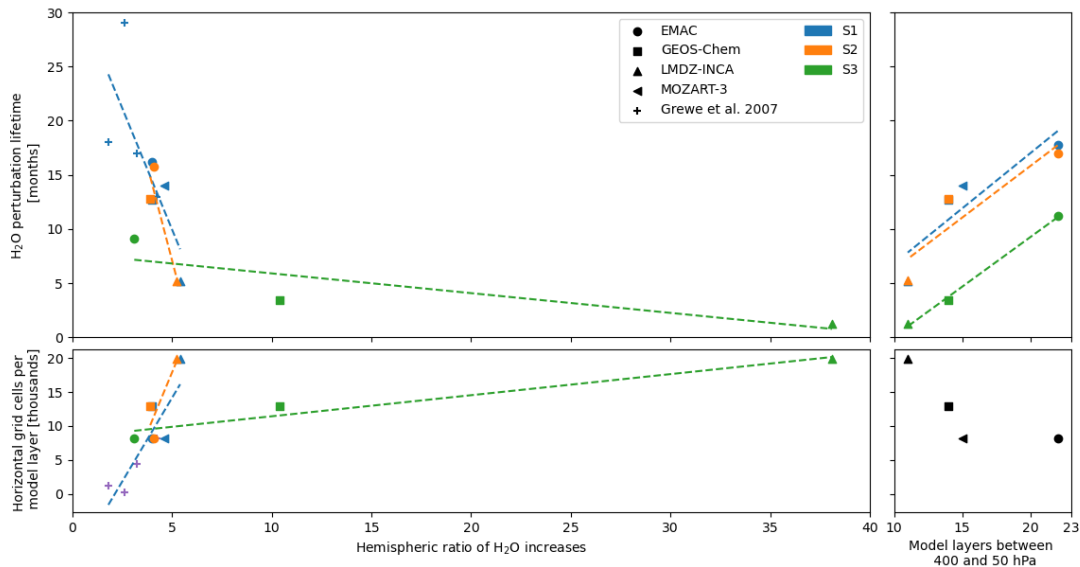


Fig A4: Hemispheric fraction of the water vapour perturbation (perturbation mass northern hemisphere / southern hemisphere) for the nominal supersonic emission scenario, over the number of cells in horizontal layers of the models used. The dashed line is a fitted first-order trend line.

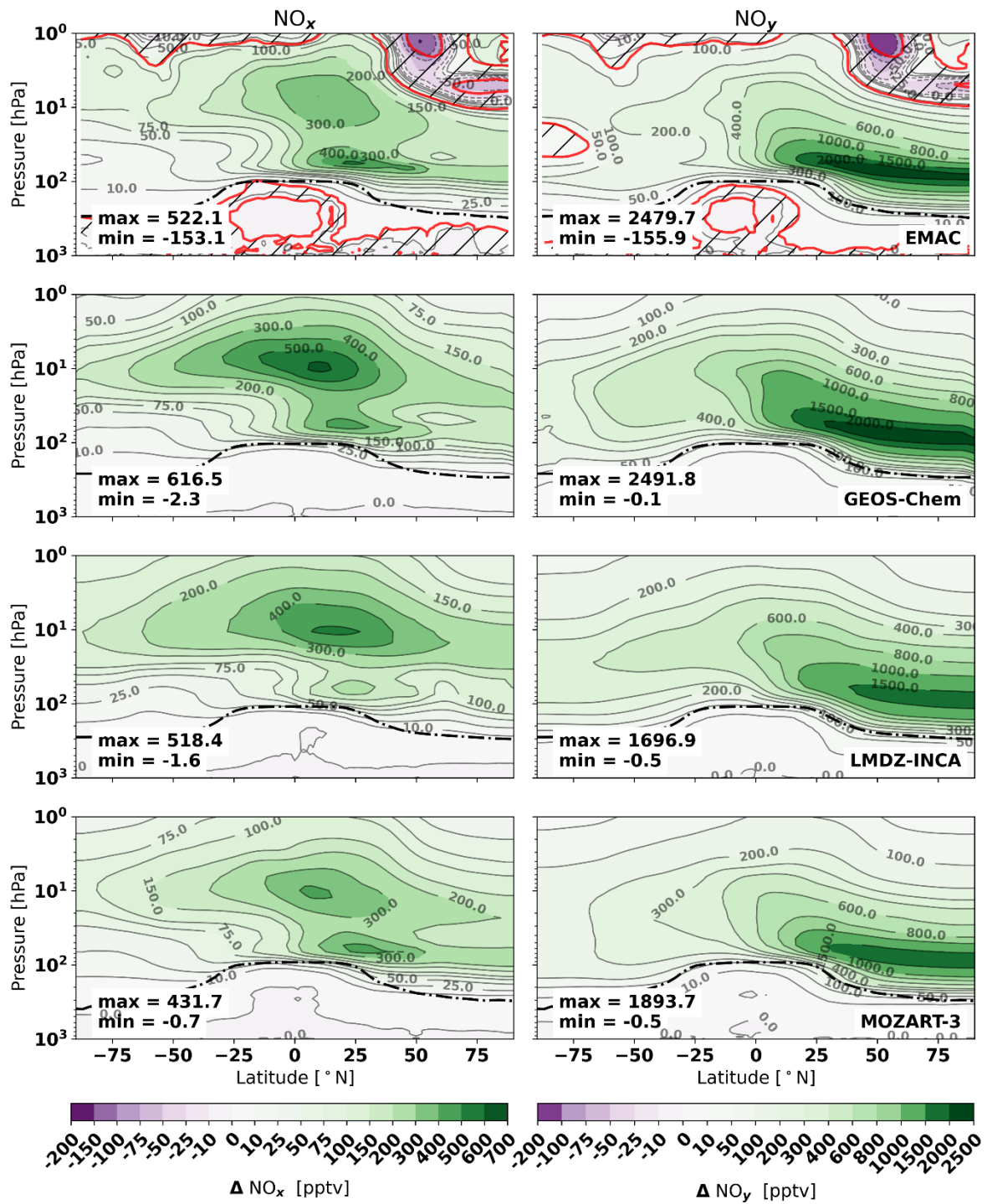
1400



1405 **Fig A5: Stratospheric H₂O perturbation over the vertical model level count for the LMDZ-INCA, GEOS-Chem, and EMAC models for the emission scenarios.**

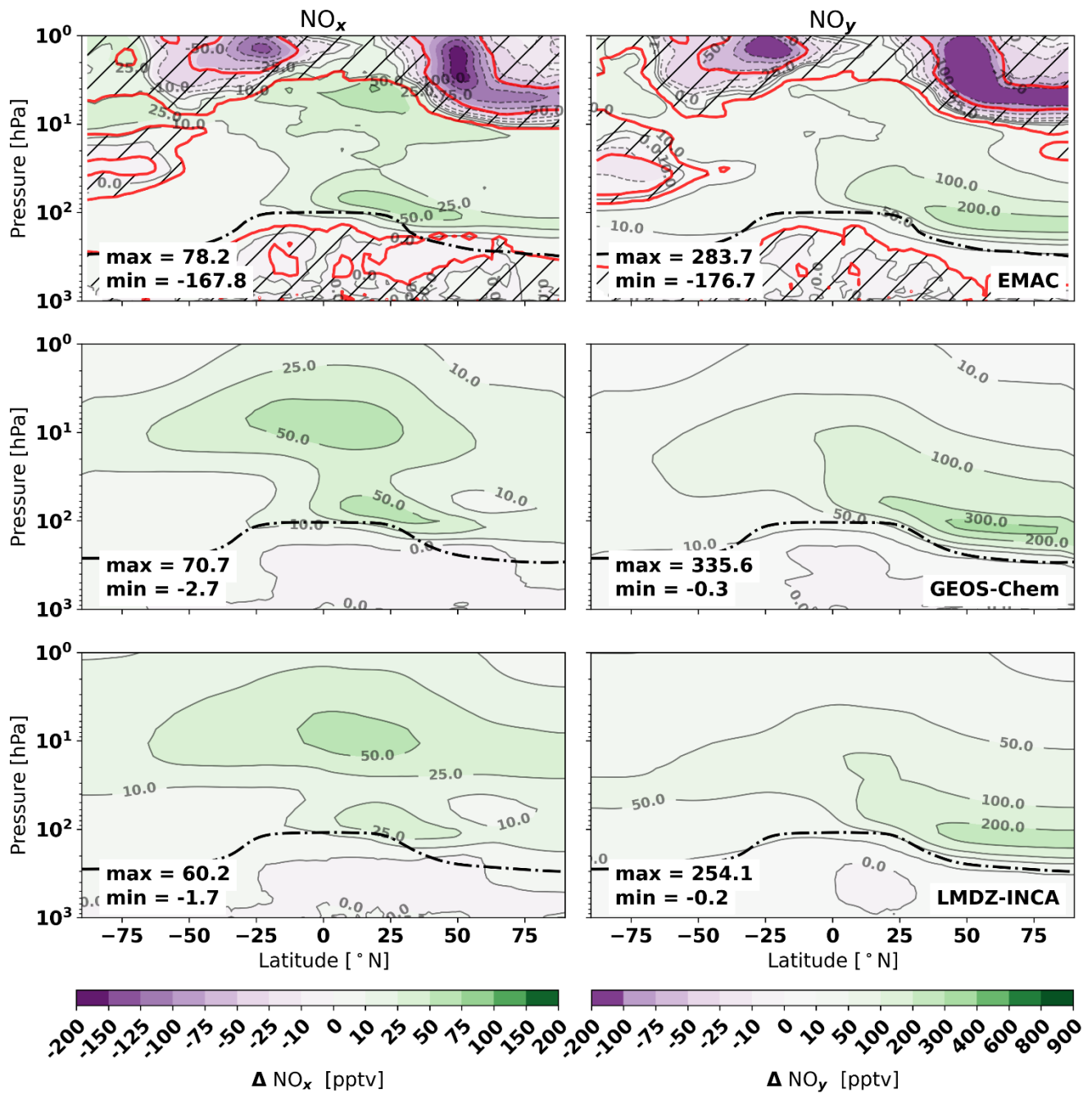


1410 **Figure A5: Comparison of the H₂O perturbation lifetime in months and the hemispheric ratio of the H₂O increases of the nominal supersonic scenario (S1) with vertical and horizontal model grid characteristics. The top left figure shows the relationship between the perturbation lifetime and the hemispheric ratio, the top right the perturbation lifetime and the number of grid layers between 400 and 50 hPa, and the bottom left shows the hemispheric ratio and the horizontal grid fidelity. Markers denote the different models and colour different scenarios. Results from Grewe et al. (2007) are included for their S1-equivalent SST scenario (S5 in Grewe et al. (2007)).**



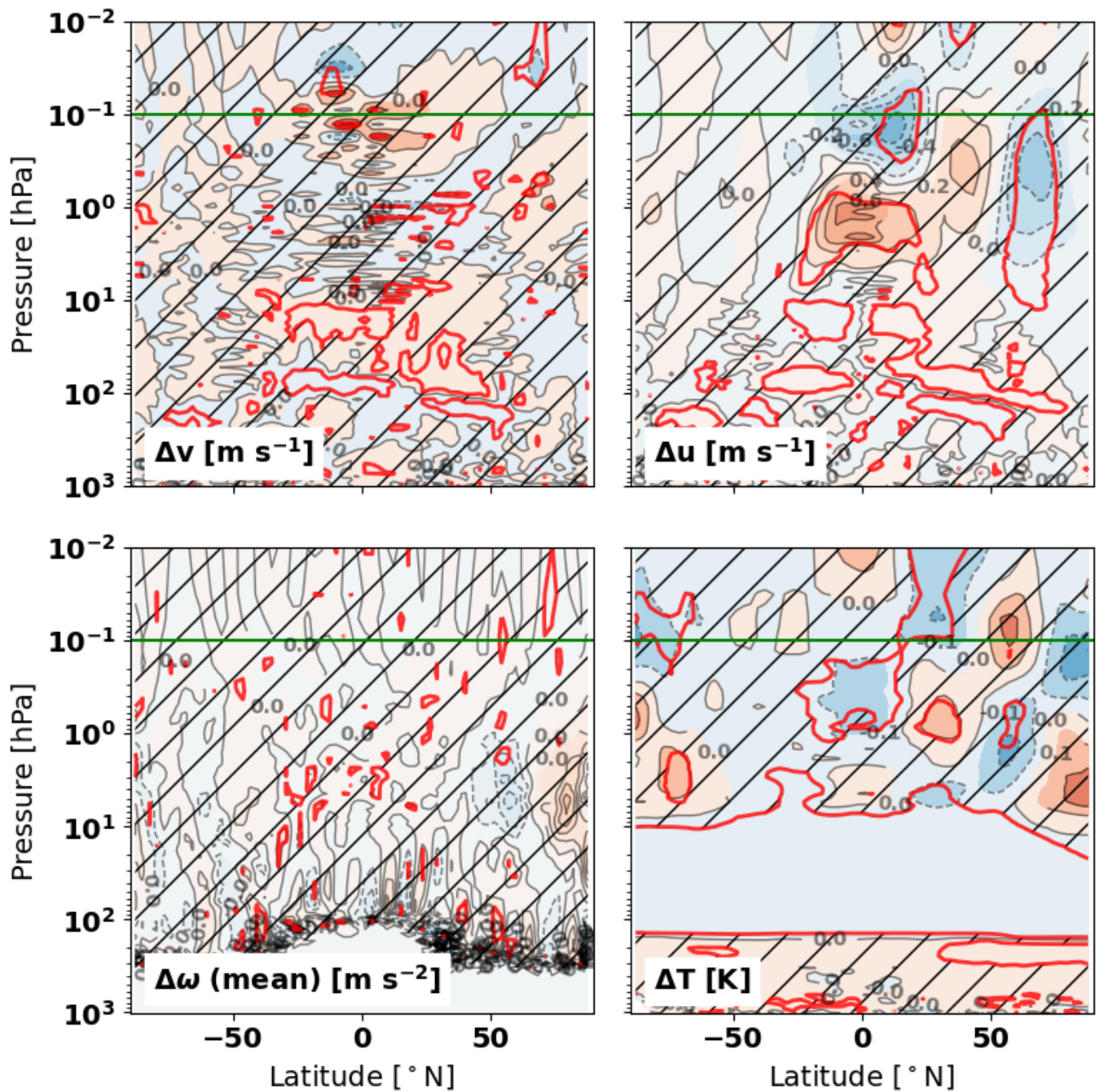
1415

Figure A66: Mean changes in NO_x (left) and NO_y (right) concentrations in the triple NO_x (SA2) emissions scenario across the models. Hatched areas enclosed by red lines indicate regions which are not statistically significant for the EMAC results. [Dash-dotted lines](#) show the mean tropopause pressure, calculated per model.



1420

Figure A7A7: Similar to Same as Figure A7A6, but for the low cruise (AS3) scenario. Hatched areas enclosed by red lines indicate regions which are not statistically significant for the EMAC results. Dash-dotted lines show the mean tropopause pressure, calculated per model.



1425

Figure A8: Changes in mean wind speeds (v, u, ω) and temperature (T) in EMAC in response to the nominal supersonic emissions scenario (S1). Hatched areas enclosed by red lines are not statistically significant over the 6 year evaluation period. Positive changes in u indicate increased eastwards velocities, the positive direction in v is northward, whereas $\Delta\omega$ shows changes in vertical acceleration.

1430

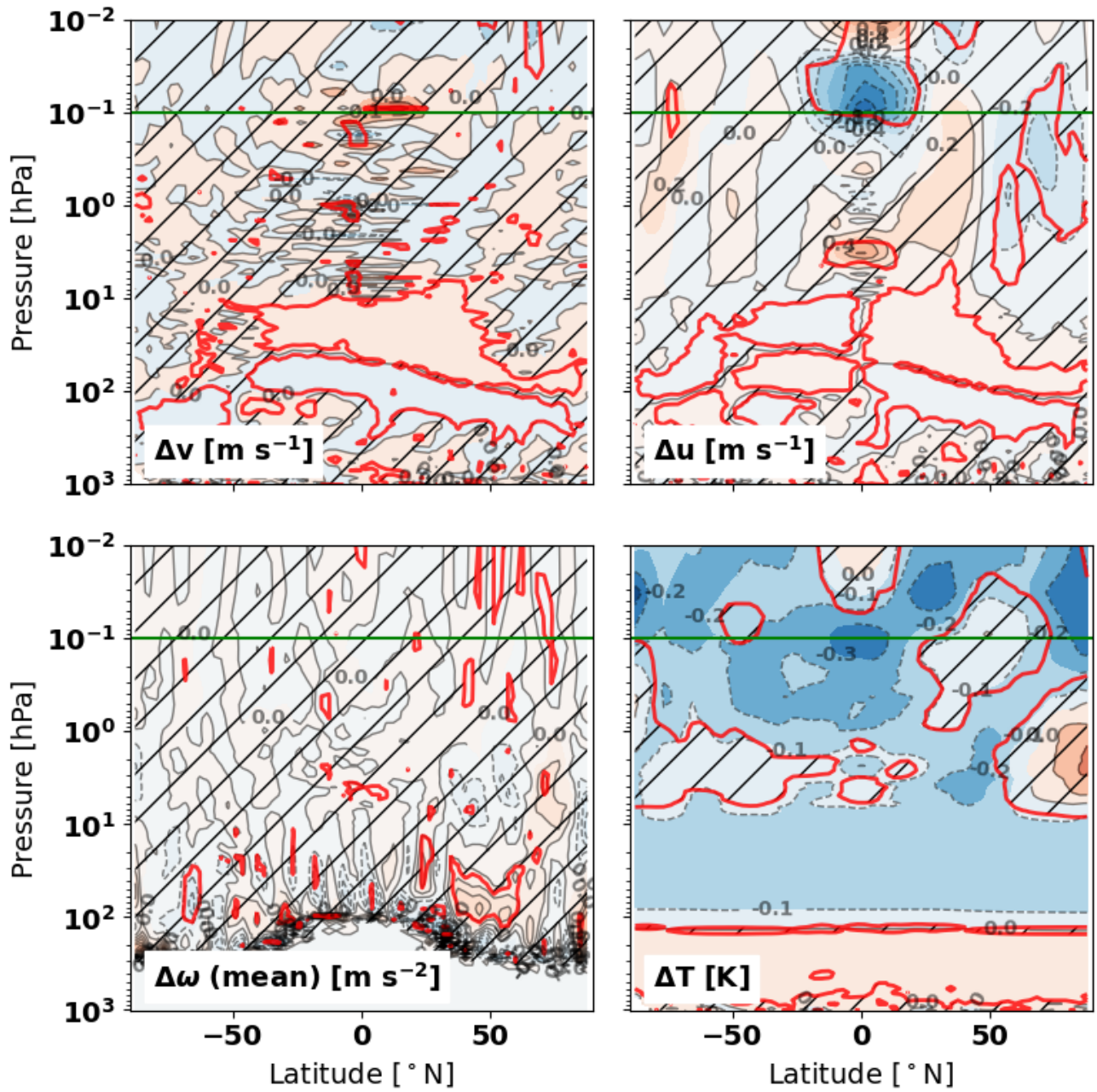


Figure A9: Same as Figure A8, but for the triple NO_x emissions scenario (S2).

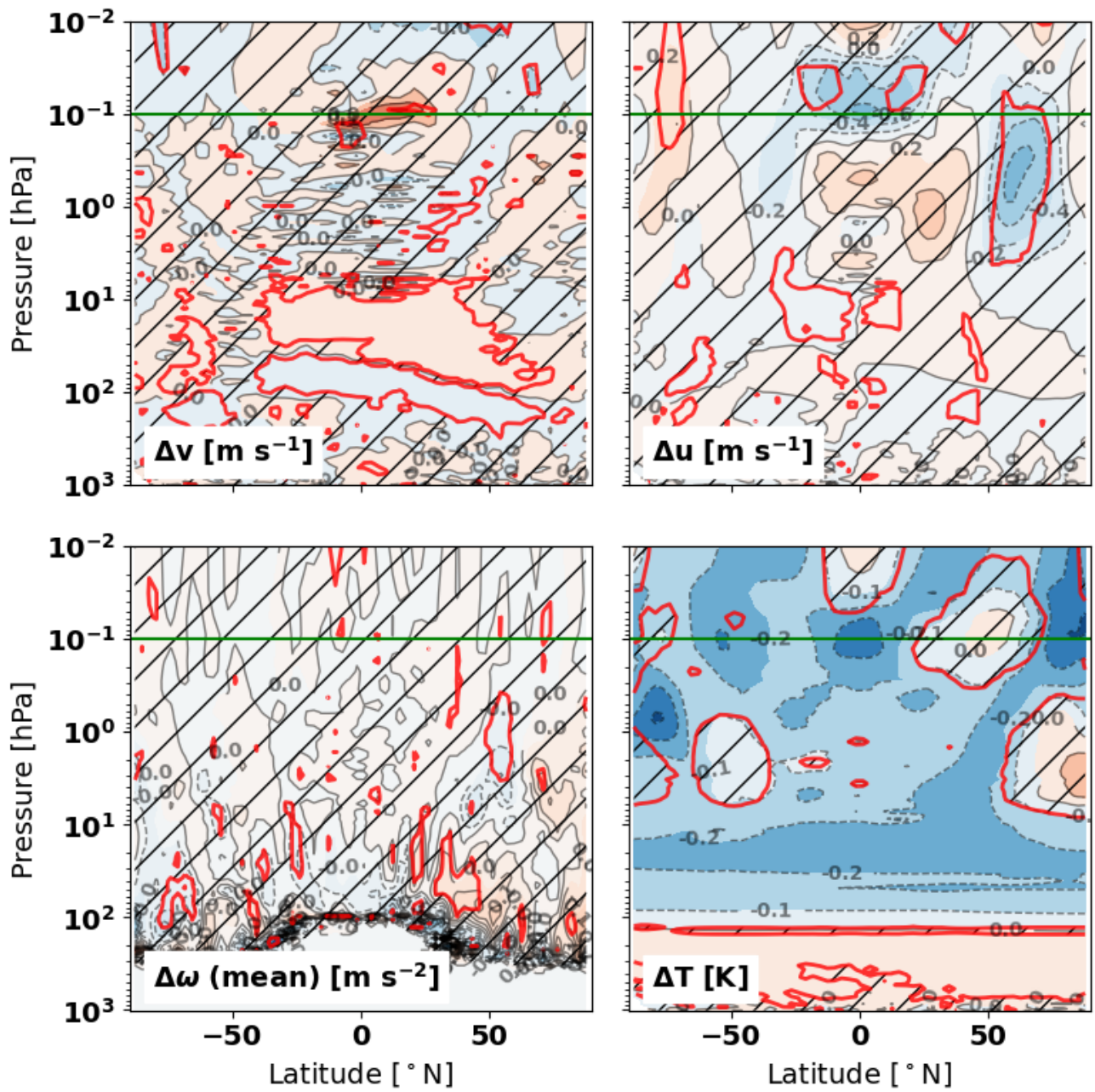


Figure A10: Same as Figure A9, but for the low cruise scenario (S3).

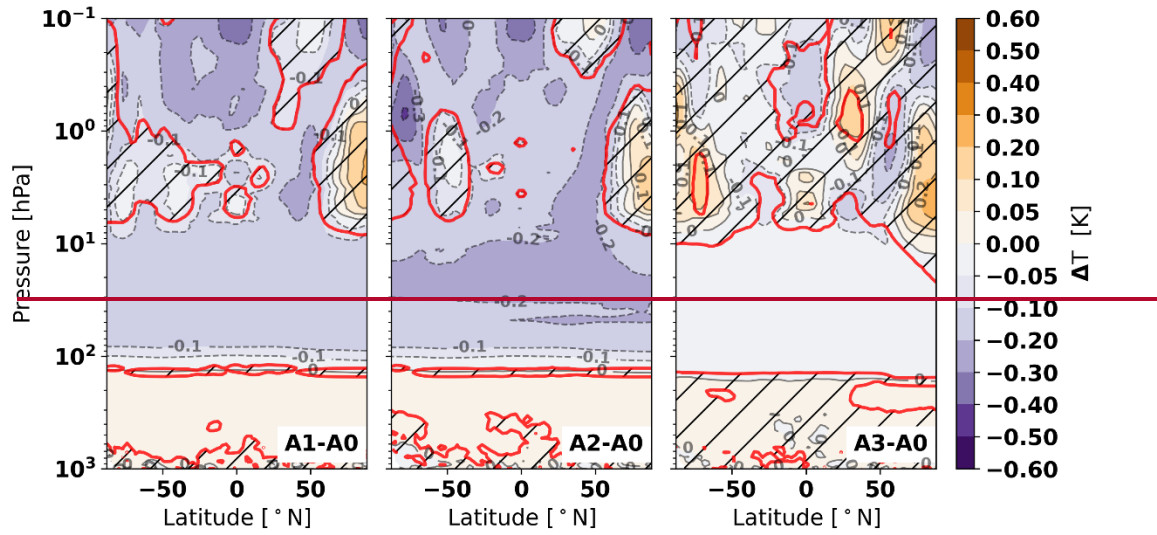
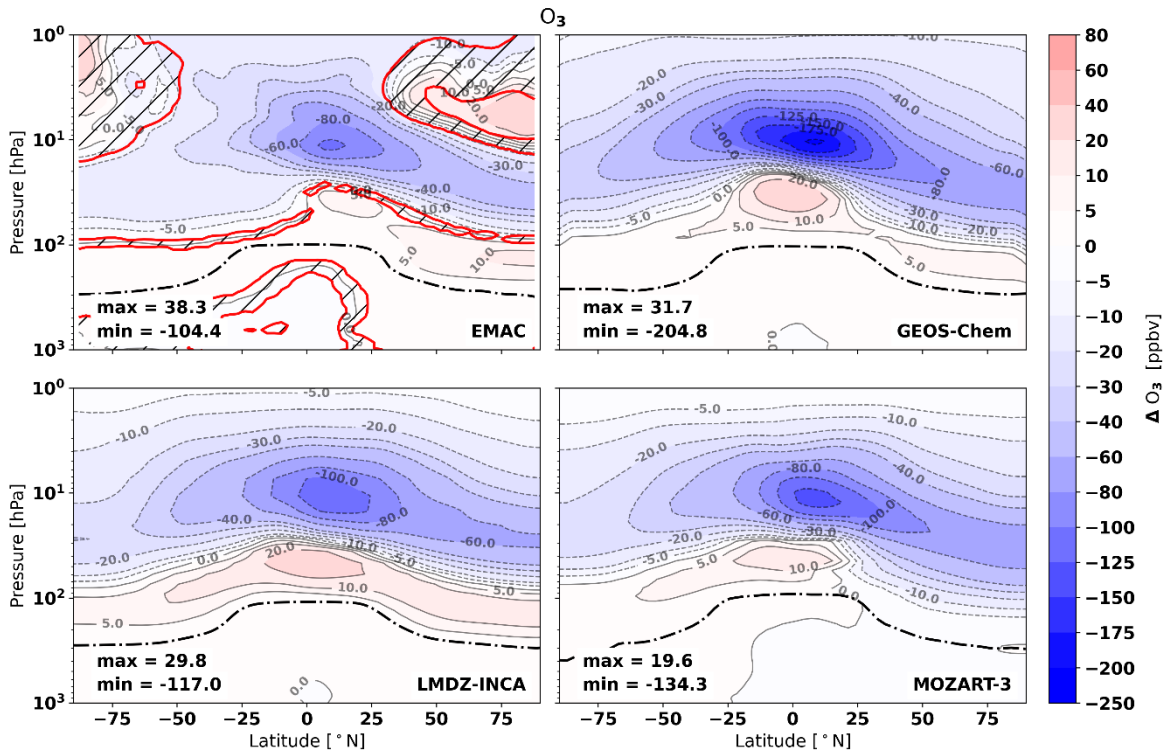
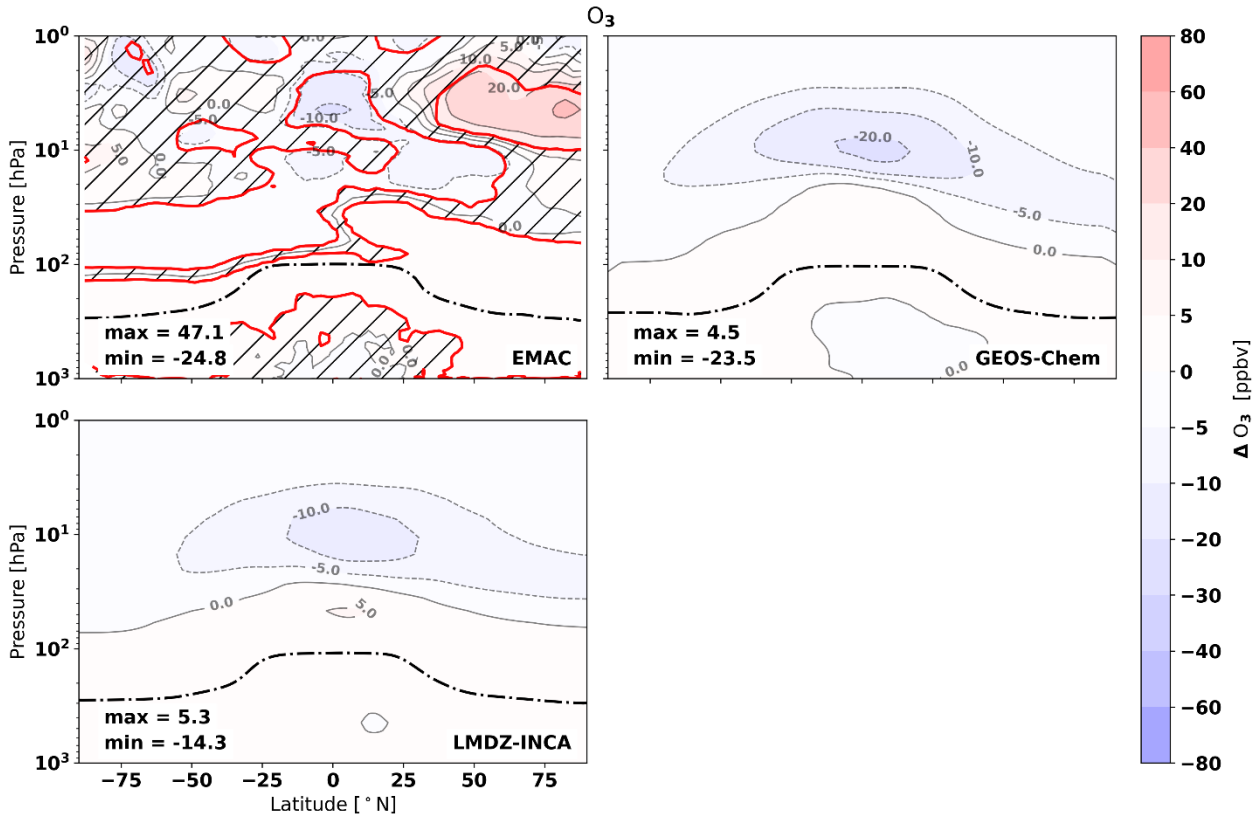


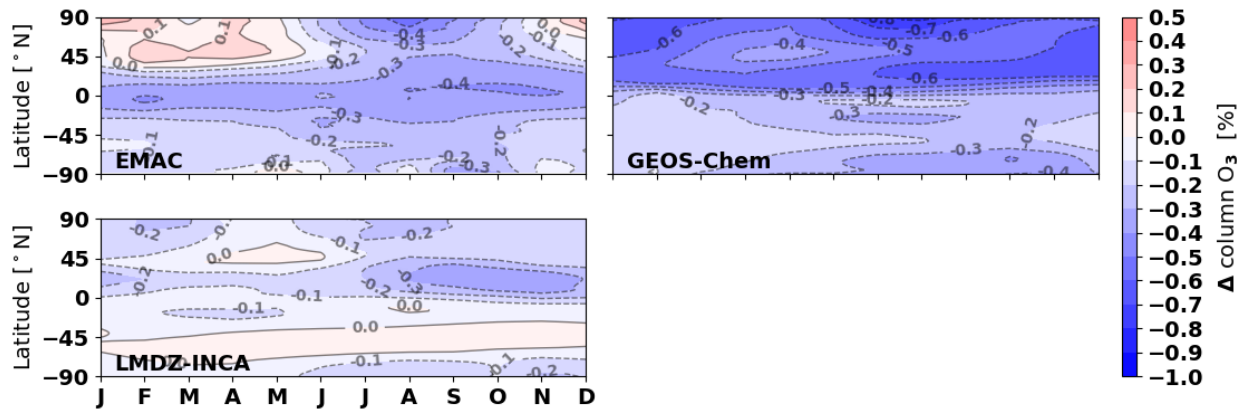
Fig A8: Average change in atmospheric temperature in Kelvin induced by the emission scenarios over the last 3 years of integration in the EMAC model. Hatched areas indicate areas where the change is not statistically significant.



1440 **Figure A19:** Changes in ozone VMR for the triple NO_x (SA2) emissions scenario. Hatched areas enclosed by red lines indicate regions which are not statistically significant for the EMAC results. Dash-dotted lines show the mean tropopause pressure, calculated per model.



1445 **Figure A102:** Similar to **Figure A11**, but for the low cruise (SA3) scenario. Hatched areas enclosed by red lines indicate regions which are not statistically significant for the EMAC results. Dash-dotted lines show the mean tropopause pressure, calculated per model.



1450 **Figure A13:** Mean monthly changes in ozone columns (in percentage) in response to the triple NO_x emissions (S2 – S0).

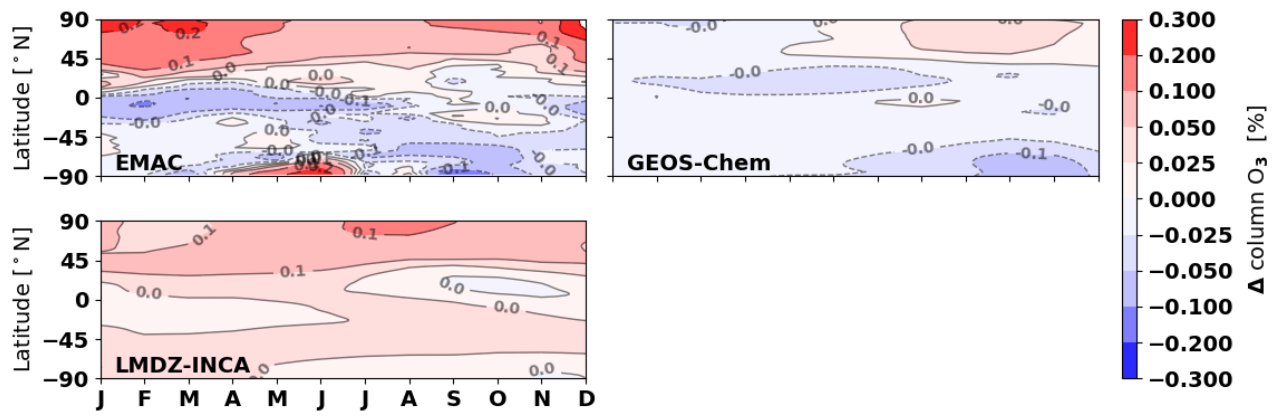
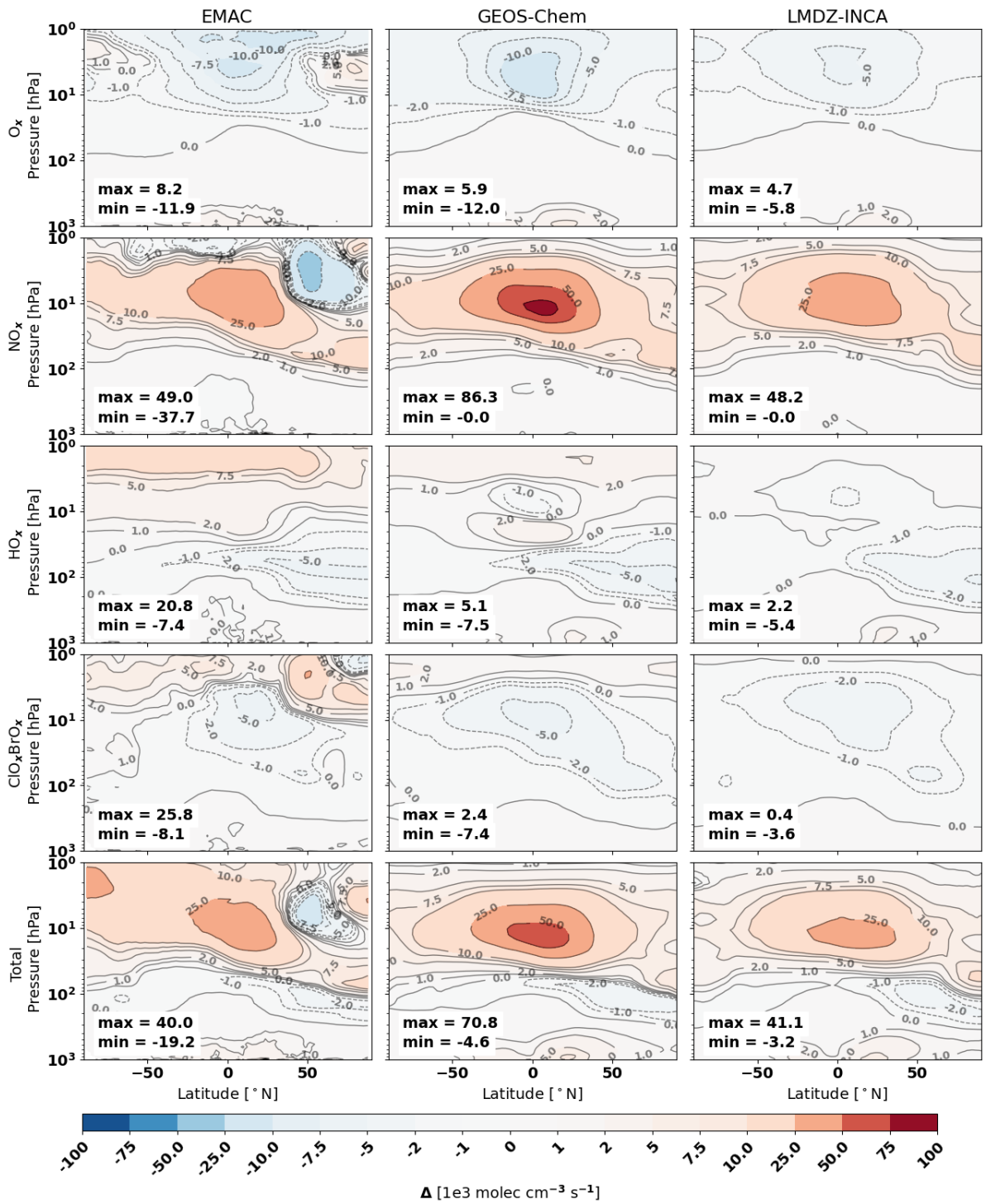


Figure A14: Similar to Figure A13, but for the low cruise (S3) scenario.



1455 Figure A145: Same as Figure 8 but for the triple NO_x (SA2) emissions scenario

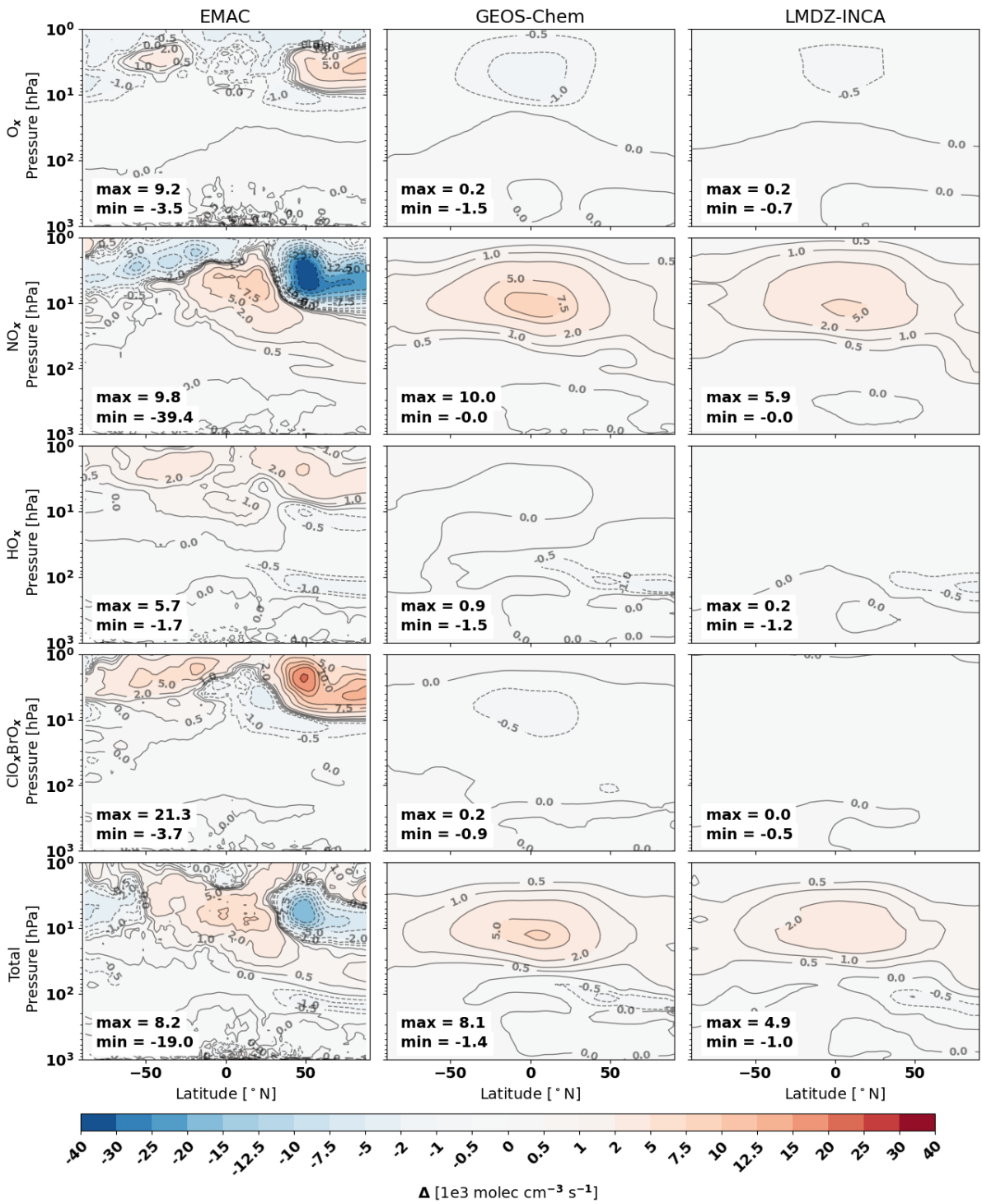
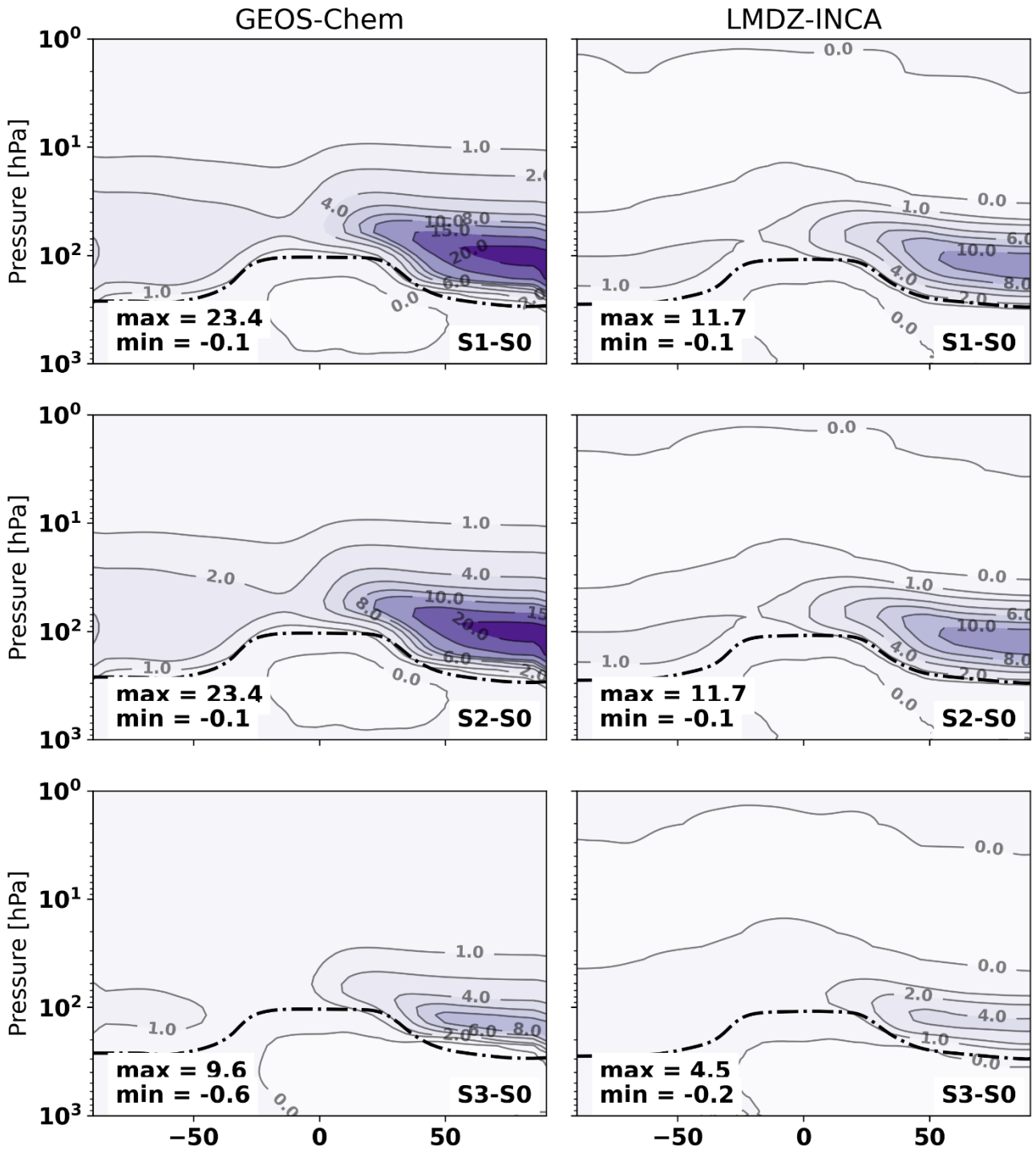


Figure A126: Same as Figure 8 but for the low cruise (SA3) emissions scenario



1460 **Figure A137:** Comparison of the black carbon aerosol perturbations in 10^{-2} ng / m^3 for the GEOS-Chem (left) and LMDZ-INCA (right) models.

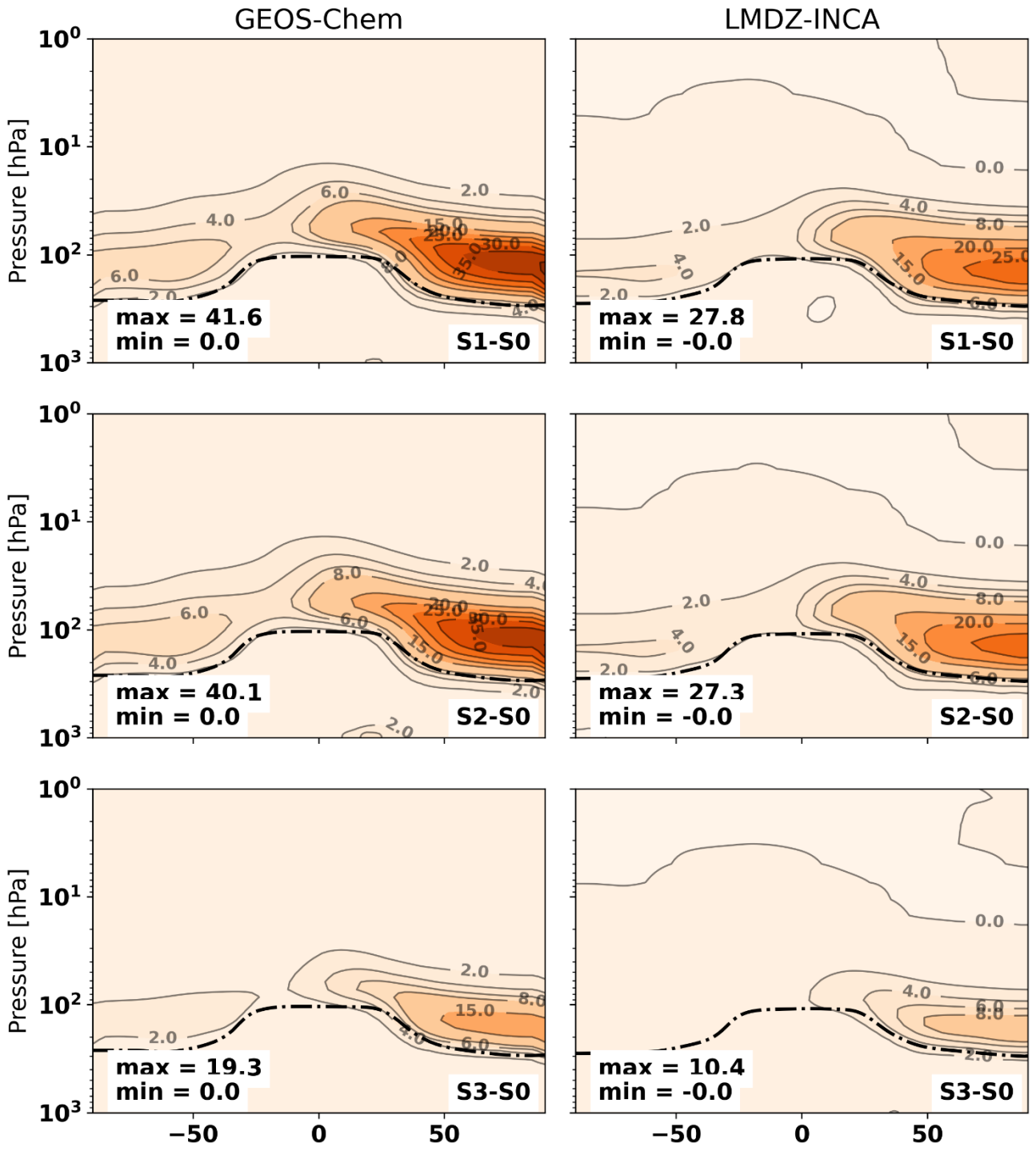
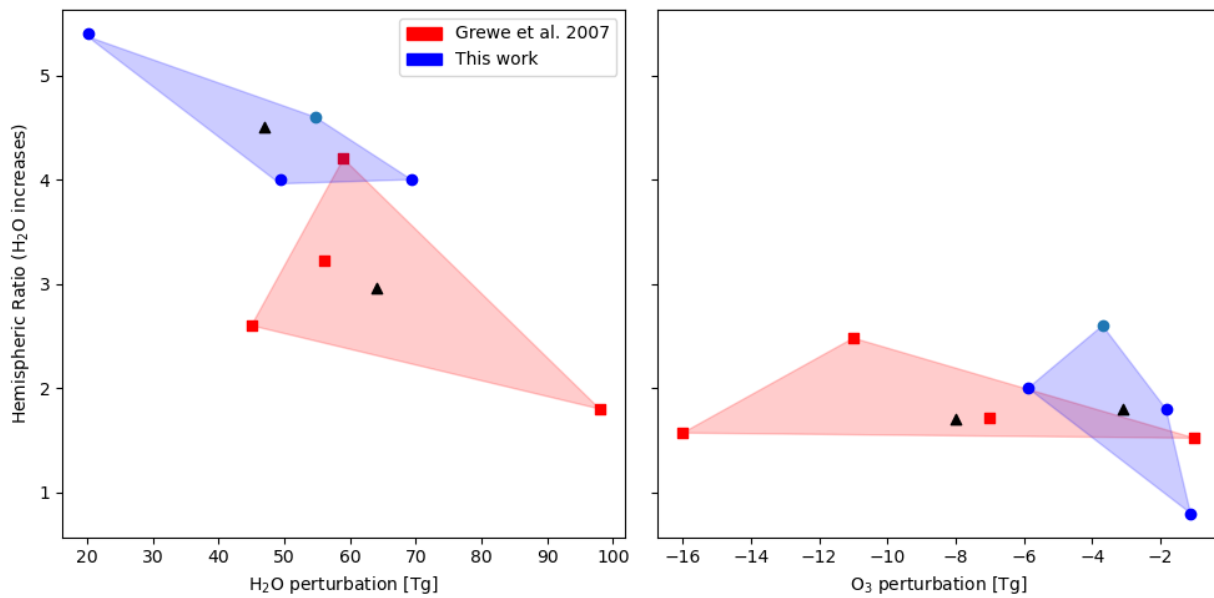


Figure A148: Comparison of the SO₄ aerosol perturbations in ng / m³ for the GEOS-Chem (left) and LMDZ-INCA (right) models.



1465

[Figure A19: Comparison of the H₂O \(left\) and O₃ \(right\) perturbations and hemispheric ratios for the models used in this work and Grewe et al. \(2007\). Black triangles represent the multi-model means.](#)